Kardar-Parisi-Zhang universality in the phase of a condensate of exciton polaritons : from the scaling of correlation functions to advanced statistics of the phase in 1+1 and 2+1 dimensions

Konstantinos Deligiannis

THÈSE

Pour obtenir le grade de

DOCTEUR DE L'UNIVERSITÉ GRENOBLE ALPES

Spécialité : **Physique Théorique**

Arrêtée ministériel : 25 mai 2016

Présentée par

Konstantinos DELIGIANNIS

Thèse dirigée par **Léonie CANET,** Professeure, UGA et LPMMC
et codirigée par **Anna MINGUZZI,** Directrice de recherche, CNRS et LPMMC

préparée au sein du **Laboratoire de Physique et de Modélisation des Milieux Condensés (LPMMC)**
dans **l'École Doctorale de Physique**

Kardar-Parisi-Zhang universality in the phase of a condensate of exciton polaritons : from the scaling of correlation functions to advanced statistics of the phase in $1+1$ and $2+1$ dimensions

Universalité de Kardar-Parisi-Zhang dans la phase du condensat d'excitons polaritons : des lois d'échelle des fonctions de corrélation aux statistiques avancées de la phase en $1+1$ et $2+1$ dimensions

Thèse soutenue publiquement le **4 Mai 2022**,
devant le jury composé de :

Monsieur Alberto Bramati
Professeur, Sorbonne Université et Laboratoire Kastler Brossel, Examinateur

Monsieur Iacopo Carusotto
Directeur de recherche, CNR-INO BEC Center, Rapporteur

Monsieur Valerio Olevano
Directeur de recherche, CNRS et Institut Néel, Président

Monsieur Nikolaos Proukakis
Professeur, Newcastle University, Rapporteur

Monsieur Alberto Rosso
Directeur de recherche, CNRS et Laboratoire de Physique Théorique et Modèles Statistiques, Examinateur

Monsieur Benoît Vermersch
Maître de conférences, UGA et LPMMC, Examinateur

Universalité de Kardar-Parisi-Zhang dans la phase du condensat d'excitons polaritons : des lois d'échelle des fonctions de corrélation aux statistiques avancées de la phase en $1+1$ et $2+1$ dimensions

Résumé

Un exciton polariton apparaît lorsqu'une paire électron-trou liée dans une microcavité semi-conductrice interagit fortement avec les photons de la cavité. En raison des pertes inévitables de photons, une injection continue est nécessaire via une source externe afin de maintenir un état stationnaire. Il a été montré que ce gaz d'exciton polariton hors-équilibre présente des caractéristiques similaires à la condensation de Bose-Einstein à l'équilibre, cependant, il a été découvert que l'ordre à longue portée est détruit par les fluctuations de la phase du paramètre d'ordre caractérisant la transition de phase. Ceci provient du fait que la dynamique effective de la phase suit l'équation de Kardar-Parisi-Zhang (KPZ) qui décrit la croissance stochastique d'une interface.

Dans ce type de problème est le champ de hauteur qui décrit le profil de l'interface. Dans la classe d'universalité définie par l'équation KPZ, on a découvert que la distribution de probabilité des fluctuations de hauteur, ainsi que leurs fonctions de corrélation, sont sensibles à la géométrie globale de la croissance, définissant ainsi des sous-classes d'universalité. Nous proposons un protocole simple qui modifie la géométrie de la phase des exciton polaritons, rendant ainsi les sous-classes associées à la géométrie plate et circulaire à $1d$, accessibles dans un système quantique complexe. Nous calculons les propriétés statistiques en un point, ainsi qu'en deux points de la phase du condensat, et nous observons un accord extrêmement satisfaisant avec les prédictions théoriques KPZ.

En $2d$, il a été avancé que la dynamique KPZ peut être entravée par la présence de tourbillons, et que Berezinskii-Kosterlitz-Thouless est le mécanisme responsable de la perte de cohérence. Beaucoup d'efforts ont été consacrés aux simulations numériques du système ces dernières années, mais son diagramme de phase est loin d'être complet, et tous les régimes possibles ne sont pas pris en compte. Nous montrons que pour une gamme de valeurs de pompe modérément élevées, les fonctions de corrélation de la fonction d'onde du condensat suivent les lois d'échelle universelles KPZ pour des paramètres pertinents sur le plan expérimental. Nous obtenons également la distribution des fluctuations de phase et montrons qu'elle est non gaussienne, comme prévu pour un processus aléatoire KPZ.

Mots-clés : universalité, physique statistique hors de l'équilibre, phénomènes critiques

Kardar-Parisi-Zhang universality in the phase of a condensate of exciton polaritons : from the scaling of correlation functions to advanced statistics of the phase in $1+1$ and $2+1$ dimensions

Abstract

An exciton polariton arises when a bound electron-hole pair in a semiconductor microcavity strongly interracts with cavity photons. Due to the unavoidable losses of photons, continuous injection is needed via an external source in order to maintain a steady state. It has been shown that this non-equilibrium exciton polariton gas displays similar characteristics to Bose-Einstein condensation in equilibrium, however, it was discovered that off-diagonal long-range order is destroyed by fluctuations of the phase of the order parameter characterizing the phase transition. This is due to the fact that the effective dynamics of the phase of the condensate follows the Kardar-Parisi-Zhang (KPZ) equation describing the stochastic growth of an interface.

A central quantity in this type of problem is the height field, which describes the shape of the interface. In the universality class defined by the KPZ equation, it was discovered that the probability distribution of height fluctuations, as well as their correlation functions, are sensitive to the global geometry of the growth, thus defining universality sub-classes. We propose a simple protocol which alters the geometry of the phase of exciton polaritons, thus making the sub-classes associated with the flat and circular geometry in $1d$ accessible in a complex quantum system. We compute one-point, as well as two-point statistical properties of the phase of the condensate, and we observe very good agreement with the KPZ theoretical predictions.

In $2d$, it was argued that the KPZ dynamics may be hindered by the presence of vortices, and that Berezinskii-Kosterlitz-Thouless is the mechanism responsible for the loss of coherence. A lot of effort has been devoted into numerical simulations of the system in recent years, but its phase diagram is all but complete, and not all possible regimes are accounted for. We report that for a range of moderately high pump values, precise KPZ scaling is found in the scaling of correlation functions of the condensate wavefunction for experimentally-relevant parameters. We also obtain the distribution of the phase fluctuations and find that it is non-Gaussian, as expected for a KPZ stochastic process.

Keywords : universality, out-of-equilibrium statistical physics, critical phenomena

Acknowledgements

Firstly, I would like to thank the members of the jury: Valerio Olevano, Alberto Bramati, Alberto Rosso, Benoît Vermersch, Iacopo Carusotto, and Nikolaos Proukakis, for accepting to review the following manuscript.

This thesis is the result of three years of work, following the transition from high-energy theoretical physics to statistical physics out-of-equilibrium. I would like to offer my sincere thanks to Léonie and Anna. Not only for the countless discussions related to our research, but also for their human side. I hope that I repaid the trust you have shown me. I would also like to thank all my colleagues at Laboratoire de Physique et Modélisation des Milieux Condensés, for all the moments in the workplace, and a special mention goes to Piero and Aniket for the fun we had during these years, both in-person and via social media. Furthermore, I thank the administrative assistants, Habiba and Camille, for being accessible, and Jean-Daniel for his help regarding informatics. A very special mention goes to my friend, Ioanna, without whom I would have lots of trouble navigating through the language barrier and the French bureaucracy. Also thanks for being a faithful comrade in the quest for searching for cold coffee in Grenoble. Furthermore, I want to deeply thank Greg, my dear friend and roommate, for lifting my spirits since November.

A special mention goes to my parents, Meni and Tasos. I'm sorry for being away from you during my studies abroad, and I hope to make up for it in the near future. I love you, and thank you for everything.

Contents

General introduction

Changes of basic states of matter occur in many types of systems, from the most simple and ever-present such as water, to exotic ones which are created in extreme conditions in laboratories across the world. Interestingly enough, these phenomena are also interdisciplinary, in the sense that they appear in diverse fields such as economics [1], sociology [2], and psychology [3].

Phase transitions

Understanding the rich mechanisms behind these phase transitions, has been one of the most challenging tasks in the heart of statistical physics for more than 100 years. Usually, the onset of these phenomena is related to the tuning of a control parameter until a transition point is reached, and the transition is classified by following the evolution of a suitable order parameter while the system changes its phase. Nowadays, this is achieved according to the following scheme: in a *first order* phase transition, the order parameter is discontinuous at the transition point, whereas it changes continuously in a *second order* phase transition. Both types can be realized in a discrete system of one-component spins in $2d$ or $3d$. Starting from a high-temperature disordered state, by reducing the temperature one observes a continuous build-up of magnetization starting at a temperature T_c in the absence of external magnetic field. It is useful to note that this onset of long-range order is usually associated with spontaneous symmetry breaking (SSB), which in this case is the discrete $\mathbb{Z}_2$. Alternatively, a first order phase transition is encountered by tuning the magnetic field at a fixed $T < T_c$ and the sign of the magnetization suddenly changes.

In order to understand how scale invariance emerges during a second order phase transition, it is instructive to define a "coarse-grained" magnetization $\tilde{m}(\vec{r})$ and look at how its fluctuations are correlated. We expect that, for a homogeneous system, its expectation value is equal to a constant, $\langle \tilde{m}(\vec{r}) \rangle \simeq \tilde{m}$, and we can define a connected correlation

function $C(\Delta r) = \langle \tilde{m}(\vec{r})\tilde{m}(\vec{r}+\Delta\vec{r})\rangle - \tilde{m}^2$. The correlation function is predicted to decay exponentially for a typical length scale ξ, which is called correlation length. When $T \gtrsim T_c$, ξ is finite but large, and magnetization fluctuations decay exponentially at large scales. As the temperature is increased, the correlation length decreases all the way until zero at $T \to \infty$. On the other hand, when $T \lesssim T_c$, long-range order starts to emerge, and clusters of the same spin start to appear. As temperature is decreased, the correlation length decreases and clusters become increasingly isolated. The point $T = T_c$ is actually a *critical point*, and the correlation length diverges, while the correlation function decays as a power-law. The system thus becomes scale invariant, and microscopic details of the system are unimportant, leading to the concept of *universality*. One can then study the system using an effective theory using collective fluctuations; the phenomenological Landau-Ginzburg theory [4], and the field-theoretical renormalization group (RG) (see the initial paper by Kadanoff [5] and a summary of the subsequent developments on this idea by Wilson [6]), which involves progressively integrating out degrees of freedom at small scales until the desired scale is reached. By doing this, one can study how the microscopic couplings "flow" as the scale is changed. Scale invariance corresponds to a fixed point where the flow stops, and one can then compute universal quantities by studying the behavior of the couplings near the fixed point. Lastly, it is useful to note that recently a new subject field arose, which has made remarkable progress in determining critical exponents with extreme precision, called conformal bootstrap, see [7] and references therein.

It is now known that the first and second order phase transitions mentioned above are not the whole story. In 1966, Stanley and Kaplan [8, 9] computed certain response functions in the high temperature limit for the XY model in $2d$, where the spins have two components. Power-law behavior of these quantities was found near a critical T_c, suggesting that a phase transition should take place, but it cannot be associated with the onset of true long-range order as in the low-temperature phase of the one-component case mentioned above, due to the Mermin-Wagner theorem [10]. This theorem states that the fluctuations of the order parameter will destroy order for dimensions $d \leq 2$ when there is SSB of a continuous symmetry such as $U(1)$. Instead, the system develops "quasi"-long-range order associated with bound pairs of vortices, and the correlation function decays with a power law. The exponent characterizing the decay is universal only on the transition point, while it depends on temperature as one pushes deep in the low-temperature phase. On the other hand, the high-temperature phase exhibits proliferation of free vortices which destroy order, and correlations decay exponentially. This *infinite order* phase transition is the well-known Berenzinskii-Kosterlitz-Thouless (BKT) phase transition [11].

Bose-Einstein condensation in equilibrium

Lots of interesting phenomena appear when "quantum" properties arise in classical systems. This can be understood in the context of a phase transition, which separates an ordinary phase in the high-temperature regime, from a more exotic one at low temperatures. Of particular interest to us is the Bose-Einstein condensation (BEC) (see [12] for the German version of Bose's article and [13] for an overview of the derivation by Einstein in 1924-1925, translated in English). According to the bosonic statistics, the mean occupation number of a quantum state with energy ϵ_i can be written as [14] $\langle n(\epsilon_i)\rangle = 1/\left(e^{\frac{\epsilon_i-\mu}{k_BT}}-1\right)$, where μ is the chemical potential, T is the temperature and k_B is the Boltzmann constant. In the limit of high temperature, we have $\mu \ll \epsilon_{\mathrm{g}}$, where ϵ_{g} is the energy of the ground state. However, as the temperature decreases, μ increases with an upper limit of ϵ_{g}, which implies macroscopic occupation of the ground state manifest in the formation of a condensate with finite density n_g. On the other hand, the excited states have low occupation. The critical temperature can be estimated by comparing the de Broglie wavelength λ_{dB} of the bosons with the inter-particle distance, which can be written as $l = \langle n\rangle^{1/d}$. For high temperatures, we have $l \gg \lambda_{dB}$, meaning that the "particle" dominates over the "wave" nature. In $3d$, at a critical temperature T_c, this is reversed and particles start behaving as waves, making the quantum nature apparent. In $2d$, it can be shown [15] that $T_c = 0$, meaning that condensation does not happen for any nonzero temperature.

The first papers that attempted to connect BEC to experimental results appeared in 1928-1932 [16–19]. In particular, at $T_c = 2.17K$ it was shown that ^{4}He exhibits a peak of the specific heat, while below T_c it displays frictionless flow, and it was called a "superfluid". These results imply that ^{4}He could undergo a phase transition at T_c, and an attempt to connect these results to BEC was made in 1938 [20]. However, it was met with skepticism, because ^{4}He is a strongly-interacting gas, thus the connection to the considerations by Bose and Einstein regarding non-interacting ideal gas could not be established. Many years later, several experimental works appeared concerning trapped weakly-interacting alkali gases, enabled by advanced techniques such as magnetic trapping and laser cooling: ^{87}Rb atoms [21], as well as ^{23}Na atoms [22] in a harmonic trap were demonstrated to exhibit true BEC. These amazing discoveries sparked a wide interest in ultra-cold atoms, and in the years that followed, a multitude of atomic species was shown to exhibit BEC. However, the critical temperature T_c was found to be extremely small in the nanoKelvin range, and in more recent years there has been a search of alternative systems displaying BEC.

Out-of-equilibrium phase transitions

While equilibrium phase transitions discussed above are very rich in terms of the underlying physics, one should note that thermal equilibrium is a rather elusive concept in the real physical world. In the case of non-equilibrium systems, it is usually impossible to track the precise microscopic dynamics of their constituents, and it has been found that an effective way to model these systems is by a Langevin equation, according to which the deterministic evolution is supplemented by a stochastic contribution. One then resorts to computing appropriate expectation values of stochastic fields over the noise distribution.

Features of scale invariance were observed in non-equilibrium systems, such as diverging correlation length, in analogous manner to second order phase transitions in equilibrium. Moreover, in some cases, it was observed that the dynamics drives the system to criticality without the need for an external parameter to be tuned, leading to novel non-equilibrium phase transitions. Theoretically, the concept of RG outlined above can be generalized in order to study these critical dynamics. A significant step in this direction was made when a path integral formulation for the Langevin equation governing the dynamics appeared by Martin-Siggia-Rose-Janssen-de Dominicis [23–25]. Here we make a crucial remark. In equilibrium, it is usually a valid strategy to study how the interactions modify the critical properties of the free theory by treating them in perturbation theory in the context of RG, but this is not always the case. Due to this, non-perturbative techniques were developed, namely an exact RG equation describing the flow of the effective average action [26]. The effective action encodes the properties of the theory after one integrates out all fluctuations, while an infrared cutoff k_{c} is introduced in the effective average action; only fluctuations with momenta $|q_{\mathfrak{fl}}| > k_{\mathrm{c}}$ are integrated out. Therefore, by reducing k_{c} one progressively integrates out fluctuations with smaller momenta (larger spatial scales), until reaching the full effective action at $k_{\mathrm{c}} = 0$. On the other hand, for $k_{\mathrm{c}} \to \infty$, no fluctuations are integrated out and the effective average action corresponds to the full action S of the theory. This procedure is the cornerstone of the modern approach to the non-perturbative, or functional RG (NPRG or FRG), which was more recently implemented in order to study non-equilibrium universal properties [27].

Drawing inspiration from the fascinating physics behind non-equilibrium phase transitions, in this thesis we focus on the celebrated Kardar-Parisi-Zhang (KPZ) equation and its associated universality class. This is associated with the "kinetic roughening" of an interface undergoing stochastic growth, namely the development of very large

fluctuations of its height as time increases. In particular, we study a system that has been shown to belong to this universality class, the Bose-Einstein condensate of exciton polaritons (EP). This system consists of bound electron-hole pairs in a semiconductor microcavity, which are called excitons, in the strong-coupling regime with cavity photons. Due to the continuous losses of photons from the microcavity, external pumping is necessary in order to maintain a steady state configuration, thus the system is intrinsically out-of-equilibrium. While many common characteristics with the Bose-Einstein condensate in equilibrium have been reported [28], the effective dynamics of the phase of the condensate follows the KPZ equation, thus KPZ fluctuations destroy the off-diagonal long-range order of the system.

It was shown in the late nineties, that one-point statistical properties (probability distribution), as well as two-point statistical properties (correlation function) of the KPZ height fluctuations, at the limit of large times, depend on the global geometry of the growth. Therefore, the universality class should be partitioned into distinct *geometry-dependent universality sub-classes*. This raises an interesting question: what does this imply for the exciton polariton system? Can these sub-classes be realized for the phase of the condensate? We will address these questions in $1d$, and in particular, we will study whether the sub-class associated with the curved ("droplet") geometry can be accessed in polariton condensates by engineering the geometry of the phase profile. We achieve this by introducing a confining potential, and we derive the KPZ equation for the phase of an inhomogeneous condensate. Indeed, we show that a precise agreement with the theoretical predictions is reached regarding the curved KPZ sub-class, both for the probability distrubutions of the phase fluctuations at one point in space, as well as for their spatial correlation function, albeit in a small region in which smooth curvature is achieved.

In $2d$, the situation is a bit more delicate. Whereas the mapping of the phase dynamics to the KPZ equation is still valid, it was suggested in the literature that the appearance of vortices will destroy the off-diagonal long-range order developed in polariton condensates. In particular, via arguments based on perturbative RG techniques, it was shown that the length scales needed for KPZ fluctuations to set in were orders of magnitude larger than the experimentally-attainable system sizes for polariton condensates. However, parts of the phase diagram are still unexplored, thanks to the extremely large dimensionality of the parameter space. Whether KPZ universality is indeed present in the exciton polariton condensate is the second question we will address in this thesis. To this end, we perform extensive numerical simulations of condensates with experimentally-relevant system sizes, exploring different parameter regimes. We

show that a vortex-free regime exists, in which conclusive KPZ scaling can be found by studying the first-order correlation function of the condensate wavefunction. Additionally, we study the phase fluctuations themselves, and we show qualitative agreement with large-scale numerical results pertaining to the $2d$ KPZ universality class in terms of one-point statistics.

This thesis manuscript is organized as follows. In chapter 1 we introduce the concept of kinetic roughening, the Edward-Wilkinson equation which is a simple model describing this process, and the need to generalize it. This leads to the KPZ equation and the universality class it defines, which is the centerpiece of our work. In particular, we will introduce exact results which have been found in one dimension, as well as the tools to probe them, and finally we will discuss about the difficulties that arise in two dimensions. In chapter 2 we review the precise mechanism under which exciton polaritons undergo Bose-Einstein condensation, the state-of-the-art, and the model we use to numerically simulate the system. Moreover, we present the mapping from this model to the KPZ equation. In chapters 3 and 4 we present our results, which concern the one-dimensional exciton polariton Bose-Einstein condensate under confinement, and the two-dimensional case, respectively. Our results are summarized in the following articles:

1. Konstantinos Deligiannis, Davide Squizzato, Anna Minguzzi and Léonie Canet "*Accessing geometry-dependent Kardar-Parisi-Zhang universality sub-classes with exciton polaritons*", Europhysics Letters (EPL) **132**, 67004 (2021),

2. Konstantinos Deligiannis, Quentin Fontaine, Davide Squizzato, Maxime Richard, Sylvain Ravets, Jacqueline Bloch, Anna Minguzzi and Léonie Canet "*Kardar-Parisi-Zhang universality in discrete two-dimensional driven-dissipative exciton polariton condensates*", arXiv:**2207.03886**, currently under peer-review.

Chapter 1

Non-equilibrium growth phenomena and the Kardar-Parisi-Zhang universality class

In this chapter, we will present the centerpiece of this thesis, the Kardar-Parisi-Zhang (KPZ) equation [29] and its universality class. We will begin by introducing the concept of self-organized criticality in order to motivate some phenomenological models which were proposed in order to model it, and we will quantify the statistics of interfaces growing under stochastic noise. In particular, we will introduce the Edwards-Wilkinson (EW) equation and the need to generalize it, leading to the KPZ equation. We will then describe universal properties of this model, and discuss their dependence on growth geometry. We note here that the KPZ equation was discovered in 1986 and has since then sparked a wide interest in both mathematics and physics communities. By now there are many comprehensive reviews covering the mathematical aspects, as well as modern developments, see for example [30–33].

1.1 Self-organized criticality

The concept of self-organized criticality was introduced in [34], and tried to shed some light on the onset of complexity in natural systems, meaning the emergence of collective phenomena that dominate over microscopic interactions between the constituents of a system. This work studied a cellular automaton, formulated in terms of a function

$f(x, y)$ defined on a $2d$ grid, with fixed boundary conditions such that $f(x, y) = 0$ on the edge of the grid. As long as $f > f_c$ at a point (x, y), where f_c is a critical value, f is constantly updated in each time step according to the following rule,

$$f(x, y) \to f(x, y) - 4, \quad f(x \pm 1, y) \to f(x \pm 1, y) + 1, \quad f(x, y \pm 1) \to f(x, y \pm 1) + 1 \tag{1.1}$$

such that nearest neighbour interactions are explicitly included, and the evolution is initialized such that $f \gg f_c$ at random points on the grid. Once $f < f_c \ \forall (x, y)$, the system stops evolving, and is in a "locally minimally stable" state. Local perturbations of such a state lead to the formation of clusters. Strikingly, power-law scaling arises in the distribution of the size of these clusters, as well as in the distribution of the lifetime of the perturbations that cause them, indicating scale invariance. This means that the macroscopic state of such a system is critical, but the crucial difference with equilibrium phenomena is that this happens without the need to tune an external control parameter, and a non-equilibrium system under non-linear interactions and noise can evolve towards criticality itself. We note here that a cellular automaton describing the time evolution of a variable via Eq. (1.1) is a sufficiently general model, therefore many systems can be identified as following similar dynamics, from the collapse of a pile of sand, to the formation of a mountain ridge.

To make these considerations apparent, we present an example in $1d$, which is illustrated in Fig. 1.1. A colony of pathogen in a petri dish, if limited by a smooth obstacle which is suddenly removed, will grow upwards. Regardless of the precise local interactions of the neighbouring molecules, which is stochastic and very complicated in nature, macroscopically a rough front emerges with fluctuations that grow over time. These are scale invariant and resemble fractals [35], and this type of phenomenon is called kinetic roughening.

In order to study the scale invariance and criticality in this type of growth, we define a stochastic function $h(t, \vec{x})$. This corresponds to the height of the growing interface at spatial position in d spatial dimensions, $\vec{x} \in \mathbb{R}^d$, and time t. We are interested in studying its statistical properties, fluctuations and correlations. Initially [30, 35–37], researchers computed the interface roughness $w^2(t, l)$, which is defined as the standard deviation of the height, averaged over many samples,

$$w(t, l) = \left\langle \sqrt{\left\langle [h(t, \vec{x}) - \langle h(t, \vec{x}) \rangle_l]^2 \right\rangle_l} \right\rangle, \tag{1.2}$$

where $\langle\cdot\rangle_l = 1/l^d \int d^d\vec{x}(\cdot)$ corresponds to a spatial average in d dimensions, carried over a volume l^d, and $\langle\cdot\rangle$ corresponds to average over different noise realisations. Strikingly, it was found by Family and Vicsek [38] that this quantity can be rewritten with the help of a scaling function g_w,

$$w(t,l) \sim t^\beta g_w\left(lt^{-1/z}\right) \sim \begin{cases} l^\alpha, & l \ll l_*(t), \\ t^\beta, & l \gg l_*(t), \end{cases} \tag{1.3}$$

for $\alpha, \beta, z \equiv a/\beta$ being the roughness, growth, and dynamical universal critical exponents, respectively. Moreover, the crossover length scale can be expressed as $l_*(t) = t^{1/z}$. We can see that once the length l surpasses this length scale, the interface width becomes independent of l itself, and rather behaves as t^β. While being historically important because it reveals scaling laws and is numerically tractable, Eq. (1.3) offers little more practically. This is because it involves spatial averages, and it is not a pure statistical quantity. We will motivate the need for defining appropriate observables in sections 1.3.2.1, 1.3.2.2 in order to unlock the full features of KPZ scaling.

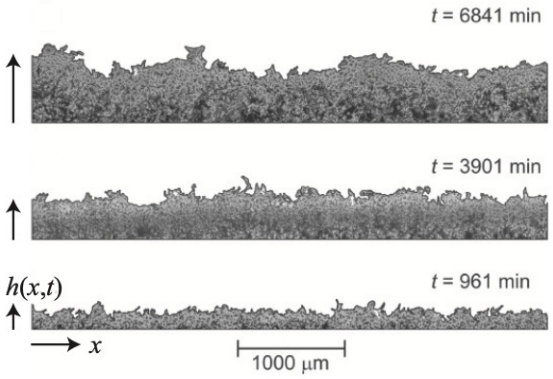

FIGURE 1.1: Experimental realisation of kinetic roughening in a complex system. Cancer cells undergo cell division and the colony grows perpendicularly to the petri dish. Snapshots of the time evolution are shown, where one can clearly identify the interface, which displays larger spatial fluctuations with increasing times. Figure taken from [32].

1.2 Phenomenological models

So far, we have established that the behavior of stochastic growth shares similar features with criticality in second order phase transitions, hence in an analogous manner the growth can be characterized in terms of universality classes. The next step is to understand the nature of the stochastic function $h(t,\vec{x})$ characterizing the growth, and then to determine the critical exponents α, β, z for the Edwards-Wilkinson (EW) and Kardar-Parisi-Zhang (KPZ) universality classes.

1.2.1 Edwards-Wilkinson equation

Historically, one of the first attempts at developing an equation which accounts for this type of growth was made in the context of cancerous cells [39], where a "seed" that is placed at a given point grows diffusively to its neighbours. The resulting model by Eden with the help of Parisi and Zhang [40–42] presents a unified approach to tackle this problem. However, due to issues mainly related with tractability of the equation and the fact that it appeared to provide redundant information for describing the universal behavior, more appropriate models have been constructed since. One important such model was proposed by Edwards and Wilkinson [43], who devised the following equation,

$$\frac{\partial h(t,\vec{x})}{\partial t} = \nu\nabla^2 h(t,\vec{x}) + \eta(t,\vec{x})\,, \tag{1.4}$$

where the noise $\eta(t,\vec{x})$ follows a Gaussian distribution with zero mean and a system-dependent variance D, namely

$$\langle\eta(t,\vec{x})\rangle = 0, \qquad \left\langle\eta(t,\vec{x})\eta\left(t',\vec{x}'\right)\right\rangle = D\delta^d\left(\vec{x}-\vec{x}'\right)\delta\left(t-t'\right) \tag{1.5}$$

and ν is also a system-dependent parameter. This equation possesses several symmetries, namely it is invariant under space and time translations, rotations and height translations, as expected for kinetic roughening. Insights on its solution can be obtained by the Fokker-Planck approach [30]. This relies on the fact that this is a Langevin equation governing the evolution of the continuous dynamic field $h(t,\vec{x})$ under the effect of noise, and this problem can be mapped to a Fokker-Planck equation for the time evolution of probability density functional for a height configuration $\{h(\vec{x})\}$ in the $d-$dimensional space, $P[\{h(\vec{x})\}]$,

$$\frac{\partial P[\{h(\vec{x})\}]}{\partial t} = -\int d^d\vec{x}\frac{\delta}{\delta h}\left\{\nu\nabla^2 h(t,\vec{x})P[\{h(\vec{x})\}]\right\} + \frac{D}{2}\int d^d\vec{x}\frac{\delta^2 P[\{h(\vec{x})\}]}{\delta h^2}. \tag{1.6}$$

A few remarks are now in order. Firstly, one can verify that this equation admits a Gaussian stationary solution,

$$P_{\text{stat}}[\{h(\vec{x})\}] = e^{-\frac{\nu}{D}\int d^d\vec{x}(\vec{\nabla}h_{\text{stat}}(\vec{x}))^2}. \tag{1.7}$$

Of course, a stationary solution and hence the notion of a "stationary state", can be applicable to a dynamical growth only in the limit where time is fixed but very large, $t_0 \to \infty$. This, combined with the fact that a diffusive process, such as the one modelled by Eq. (1.4), can be expressed as a Wiener process [44] in $1d$, tells us that there should be a limit, where one can map P_{stat} to the probability density of a Wiener process; indeed this is the case, if x is interpreted as t, one has $h_{\text{stat}} \to W$, where W is a Wiener

process. In other words, in the stationary state, for large t_0, the interface behaves like a Wiener process in the spatial domain. This allows us to readily deduce the roughness exponent α from the correlation function,

$$\left\langle (W(t) - W(0))^2 \right\rangle \simeq t\,, \tag{1.8}$$

and according to the aforementioned mapping, the same correlation function corresponds to the average squared displacement

$$\left\langle (h_{\text{stat}}(x) - h_{\text{stat}}(0))^2 \right\rangle \simeq x \tag{1.9}$$

in the appropriate long-time limit, and so $\alpha = 1/2$ from the scaling Eq. (1.3). Note that this quantity is predicted to have the same power-law behavior as the roughness of the interface $w^2(x, t_0)$ from Eq. (1.3), but with a different scaling function. In d dimensions, the roughness, growth and dynamical critical exponents α, β, z can be extracted from demanding Eq. (1.4) be invariant under a scale transformation that is defined as follows,

$$x \to bx \qquad\qquad t \to b^z t \qquad\qquad h \to b^\alpha h\,, \tag{1.10}$$

from which we find

$$\alpha = \frac{2-d}{2} \qquad\qquad \beta = \frac{2-d}{4} \qquad\qquad z = 2. \tag{1.11}$$

In $1d$, this is in agreement with the prediction for α from the Wiener process.

1.2.2 Kardar-Parisi-Zhang equation

Despite the EW equation being a first step towards theoretically understanding stochastic growth, experiments conducted for various systems did not show the predicted scaling laws of Eq. (1.3). The EW equation is linear, and hence can be solved exactly for the statistics of the height fluctuations, but a crucial ingredient is missing; it does not account for kinetic roughening, and the dynamics is only driven by smoothening caused by diffusion. In other words, Eq. (1.4) implies that the growth occurs always vertically at a given point, while it is more natural to assume that it occurs normally to this point. This is illustrated in Fig. 1.2.

It is straightforward to show via a geometric argument that this feature corresponds to including one more term to the EW equation, corresponding to the first relevant

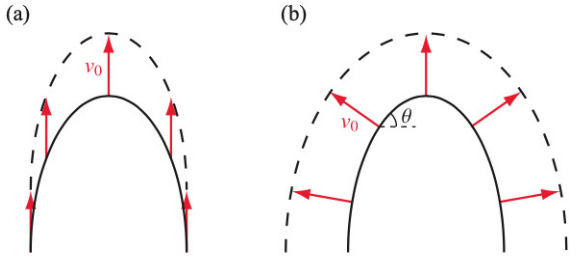

FIGURE 1.2: Growth corresponding to EW model (a), and in a more natural setting (b), where the growth occurs along the local normal to the surface (see text). Figure taken from [32].

non-linearity. By doing so, one obtains the Kardar-Parisi-Zhang (KPZ) [29] equation,

$$\frac{\partial h(t,\vec{x})}{\partial t} = \nu\nabla^2 h(t,\vec{x}) + \frac{\lambda}{2}(\vec{\nabla}h(t,\vec{x}))^2 + \eta(t,\vec{x})\,, \tag{1.12}$$

where $\eta(\vec{x},t)$ is still a Gaussian white noise, whose properties are the same as in Eq. (1.5). The KPZ equation crucially obeys one more symmetry which is not satisfied by the EW equation, and this is the statistical tilt symmetry. This can be proven via mapping to the stochastic Burger's (SB) equation [45] for the KPZ "velocity" $\vec{u}(t,\vec{x}) = -\lambda\vec{\nabla}h(t,\vec{x})$, which reads

$$\frac{\partial\vec{u}}{\partial t} + (\vec{u}\cdot\vec{\nabla})\vec{u} = \nu\nabla^2\vec{u} + \vec{\xi}\,,\ \text{for}\ \vec{\xi} = -\lambda\vec{\nabla}\eta. \tag{1.13}$$

This equation describes a randomly forced infinitely compressible fluid, and admits the well-known Galilean symmetry,

$$t \to t' = t\,, \tag{1.14a}$$

$$\vec{x} \to \vec{x}' = \vec{x} + \lambda\vec{u}_0 t\,, \tag{1.14b}$$

$$\vec{u}(t,\vec{x}) \to \vec{u}'(t',\vec{x}') = \vec{u}(t',\vec{x}') - \vec{u}_0\,, \tag{1.14c}$$

where $\vec{u}_0$ is a constant vector. Crucially, the coefficient of the non-linearity λ can be shown to not change with scale in the level of field theory. The importance of this symmetry, which corresponds to the statistical tilt symmetry of the KPZ equation, becomes apparent from the realisation that the covariant time derivative, from which the left-hand side of the SB equation originates,

$$\hat{D} = \frac{\partial}{\partial t} + \vec{u}\cdot\vec{\nabla} \tag{1.15}$$

should be scale-invariant. By using the scale transformation Eq. (1.10) in Eq. (1.15), we find

$$\hat{D} \to \hat{D}' = b^{-z}\left(\frac{\partial}{\partial t} + b^{\alpha+z-2}\vec{u}\cdot\vec{\nabla}\right). \tag{1.16}$$

The global prefactor b^{-z} can be absorbed by redefining the field, and the two components exactly match each other under change of scale if the following exponent identity is true,

$$\alpha + z = 2\,,\ \forall d \tag{1.17}$$

This allows us to extract all three scaling exponents in $1d$, since only then Eq. (1.7) is also a solution to the Fokker-Planck equation corresponding to the KPZ equation. This can be shown formally in the discrete limit, but after using an appropriate spatial discretization prescription for the nonlinearity [46], the continuum limit can be safely taken. We have

$$\begin{aligned}\frac{\partial P[\{h(\vec{x})\}]}{\partial t} = &-\int d^d\vec{x}\frac{\delta}{\delta h}\left\{\left[\nu\nabla^2 h(t,\vec{x}) + \frac{\lambda}{2}(\vec{\nabla}h(t,\vec{x}))^2\right]P[\{h(\vec{x})\}]\right\} \\ &+\frac{D}{2}\int d^d\vec{x}\frac{\delta^2 P[\{h(\vec{x})\}]}{\delta h^2},\end{aligned} \tag{1.18}$$

By inserting the stationary distribution Eq. (1.7) in Eq. (1.18), one finds that the $\lambda-$ dependent contributions are

$$-\lambda\int d^d\vec{x}\{\nabla^2 h(t,\vec{x})P_{\rm stat}[h(t,\vec{x})] - \frac{\nu}{D}(\vec{\nabla}h(t,\vec{x}))^2\nabla^2 h(t,\vec{x})P_{\rm stat}[h(t,\vec{x})]\}.$$

The two terms can be treated separately. The first integral can be brought to a form of total derivative which vanishes on the boundaries, under the assumption that the field vanishes at infinity. The second integral is zero only in $1d$ because it can also be brought to a total derivative in this case,

$$\int dx\left(\frac{\partial h(t,x)}{\partial x}\right)^2\frac{\partial^2 h(t,x)}{\partial x^2} = \frac{1}{3}\int dx\frac{\partial}{\partial x}\left(\left(\frac{\partial h(t,x)}{\partial x}\right)^3\right).$$

This is not the case in dimensions $d \neq 1$, due to the more complicated contraction structure in terms of spatial indices.

By comparing with the Wiener process as was done in the previous section, one concludes that $\alpha = 1/2$, and by using Eq. (1.17) one finds

$$\alpha = \frac{1}{2} \qquad \beta = \frac{1}{3} \qquad z = \frac{3}{2}. \tag{1.19}$$

Let us emphasize that determining the scaling exponents is only a part of the story, and the stationary probability density at $t \to \infty$ does not at all correspond to completely solving the theory, even in $1d$. This is because, besides knowledge of the universal spatial fluctuations at the stationary state attained by systems that belong to the KPZ

universality class, one must also look at temporal fluctuations at fixed spatial point x_0 and classify their statistics.

1.3 Exact results in $1d$

1.3.1 Long-time limit of the interface height

The following behavior, which was derived in order to generalize certain exact results of integrable systems belonging to the KPZ universality class, is widely used and describes the time evolution of the height profile at a fixed spatial point,

$$h(t) \to u_\infty t + (\Gamma t)^\beta \chi, \tag{1.20}$$

where we can see that in the long time limit, the evolution consists of two terms. The first corresponds to growth of the mean profile, which is deterministic and linear in time. By computing the mean derivative,

$$\left\langle \frac{\partial h(t)}{\partial t} \right\rangle = u_\infty + \beta \Gamma^\beta t^{\beta-1} \left\langle \frac{\partial \chi}{\partial t} \right\rangle, \tag{1.21}$$

where $\beta < 1$ for the KPZ universality class in any dimension, it is clear that u_∞ is the asymptotic velocity in the limit $t \to \infty$. The second term grows in time with the KPZ exponent β and contains the random variable χ which captures the rescaled height fluctuations. The goal of this section is to link the statistics of this stochastic variable with KPZ universality. We note here that both u_∞, Γ are found to have a non-trivial dependency on the KPZ parameters ν, λ, D [47], and are hence system-dependent constants. Therefore, we expect that the only role they can play in determining universal statistics are in terms of appropriate normalizations.

1.3.2 Geometry dependence

1.3.2.1 One-point statistics

An important first step was made in this direction when the probability density function in the long-time limit at a fixed spatial point x_0 was computed [48, 49] for the totally asymmetric simple exclusion process (TASEP), a discrete model which was known to exhibit the KPZ scaling in $1d$, and more details about which will be given soon. The resulting distribution of the temporal fluctuations, under suitable rescaling, is distinctly non-Gaussian, and its mathematical expression, as well as its higher-order moments,

were computed exactly. These works ultimately inspired several studies by mathematicians [50], as well as physicists [51–56], to tackle the more general question; can an analytic solution for the universal one-point statistics of the solution of the KPZ equation be found in all times, provided that it is an equation for a continuous field? In order to answer this question, one has to formally define what it means to solve the KPZ equation. In order to do so, it is instructive to use the Cole-Hopf transformation [32],

$$h = \frac{2\nu}{\lambda} \ln Z \,, \tag{1.22}$$

and by substituting to Eq. (1.12) we arrive at the stochastic heat equation (SHE),

$$\frac{\partial Z}{\partial t} = \nu \nabla^2 Z - \frac{\lambda}{2\nu} Z \text{“} \times \text{”} \eta. \tag{1.23}$$

The symbol “ $\times$ ” means that we must adopt either the Itô or Stratonovich convention in order to make sense of the multiplicative noise [44], but the equation is now free of the non-linearity. This is particularly important, because this term is actually malignant in the KPZ equation; we have showed that at least in $1d$, the interface in the stationary state is a Brownian motion (Wiener process) in space, therefore it does not make sense to take the square of its derivative, as the height field roughens its spatial derivative will diverge. However, on one hand, according to Bertini and Giacomin [57], the solution of the KPZ equation can be defined via the solution of the SHE, and it was further shown that this procedure can be circumvented, as proven by Hairer [58], who eventually provided a rigorous mathematical foundation to the KPZ equation itself.

Provided that a solution of the KPZ equation can formally be written, one can now prove that the probability density function actually interpolates between a Gaussian in the short-time limit, and the non-trivial distribution found by the authors of [48, 49] in the long-time limit. However, it is important to note that these works dealt with a discrete model describing a growth in which a curved interface in the shape of a parabola is developed, and the latter works [50–54] assumed an initial condition for the KPZ equation which is appropriate for this particular growth. Therefore, the natural question to be asked is whether different initial conditions, which determine the asymptotic shape the interface takes while undergoing growth, plays a role in the asymptotic probability density function. Intuitively, the answer to this question is negative. The linear term in Eq. (1.20) simply tells us that the mean profile grows linearly with time, but crucially, this term is independent of the geometry and of the spatial position. Therefore, by subtracting it from the height at any space point, we can access the growing fluctuations $\delta h = h(t) - u_\infty t$. Then, the probability density once the power-law is removed, $P[\delta h/t^\beta] = P[\chi]$ has no reason to depend on the growth geometry. As we will see,

however, this is not the case.

We will now briefly consider the asymmetric simple exclusion process (ASEP) [59, 60], in order to illustrate whether the geometry dependence we mentioned indeed exists. Additional details related to the calculations and the actual mathematical theorems can be found in the excellent reviews [32, 33].

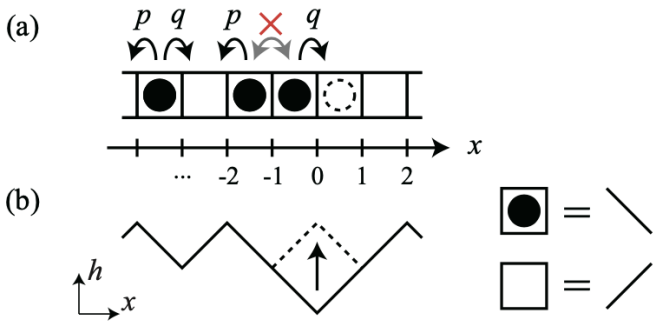

FIGURE 1.3: (a) Schematic representation of the ASEP, (b) mapping to an interface growth problem by introducing valleys and mountains depending on the hopping. The black dot corresponds to an occupied site. Figure taken from [32].

ASEP is defined on a lattice with $x_i \in \mathcal{Z}$ as shown in Fig. 1.3. Inbetween spatial coordinates x_i, x_{i+1} there are sites which are either occupied or empty. Empty sites can only be filled by hopping from neighbouring occupied sites, which happen independently, and a hopping rate q is assigned to the right and $p = 1 - q$ to the left. This system can be mapped to an interface growth of a height function $h(t, x)$ as shown in the same figure, by introducing a descending slope from x_i to x_{i+1} if the site is occupied, and an ascending slope if the site is empty. Once it gets filled, the height at some x_0 increases by $\Delta h(t, x_0) = h(x_0, t) - h(x_0, 0)$, and in time this is equal to the net number of hops passing through x_0, which is $\Delta N = N_{\rightarrow}(x_0) - N_{\leftarrow}(x_0)$. This type of stochastic growth was known to belong to the KPZ universality class, and interesting physics can be extracted by looking at the temporal fluctuations of the quantity $h(t, x_0)$ at a given point x_0, which is taken to be $x_0 = 0$ due to translational invariance.

The results mentioned so far were derived for $p = 0$, which defines the TASEP. The initial condition for this growth is a step function, such that the sites for $x < 0$ are occupied and for $x > 0$ are empty. According to the mapping illustrated in Fig. 1.3 and described above, the corresponding height profile $h(t = 0, x)$ would then be a wedge. Alternatively, if one uses an initial condition where alternating sites are occupied from $-\infty$ to ∞, the height profile $h(t = 0, x)$ would be a jagged, but globally flat interface. Lastly, one can envisage an initial condition where the occupation of each site is initially selected

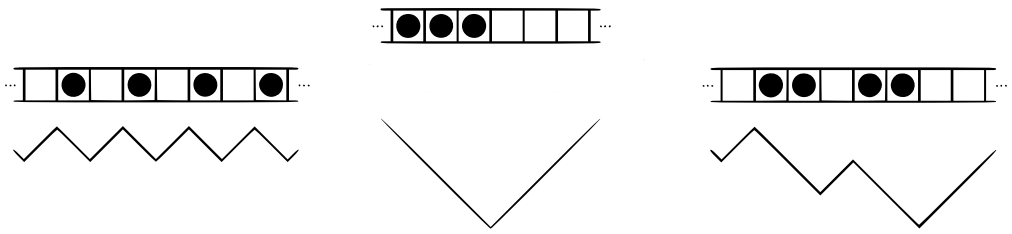

FIGURE 1.4: Schematic representation of three important initial conditions of the TASEP and the corresponding initial height profiles $h(t = 0, x)$ by mapping to an interface growth problem, in a similar manner to Fig. 1.3. Figure taken from [32].

randomly, but with a fixed probability of $1/2$, in order to ensure the globally flat shape. Due to this randomness, $h(t = 0, x)$ would display significantly larger fluctuations. These three cases are shown in Fig. 1.4. We note that these are simply the main ones, and historically combinations of them have also been investigated [33], leading to interesting results.

Here we make a crucial remark. The scaling exponents are the same despite the different initial condition for the TASEP, after all it is in the KPZ universality class. However, it turns out that in terms of the one-point statistics as defined in the beginning of this section, the probability density functions for the reduced fluctuations χ in Eq. (1.20) have markedly different forms. At the level of the discrete models, this is traced back to the different symmetries that arise in the combinatorics involved in their study, and which crucially depend on the initial condition. This leads to partitioning the universality class to geometry-dependent universality sub-classes, according to the initial condition of the growth. The same results were obtained in the continuum, and have more recently been observed in a series of beautiful experiments [61–63], thus conclusively proving that such a partitioning is not merely an artifact of the discrete models.

The wedge initial condition is associated with the circular KPZ sub-class, the characteristic trait of which being the propagation of the interface fluctuations in the radial direction due to the inherent curvature. Its one-point statistics in the long-time limit follow the one of the Tracy-Widom Gaussian Unitary Ensemble (TW-GUE), which corresponds to the probability density function of the largest eigenvalues of random $N \times N$ matrices belonging to this ensemble, in the limit $N \to \infty$ and after appropriate rescaling. The celebrated early works on TASEP by Baik, Deft and Johansson in 1999 and 2000 sparked a wide interest in the field, and during the next decade, in parallel with research on the statistics of the exact solution of the KPZ equation with this initial condition, the flat one was also extensively studied [64–69]. It was proven that the distribution in this case corresponds to the one of the Tracy-Widom Gaussian Orthogonal Ensemble

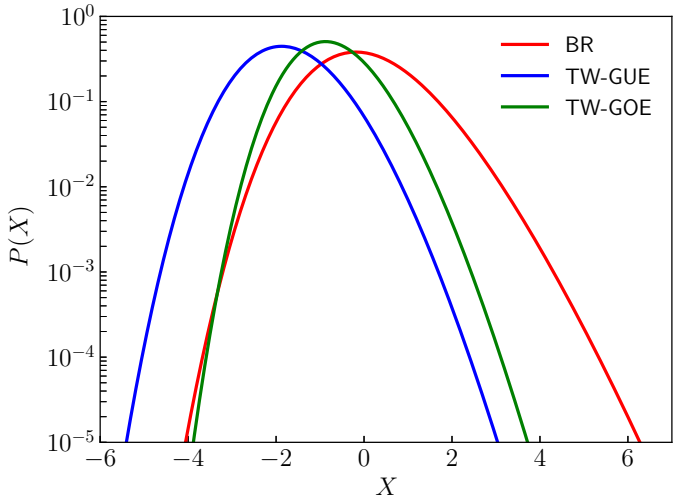

FIGURE 1.5: The three distributions of relevance in the $1d$ KPZ universality class. The numerical data is available online, courtesy of M. Prähofer and H. Spohn, at [75]. One can see that the distributions are clearly non-Gaussian and are distinct among themselves. Exact values of their skewness and excess kurtosis, which quantify the asymmetry and the length of the tails, respectively, can be found in [76].

(TW-GOE). Regarding the initial condition which corresponds to the random occupation of sites, taken to be a Brownian motion in space for the interface height, the result corresponds to the Baik-Rains (BR) distribution [70–73]. In this case, the sub-class is referred to as stationary, because the distribution of $h(x,0)$ is the Gaussian stationary solution of the Fokker-Planck equation related to the KPZ equation in $1d$, Eq. (1.7). By using Eq. (1.20), we have

$$\chi \xrightarrow{\text{1-pt dist.}} \begin{cases} \chi_{\text{TW-GOE}}, \text{ flat sub-class}, \\ \chi_{\text{TW-GUE}}, \text{ circular sub-class}, \\ \chi_{\text{BR}}, \text{ stationary sub-class} \end{cases} \quad \text{for } t \to \infty. \tag{1.24}$$

Here $\chi_{\text{BR}}, \chi_{\text{TW-GUE}}, \chi_{\text{TW-GOE}}$ follow the Baik-Rains, TW-GUE and TW-GOE probability distributions, respectively. The three distributions are shown in Fig. 1.5. We note here that the same results were found in parallel for another important discrete model in the KPZ universality class, the polynuclear growth (PNG). In particular, using appropriate initial conditions corresponding to growth under the aforementioned geometries [74] confirmed the results for the wedge and flat initial conditions of the TASEP.

We therefore conclude that there is a deep connection between the KPZ universality class in $1d$ and random matrix theory, the realm where Tracy-Widom [77] statistics lie, which is robust at least at the level of one-point statistics for the flat and circular sub-classes. As we will see in the next section, this correspondence does not hold for multi-point

statistics. The BR distribution, and thus the one-point statistics for the stationary subclass, has no connection to random matrix theory, and was rather discovered when a need for another distribution with zero mean arose during the investigation of a particular extension of the circular PNG problem, which was used to model the stationary PNG interface.

1.3.2.2 Two-point statistics

After discussing the probability density functions which constitute statistics of fluctuations at a single space point, it is instructive to proceed with correlation functions, namely the joint probability at different space/time points in $1d$, $\{h(t_1,x_1)h(t_2,x_2)\}$. The first quantity that was studied [78] in the context of the $1d$ PNG problem is the spatial correlation function,

$$C_{t_0}(\Delta x) = \langle h(t_0,x+\Delta x)h(t_0,x)\rangle - \langle h(t_0,x+\Delta x)\rangle \langle h(t_0,x)\rangle \equiv \langle h(t_0,x+\Delta x)h(t_0,x)\rangle_c \,. \tag{1.25}$$

By using Eq. (1.20), one is then interested to find the long-time limit of this expression. One finds

$$C_{t_0}(\Delta x) \to (\Gamma t_0)^{2\beta} \langle \chi_1 \chi_2 \rangle_c \,, \tag{1.26}$$

where χ_1, χ_2 correspond to random numbers representing the fluctuations at the two space points. If the KPZ dynamical scaling is present, then the only relevant variable in the long-time limit is $\zeta \sim x/t^{2\beta}$ [79], and not space or time separately, Therefore the local evolution of the height can be written as

$$h(t,x) \to u_\infty t + (\Gamma t)^\beta \chi(t,\zeta),$$

which, in turn, means that $\langle \chi_1\chi_2\rangle_c \equiv \langle \chi(t_0,\zeta)\chi(t_0,\zeta+\Delta\zeta)\rangle_c$. Crucially, in the long-time limit, this quantity should not depend on time anymore; the only such dependence should be encoded in the spatial correlation of the field itself, Eq. (1.25). In a similar manner as for the mapping of the stationary solution probability density function to a Brownian motion at the end of section 1.2.1, the scale-invariant fluctuations can be mapped to a stochastic process in this limit, and ζ is interpreted as the time τ of this process. Therefore, the (originally spatial) correlation function should be mapped to a time correlation function of this process. Indeed, for the circular sub-class, this limit process is called Airy_2 [78, 80], while for the flat one it is called Airy_1 [67, 81]. In a similar manner to Eq. (1.24) for convergence in terms of 1-point statistics, we can now

write

$$\chi(t_0,\zeta) \xrightarrow{\text{2-pt dist.}} \begin{cases} \mathcal{A}_1(\zeta), & \text{flat sub-class,} \\ \mathcal{A}_2(\zeta) - \zeta^2, & \text{circular sub-class,} \end{cases} \tag{1.27}$$

where $\mathcal{A}_i$ corresponds to the Airy$_i$ process. We note here that the $-\zeta^2$ contribution naturaly arises in the context of the circular sub-class, and corresponds to the deterministic parabolic shape of the droplet in the PNG model [78]. For the stationary case, it was found that the fluctuations field $\chi(\zeta,t)$ is correctly accessed if one further subtracts the $h(x=0,t=0)$ term as well, namely

$$h_{\text{stat}}(t,x) - h(t=0,x=0) \to u_\infty t + (\Gamma t)^{2\beta}\chi_{\text{stat}}(\zeta,t), \tag{1.28}$$

otherwise one ends up with the trivial Brownian motion in space. The novel limit process in this case is the Airy$_{\text{stat}}$ in terms of 2-point statistics [82]. The connection with the results of section 1.3.2.1 is of course established for fixed ζ for all three sub-classes. We note here that one can associate certain dynamics of the appropriately rescaled largest eigenvalue of TW-GUE matrices, called Dyson's Brownian motion [83], to the Airy$_2$ process [84], but this is not the case for the TW-GOE matrices [85]. Therefore, the apparent correspondence between the mathematics of KPZ and random matrix theory in terms of 1-point statistics, indeed ceases to exist for 2-point statistics.

1.4 Results in $2d$

While statistics of $1d$ interfaces belonging to the KPZ universality class are well studied and many exact results are available, mainly because of a multitude of integrable systems that belong to this class, this is not the case in $2d$. We stress that this section is not intended to serve as a complete overview of the developments on this subject, and we rather present certain historically important developments.

1.4.1 Numerical simulations

Historically, numerical simulations were used extensively in order to tackle the determination of the scaling exponents in the $2d$ KPZ universality class. As was the case in $1d$, significant attempts were made to simulate discrete models belonging to the KPZ universality class, see for example Refs. [86–97], or the KPZ equation itself [98–101]. We note that, in Refs. [88, 90], a $d-$dependent closed form for the exponents was proposed, according to which $\alpha = 2/5, \beta = 1/4, z = 8/5$ in $2d$, however, it was suggested that strong crossover effects might limit the accuracy of this type of ansätze. Furthermore, a

particularly important result appeared in Ref. [102], according to which, the spatial discretization used in the prior attempts to numerically simulate the continuum model was unstable, due to divergences appearing for large value of the non-linearity parameter. Nowadays, the most reliable predictions have come from efficient numerical simulations of very large systems [103]. In Ref. [104] it was shown that Eq. (1.20) holds for $\beta \simeq 0.24$ in $2d$, and the concensus among the literature is now that $\alpha \simeq 0.39$ is a valid approximation for sufficiently large systems in $2d$.

Regarding the partitioning to geometry-dependent sub-classes, numerics have also turned out to be very useful. For the analog of the $1d$ stationary sub-class, universal ratios of cumulants of the reduced height fluctuations were computed [92, 105, 106], as well as for the analogs of the flat and curved $1d$ sub-classes [104, 107–109]. It was quantitatively shown that the skewness and excess kurtosis do not match if the geometry is different. However, qualitatively, the corresponding one-point statistics cannot be matched to the BR or TW distributions, and exact results are still missing. Therefore, phenomenological fitting distributions were proposed for the reduced height fluctuations, namely the generalized Gumbel distribution and the Pearson distribution. Regarding 2-point statistics, the connected spatial correlation function was computed for the flat sub-class [110], and the difference from its $1d$ analog, the Airy_1 covariance, was highlighted.

1.4.2 Analytical results

Analytical attempts on extracting universal results for the $2d$ KPZ universality class are notoriously difficult to come by. Regarding the critical exponents, the Galilean transformation leaves the KPZ equation invariant in $2d$, and this results to the exponent identity Eq. (1.17), but one cannot infer what is the exact value for χ because there is no closed form of a stationary solution and hence no mapping to the Wiener process. One can show that this originates from the absence of the time-reversal symmetry in $2d$. However, using perturbative field-theoretical techniques, the first predictions of an analytical expression of the critical exponents appeared in 1998 [111], which were in agreement with the earlier numerical simulations by Kim and Kosterlitz in 1989, and a few years later a more refined prediction appeared [112], according to which $z \simeq 1.62$. A particularly important result appeared in 1999 [113], where it was shown that the perturbative RG flow of the effective KPZ coupling $g_{\text{KPZ}} = \frac{\lambda^2 D}{\nu^3}$ can be computed exactly to all orders, but this yields a run-away flow to infinity, instead of a fixed-point solution, which would be associated with roughening and KPZ dynamics. This means that non-perturbative RG should be used in order to capture the relevant fixed point, raising doubts about the validity of the previous results. Using this framework, some

results have appeared more recently [114, 115]. Indeed, it was shown that the strong-coupling fixed point is not at all connected with the Gaussian fixed point associated with EW dynamics, which explains the failure of perturbation theory. A prediction for the growth exponent $\alpha = 0.33$ was given in [114], while a more refined calculation [116] predicts $\alpha = 0.373$. In the latter work, the dimensionless variance of the distribution of the rescaled fluctuations in the analog of the stationary sub-class, as well as the full scaling function, were also found.

Chapter 2

Quantum fluids of light

As explained in chapter 1, experimentalists began searching for alternative systems with more favorable properties, as part of the quest to increase the critical temperature at which Bose-Einstein condensation takes place. In particular, it was suggested that hybrid light-matter systems such as exciton polaritons (EP), which exhibit a lighter mass, could be excellent candidates for BEC, and thus make quantum physics observable in an unprecedented manner. However, it was later realized that the nature of the BEC transition undergone in these systems is of non-equilibrium nature, in stark contrast to the BEC at equilibrium, where the control parameter is either the temperature, or the particle number. In this chapter, we will present the exciton polaritons mentioned above, which are formed by the strong coupling of excitons and cavity photons. In particular, we will describe the mechanism of their creation, and discuss the possibility of formation of a BEC in such systems. We will also describe in detail the mapping of the dynamics of the phase of the EP to the KPZ equation, and highlight the consequences of the mapping to the development of coherence in polariton condensates.

2.1 Physical system

2.1.1 Excitons

One of the two ingredients of the system, excitons, are formed in semiconductors. The process is conceptually simple, as an electron can be excited from the valence band to the conduction band, leaving behind a lack of negative charge. This is interpreted as a quasi-particle of positive charge, which is called a hole, as shown in Fig. 2.1. Due to the opposite charges, the Coulomb interaction favors the formation of an excited electron-hole bound state called exciton. Excitons are formed both in bulk materials, and also

in bidimensional structures obtained in quantum wells (QW), in which a material with small bandgap (*e.g.* GaAs) is sandwitched between two layers of material with wider bandgap (*e.g.* AlAs). In the latter case, confinement along the direction of change of material (usually taken to be the z direction) is achieved, while the electrons are free to roam in the xy plane on the material with the smaller bandgap. Excitons are characterized by their mass m_{x}, which is usually taken to be the sum of the effective masses of the electron and the hole, $m_{\mathrm{x}} = m_e + m_h$. Moreover, excitons are approximated by the hydrogen atom, and their binding energy and radius can be characterized by the effective Rydberg and the Bohr radius, which read [117]

$$R_y^* = \frac{\tilde{\mu} e^4}{2\epsilon_d^2 \hbar^2} \quad , \quad \alpha_B^* = \frac{\hbar^2 \epsilon_d}{\tilde{\mu} e^2} \, , \tag{2.1}$$

where $\tilde{\mu}$ is the reduced mass of the electron-hole system, which is given by $\tilde{\mu}^{-1} = m_e^{-1} + m_h^{-1}$, e is the electron charge, and ϵ_d the static dielectric constant of the material. For a more comprehensive review on the subject of excitons, we refer the reader to [118].

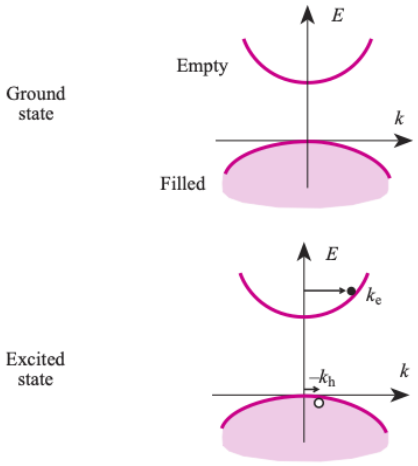

FIGURE 2.1: Ground and excited state energy of a semiconductor as a function of the wavevector. In the ground state, the valence band is filled, whereas the conduction band is empty. An electron can be excited via external stimulation, leaving behind a lack of negative charge (hole). The electron and the hole bind together to form an exciton, due to the Coulomb interaction. Figure taken from [119].

2.1.2 Cavity photons

The other basic ingredient of the system is cavity photons. A major feature is that they must be confined in the same semiconductor material, such that they overlap with the QW hosting the excitons. For this purpose, two Bragg mirrors are widely used, which can be engineered to offer very high reflectivity, in order to create a "microcavity" [120]. More specifically, by placing them at relative distance L along the z axis, one can show that an incident photon is effectively confined on the direction z perpendicular to the

mirror planes, for specific wavelengths which depend on L and certain characteristics of the mirrors. This implies that the momentum along this direction is quantized,

$$k_z = N\frac{2\pi}{L}, \text{ with } N \in \mathbb{Z}. \tag{2.2}$$

A crucial point is that confinement gives rise to an effective mass for the photon, since the dispersion relation in the microcavity [28],

$$\omega_c(k_\parallel) = \frac{c}{n_0}\sqrt{k_z^2 + k_\parallel^2} \simeq \frac{ck_z}{n_0}\left(1 + \frac{k_\parallel^2}{2k_z^2}\right), k_z \gg k_\parallel\,,$$

can be written as

$$\omega_c(k_\parallel) = \omega_c(k_\parallel = 0) + \frac{\hbar}{2m_{\text{cav}}}k_\parallel^2\,, \tag{2.3}$$

where $\omega_c(k_\parallel = 0) = ck_z/n_0$ and $m_{\text{cav}} = \hbar\omega_c(k_\parallel = 0)/(c^2/n_0^2)$ for dielectric medium of refractive index n_0. Here, one should notice that, due to the c^{-2} dependence, the effective mass m_{cav} is typically very small, of the order of $m_{\text{cav}} \simeq 10^{-5}m_{\text{e}}$. Furthermore, we stress that despite the enormous reflectivity of the mirrors, an incident photon will not stay in the cavity forever, bur rather will escape from the cavity due to the non-ideal mirrors. In typical EP experiments, the timescale is of a few picoseconds, see *e.g.* [121–123].

2.1.3 Exciton polaritons

The strong coupling between the confined photonic degrees of freedom with the excitons in a semiconductor microcavity was first discussed in [124]. This originates from a minimal light-matter coupling in the microscopic Hamiltonian [117], of the form

$$\mathcal{H} = \frac{1}{2m_e}\left(\vec{p} - \frac{e}{m_e}\vec{A}\right)^2\,, \tag{2.4}$$

where $\vec{p}$ corresponds to momentum of the exciton, $\vec{A}$ to the vector potential of the electromagnetic field and the coupling constant is $\vec{p}\cdot\vec{A} \propto \Omega_R$. We describe photons and excitons by annihilation and creation operators $\hat{a}, \hat{a}^\dagger$, denoted with a subscript "x" or "c" for excitons and photons, respectively. In particular, in second quantization, the

Hamiltonian of the system in Eq. (2.4), can be written as $\mathcal{H} = \mathcal{H}_\mathrm{c} + \mathcal{H}_\mathrm{x} + \mathcal{H}_\mathrm{xc}$, where

$$\mathcal{H}_\mathrm{c} = \int_k \hbar\omega_\mathrm{c}(k)\hat{a}_\mathrm{c}^\dagger(k)\hat{a}_\mathrm{c}(k)\,, \tag{2.5a}$$

$$\mathcal{H}_\mathrm{x} = \int_k \hbar\omega_\mathrm{x}(k)\hat{a}_\mathrm{x}^\dagger(k)\hat{a}_\mathrm{x}(k)\,, \tag{2.5b}$$

$$\mathcal{H}_\mathrm{xc} = \int_k \hbar\Omega_R\left[\hat{a}_\mathrm{c}^\dagger(k)\hat{a}_\mathrm{x}(k) + \hat{a}_\mathrm{x}^\dagger(k)\hat{a}_\mathrm{c}(k)\right]. \tag{2.5c}$$

Here $\mathcal{H}_\mathrm{xc}$ corresponds to the light-matter interaction and the interaction constant Ω_R is called the Rabi frequency. The requirement of strong coupling is satisfied if Ω_R is the dominant energy scale in the system, in particular $\Omega_R > \gamma$, where γ represents the loss rate from the cavity. In order to diagonalize the total Hamiltonian of the system $H_\mathrm{tot} = H_\mathrm{c} + H_\mathrm{x} + H_\mathrm{xc}$, we introduce new operators,

$$\hat{\psi}_\mathrm{LP}(k) = X(k)\hat{a}_\mathrm{x}(k) + C(k)\hat{a}_\mathrm{c}(k)\,, \tag{2.6}$$

$$\hat{\psi}_\mathrm{UP}(k) = -C(k)\hat{a}_\mathrm{c}(k) + X(k)\hat{a}_\mathrm{x}(k)\,, \tag{2.7}$$

where $X(k), C(k)$ are called Hopfield coefficients. We note here that the very large mass of the excitons m_x compared to the effective mass of the photons m_cav leads to approximating the exciton dispersion with a constant, $\omega_\mathrm{x}(k) \simeq \omega_{\mathrm{x},0}$. On the other hand, the dispersion relation of the photon is well approximated by a parabola, as can be seen from Eq. (2.3). The eigenenergies of the system are found to be

$$E_\mathrm{LP}(k) = \frac{\hbar}{2}\left(\omega_\mathrm{c}(k) + \omega_\mathrm{x}(k)\right) - \hbar\sqrt{\frac{\left(\omega_\mathrm{c}(k) - \omega_\mathrm{x}(k)\right)^2}{4} + \Omega_R^2}\,, \tag{2.8a}$$

$$E_\mathrm{UP}(k) = \frac{\hbar}{2}\left(\omega_\mathrm{c}(k) + \omega_\mathrm{x}(k)\right) + \hbar\sqrt{\frac{\left(\omega_\mathrm{c}(k) - \omega_\mathrm{x}(k)\right)^2}{4} + \Omega_R^2}. \tag{2.8b}$$

We therefore find that, in the case of strong light-matter coupling, two new hybrid eigenstates with different energies arise, as linear superpositions of the excitonic and photonic modes due to Rabi splitting [125]. The new eigenstates are called Lower Polariton (LP) and Upper Polariton (UP), see Fig. 2.2 for a pictorial representation of some possible pumping schemes, and Fig. 2.3 for the full dispersion relation. Particles in these new eigenstates are created (destroyed) by $\hat{\psi}_\mathrm{LP}^\dagger, \hat{\psi}_\mathrm{UP}^\dagger$ ($\hat{\psi}_\mathrm{LP}, \hat{\psi}_\mathrm{UP}$) respectively. As we will describe below, the population of the UP branch is usually negligible when compared to the LP where condensation takes place, hence the order parameter is usually associated with ψ_LP.

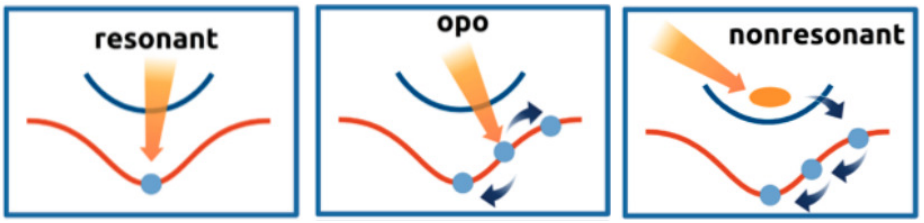

FIGURE 2.2: Three different pumping schemes for creation of EPs. A first method consists of shining a laser where the photons carry momentum $k = k_{\mathrm{LP,\,min}}$ (left). Alternatively, by pumping in-between the minimum and the inflection point of the LP branch (middle), pairs of polaritons can scatter to two distinct states while being allowed to do so by the conservation of momentum. This results to massive occupation of two states, called the signal (minimum of the LP branch) and the idler (close to the maximum of the LP branch), and the system is in the optical parametric oscilator (OPO) regime. A third approach consists of pumping high-energy excitons with no particular phase (right), which eventually relax down and condense to the minimum of the LP, see also Fig. 2.3. We refer the reader to [28] for a more complete account of the intricacies associated with each pumping scheme. Figure taken from [126].

2.1.4 Driven-dissipative Bose-Einstein condensation

Intense debate has sparked (see *e.g.* [127]) on what is the precise nature of this kind of non-equilibrium phase. Answering this question is non-trivial due the fact that equilibrium BEC formation and lasers have some common features. Indeed, for a long time, the close analogy between lasers and second-order phase transitions was known [128, 129].

In the case of lasers, the steady state is of non-equilibrium character and results from balance between pump and losses; this is of fundamental importance for population inversion, which is the cornerstone of a standard lasing process. Moreover, the defining characteristic of such a system is that off-diagonal long-range order (ODLRO) is displayed, which means that the electromagnetic field $\hat{E}(x)$ displays first-order coherence

$$\lim_{|\vec{x}-\vec{x}'|\to\infty} \left\langle \hat{E}^{\dagger}(\vec{x})\hat{E}(\vec{x}') \right\rangle \neq 0\,, \tag{2.9}$$

and light emitted by a laser device above its threshold remains coherent over large distances. However, it should be noted that weak light-matter coupling is enough for stimulated emission and hence for a lasing process. On the other hand, a BEC phase transition happens at equilibrium. Therefore, we deduce that the strong light-matter coupling, which amounts to new eigenstates of the system being formed, automatically rules out an optical laser, while the non-equilibrium character of the system due to the inherent drive and dissipation rules out an equilibrium BEC phase transition. The answer as to what exactly EPs are thus must lie somewhere in the middle between these two limiting cases [130].

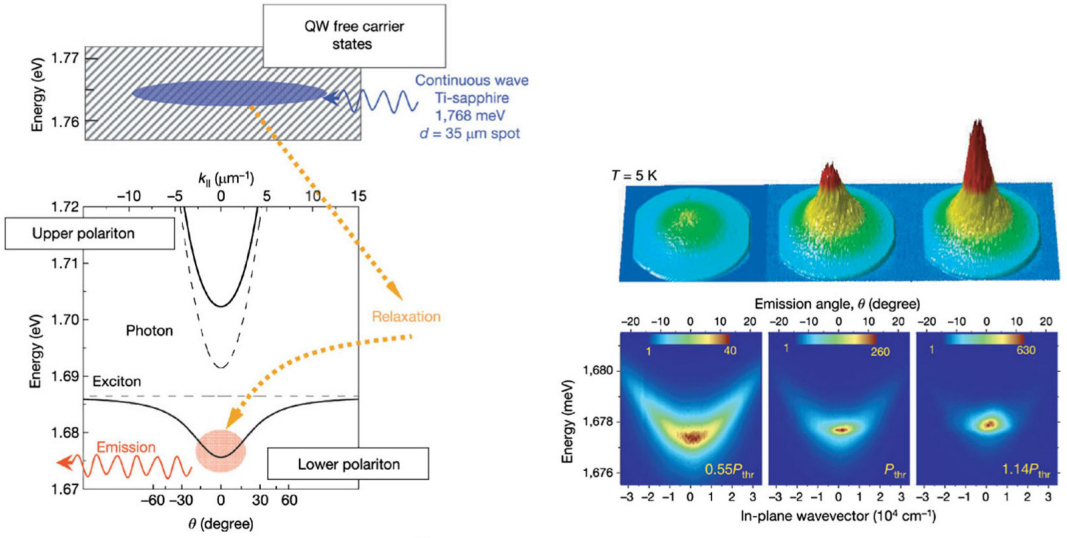

FIGURE 2.3: Experimental setup used in [122] under a non-resonant pumping scheme. Energy dispersion of the polariton modes versus in-plane wave vector $k_{\|}$ and the incidence angle θ (left). The excitonic dispersion is clearly identified as a constant $\omega_{x,0}$, while the photon one is a parabola (dashed lines). The UP and LP branches are also clearly visible (solid lines). The pump is tuned at an energy level even higher than the UP branch, and the excess amount is eventually relaxed to the bottom of the LP branch, via a variety of mechanisms, such as lattice phonon interaction and exciton scattering. We refer the reader to the excellent review [120] where this point is discussed in detail. Macroscopic population of this state then follows, which is associated with a hybridized Bose-Einstein condensation, as proven in this work. Emitted energy as function of $k_{\|}$ for three different pump powers, corresponding to below threshold, exactly at threshold, and above threshold (left to right), as well as energy distribution around a cone. Below threshold the energy is rather broadly distributed, while above threshold a clear consolidation at the lowest quantum state $k_{\|} = 0$ is observed.

So far it has been established that ODLRO is established in the EP system via emission of coherent light, using a variety of different pumping schemes. Experimentally, this was shown in the context of pumping close to the inflection point of the LP (Fig. 2.2, second panel) [131–133], and was predicted theoretically in [134] to correspond to a sort of Bose-Einstein condensation, where the symmetry breaking associated with the transition is of a $U(1)$ between the signal and idler modes. On the other hand, the quest for achieving spatiotemporal coherence in the case of non-resonant pumping (Fig. 2.2, third panel) [121, 135–137] also started. The first observation of an BEC of EP was experimentally reported in [122]. The experimental realisation is shown in Fig. 2.3, as well as results regarding occupation of the state of lowest in-plane momentum. In this work, a well-defined pumping intensity threshold is identified, above which much longer temporal coherence is reported, due to the formation of a BEC. Moreover, build-up of spatial coherence is found, which was linked to the formation of a condensate. In equilibrium BEC, this implies the development of ODLRO, however, it was later proven that KPZ fluctuations destroy ODLRO in this non-equilibrium setting, and this is the object we study in this thesis.

2.2 Gross-Pitaevskii Equation

Given that we established some form of Bose-Einstein condensation phenomenon happening in the case for EPs under incoherent pumping, we will now construct a phenomenological model for the description of the system. We note here that this type of pumping scheme will be assumed throughout this thesis, unless stated otherwise. This is because no coherence is able to be inherited from the pump laser, which is a necessary ingredient for the emergence of KPZ physics in the system. While this fact directly rules out the coherent pump where the incident momenta are in resonance with the minimum of the LP branch, the OPO regime depicted in the central panel of Fig. 2.2 is not ruled out and also exhibits KPZ physics. In this case, one has to deal with a 3-mode system (pump, signal, idler), and moreover, according to the analysis performed in [138, 139], this setup encounters strong sensitivity of the outcome to the pump characteristics.

2.2.1 From many-body to mean-field theory

The model presented in this section was introduced in [140, 141] and takes into account the physical features of the system described above. A significant simplification of the problem is achieved by the fact that the EP are described by a single classical field, as long as the particles populate almost exclusively the minimum of the LP, and hence they behave as a macroscopic condensate. In this case, a complex generalization of the well-known Gross-Pitaevskii equation (gGPe) [142] used in equilibrium systems can be employed. The gGPe is a non-linear Schrödinger equation for the classical mean-field $\psi = \psi(t,x) = \left\langle \hat{\psi}_{\mathrm{LP}}(t,x) \right\rangle$, which in our case describes the EP in the LP branch. A rate equation describing the excitonic reservoir is coupled to the gGPe, in order to explain the scattering of the high-energy carriers which allows the population of the condensate. We note that the precise mechanism under which the relaxation from the reservoir to the condensate happens is extremely complex and involves many different processes [143]. However this model has been found to be effective in predicting experimental results, without the need to incorporate the precise mechanisms underlying the gain in detail. In the most general case, the gGPe and the rate equation of the reservoir read:

$$i\hbar\frac{\partial\psi}{\partial t} = \left[\mathcal{F}^{-1}\left[E_{\mathrm{LP}}(k)\right] + \frac{i\hbar}{2}\left(Rn_r - \mathcal{F}^{-1}\left[\gamma_l(k)\right]\right) + 2g_r n_r + g\left|\psi\right|^2\right]\psi\,, \tag{2.10a}$$

$$\frac{\partial n_r}{\partial t} = P - \gamma_r n_r - Rn_r\left|\psi\right|^2. \tag{2.10b}$$

In Eqs. (2.10a, 2.10b), the reservoir density n_r is stimulated by pumping P, and is continuously depleting with a rate γ_r. The gain from the reservoir into the condensate is introduced via an amplification term R. The Gross-Pitaevskii equation includes an

imaginary term corresponding to the deterministic effects of the drive and dissipation, as well as contact polariton-polariton interactions and polariton-reservoir interactions, with coupling constants indicated by g, g_r respectively. The polariton loss-rate, which is in general momentum-dependent, is indicated by $\gamma_l(k)$, whose full expression is given in Eq. (2.12) below.

In order to write the dispersion relation for the LP branch, we take into account certain approximations. As can be seen in Fig. 2.3, polaritons under incoherent pumping eventually condense at the minimum of the LP branch, which corresponds to the lowest momentum state. Without loss of generality, we focus on the case where the system has zero detuning δ, namely $\delta \equiv \omega_{\mathrm{x},0} - \omega_{\mathrm{c},0} = 0$, with the generalization for $\delta \neq 0$ being straightforward, also from an experimental point-of-view. This choice simplifies Eq. (2.8a), and we can expand,

$$E_{\mathrm{LP}}(k) \simeq \hbar\omega_{\mathrm{LP}} + \frac{\hbar^2}{2m_{\mathrm{LP}}}k^2 - \frac{1}{2\hbar\Omega_R}\left(\frac{\hbar^2}{2m_{\mathrm{LP}}}k^2\right)^2 , \tag{2.11}$$

where $\omega_{\mathrm{LP}} = \omega_{\mathrm{c},0} - \Omega_R$ and $m_{\mathrm{LP}} = 2m_{\mathrm{cav}}$ and $k = |\vec{k}|$. By including up to quartic corrections, we are able to take into account excitation modes not strictly at the bottom of the LP branch.

As extensively discussed in the literature, in order to construct a more faithful model, it is expected that an extra momentum dependence should arise, coming either from the drive, or dissipation of the condensate [143]. This has been mostly carried out by introducing a frequency-selective pump, see *e.g.* [144, 145]. We will rather choose to introduce a momentum dependence on the polariton loss-rate. Our choice is motivated by the fact that there is experimental evidence of a momentum-dependent linewidth. On the other hand, the precise details of the pumping mechanism and the relaxation are not known in the incoherent pumping case. Therefore, we take

$$\gamma(k) = \gamma_0 + k^2\gamma_2 , \tag{2.12}$$

where $\gamma_0 \simeq 1/\tau_{\mathrm{pol}}$, for typical polariton lifetime τ_{pol}, and γ_2 corresponds to an increase of losses at finite wavevector $k = |\vec{k}|$. We note that, while the momentum dependence was measured as being linear in the wavevector in the experiment carried out in [146], in principle the functional form is a characteristic of the given experiment [147] and indeed a quadratic dependence was recently used [148]. Furthermore, the quadratic dependence in Eq. (2.12) is rather convenient, due to its well-defined Fourier transform.

2.2.1.1 Adiabatic approximation

After introducing the full model, we can make a further approximation, in the case where $\gamma_r \ll \gamma_l$. This means that the characteristic timescale for the reservoir dynamics is much longer than the one for the condensate, $\tau_\mathrm{r} \gg \tau_\mathrm{pol}$. Therefore, for the relevant timescale of the polaritons, the reservoir density can be thought of as being approximately constant, and hence the rate equation Eq. (2.10b) can be directly integrated, which leads to

$$n_r = \frac{P}{\gamma_r + R\left|\psi\right|^2}. \tag{2.13}$$

After substituting this expression, along with the dispersion relation Eq. (2.11) and the polariton loss rate Eq. (2.12) into Eq. (2.10a), we finally arrive at

$$\begin{aligned} i\hbar\frac{\partial\psi}{\partial t} = \Bigg[\left(-\frac{\hbar^2}{2m_\mathrm{LP}}\nabla^2 + i\hbar\frac{\gamma_2}{2}\nabla^2\right) + \frac{i\hbar\gamma_0}{2}\left(\frac{p}{1+\frac{|\psi|^2}{n_s}} - 1\right) \\ +2g_r\frac{P}{\gamma_r\left(1+\frac{|\psi|^2}{n_s}\right)} + g\left|\psi\right|^2\Bigg]\psi\,, \end{aligned} \tag{2.14}$$

where we have performed the inverse Fourier transforms to express the dispersion relation and the loss rate in real space, and we have further defined a dimensionless pump parameter $p \equiv P/P_\mathrm{th} = PR/(\gamma_0\gamma_r)$. We have also introduced the saturation density $n_s = \gamma_r/R$. It should be stressed that n_s is not known experimentally, due to the aforementioned difficulties in accessing the precise mechanisms for stimulating the LP branch in the incoherent pump case. On the other hand, the pump is very well controlled, and in fact p naturally acts as a control parameter for the phase transition.

2.2.1.2 Steady-state solution

We are interested in finding a stationary, steady-state solution of Eq. (2.14). So far we have been interested in a homogeneous condensate, since there is no external potential in the system. The full case where a confinement potential is introduced is crucial to our work and will be presented in chapter 3. For a homogeneous condensate, we substitute $\psi(t) = \sqrt{n_0}e^{i\theta_0(t)}$, where n_0 is a uniform and constant density, and θ_0 is the global phase. The real and imaginary parts of the resulting equation read

$$\partial_t\theta_0 = -gn_0 - 2g_r\frac{P}{\gamma_r\left(1+\frac{n_0}{n_s}\right)}\,, \tag{2.15a}$$

$$0 = \frac{\hbar\gamma_0}{2}\left(\frac{p}{1+\frac{n_0}{n_s}} - 1\right). \tag{2.15b}$$

By examining these equations, we see that $n_0 = 0$ is the stable solution if $P \leq P_{\text{th}}$, while a steady-state density proportional to p is found when $P > P_{\text{th}}$,

$$n_0 = n_s(p - 1), \tag{2.16}$$

thus reinforcing the claim that p naturally corresponds to the control parameter. The macroscopic phase of the condensate in the steady state is uniquely fixed, the $U(1)$ symmetry is broken and a non-equilibrium phase transition takes place.

2.2.2 Statistical fluctuations beyond mean-field

The mean-field model described in the previous section is based on treating the many-body quantum fields as classical complex fields which correspond to their expectation value. This assumption explicitly excludes the presence of fluctuations, and the only excitations around the MF solution one can study are the Bogoliubov excitations caused *e.g.* by an external perturbation. In an equilibrium condensate, this was introduced in [142], and the Bogoliubov modes were characterized. On the other hand, for a non-equilibrium condensate under incoherent pumping, key differences in the behavior of the Bogoliubov modes were found [149], especially in the low-momentum sector. The mean-field model, however, is approximate since it neglects statistical fluctuations which naturally arise from the stochastic nature of the drive and dissipation. To account for such fluctuations, a stochastic element must be added to the Gross-Pitaevskii equation. We refer the reader to the work by Gardiner and Davis [150] and references therein for details regarding the calculations, and we present here the main ideas, which were applied in the case of polaritons under incoherent pumping in [141].

2.2.2.1 Quantum and statistical fluctuations

The main idea behind the inclusion of a stochastic contribution to the system comes from its interplay with an excitonic reservoir, which replenishes polaritons. Going back to the quantum mechanical treatment of the problem, the total Hamiltonian of our system, since we disregard the UP, can be written as

$$\mathcal{H} = \mathcal{H}_0 + \mathcal{H}_{\text{s-r}}, \text{ with } \mathcal{H}_0 = \mathcal{H}_{\text{LP}} + \mathcal{H}_{\text{r}}. \tag{2.17}$$

We recall that LP are created (annihilated) by the operator $\hat{\psi}^\dagger_{\text{LP}}$ ($\hat{\psi}_{\text{LP}}$), which we will indicate as $\hat{\psi}^\dagger$ ($\hat{\psi}$) for short-hand notation, and here we also consider excitons in the reservoir which are created (annihilated) by the operator $\hat{\phi}^\dagger$ ($\hat{\phi}$). The Hamiltonians read

$$\mathcal{H}_{\mathrm{LP}} = \int_x \hat{\psi}^\dagger(x)\mathcal{F}^{-1}[E_{\mathrm{LP}}(k)]\hat{\psi}(x) + \frac{g}{2}\hat{\psi}^\dagger(x)\hat{\psi}^\dagger(x)\hat{\psi}(x)\hat{\psi}(x)\,, \tag{2.18a}$$

$$\mathcal{H}_{\mathrm{r}} = \int_x \hat{\phi}^\dagger(x)\mathcal{F}^{-1}[E_{\mathrm{R}}(k)]\hat{\phi}(x) + \frac{g_r}{2}\hat{\phi}^\dagger(x)\hat{\phi}^\dagger(x)\hat{\phi}(x)\hat{\phi}(x)\,, \tag{2.18b}$$

where a contact two-body polariton-polariton interaction of strength g has been included, as well as interaction among the excitons in the reservoir g_r, which is of the same order of magnitude [28]. The dispersion relations for the LP is given in Eq. (2.11), whereas the one for the excitons is treated as a constant due to the large mass, however in principle it is also a parabola, albeit extremely shallow. Regarding the coupling term $\mathcal{H}_{\text{s-r}}$, it involves mixing of operators, such that particles can be transferred between the reservoir and the LP,

$$\mathcal{H}_{\text{s-r}} = \int_x g_c \left(\hat{\phi}^\dagger(x)\hat{\phi}(x)\hat{\phi}(x)\hat{\psi}^\dagger(x) + \hat{\phi}^\dagger(x)\hat{\phi}^\dagger(x)\hat{\phi}(x)\hat{\psi}(x)\right) = H_{\mathrm{gain}} + H_{\mathrm{loss}}\,, \tag{2.19}$$

where also g_c is of the same order as g, g_r. We note here that, in principle, there are more terms involved, such as terms including three LP operators $\psi, \psi^\dagger$, as well as $H_{\mathrm{MF}} = g_c \int_x \phi^\dagger\phi\psi^\dagger\psi$. The former is assumed to be negligible in [141], while the latter does not contribute to exchange of particles between the two subsystems, but rather only to constant mean-field shifts.

We write a von Neumann equation for the total density matrix in the Schrödinger picture,

$$\frac{d\rho}{dt} = -i\left[\mathcal{H}, \rho\right]\,, \tag{2.20}$$

and the reduced density matrix for the LP is obtained by tracing out the reservoir and reads

$$\rho_{\mathrm{LP}} = \mathrm{Tr}_r \rho. \tag{2.21}$$

It is advantageous now to switch to the interaction picture, and we introduce a superscript "I" to denote the quantities expressed in this picture. We have

$$\mathcal{H}^{(I)}_{\text{s-r}} = e^{i\mathcal{H}_0 t}\mathcal{H}_{\text{s-r}}e^{-i\mathcal{H}_0 t}\,, \tag{2.22a}$$

$$\rho^{(I)} = e^{i\mathcal{H}_0 t}\rho e^{-i\mathcal{H}_0 t}\,, \tag{2.22b}$$

$$\frac{d\rho^{(I)}}{dt} = -i\left[\mathcal{H}^{(I)}_{\text{s-r}}, \rho^{(I)}\right]. \tag{2.22c}$$

We note here that the definition of the reduced density matrix for the LP, once the reservoir is traced out, reads in the interaction picture

$$\rho_{\mathrm{LP}}^{(I)} = \mathrm{Tr}_{\mathrm{r}}\rho^{(I)}. \tag{2.23}$$

In order to access its time evolution, we write the formal solution of Eq. (2.22c) after two iterations,

$$\rho^{(I)}(t) - \rho^{(I)}(0) = -i\int_{t'}\left[\mathcal{H}_{\text{s-r}}^{(I)}(t'), \rho^{(I)}(0)\right] - \int_{t'}\int_{t''}\left[\mathcal{H}_{\text{s-r}}^{(I)}(t'), \left[\mathcal{H}_{\text{s-r}}^{(I)}(t''), \rho^{(I)}(t'')\right]\right], \tag{2.24}$$

and by taking the partial trace in order to access the desired $\rho_{\mathrm{LP}}^{(I)}$ from Eq. (2.23), we finally obtain

$$\rho_{\mathrm{LP}}^{(I)}(t) - \rho_{\mathrm{LP}}^{(I)}(0) = -\int_{t'}\int_{t''}\mathrm{Tr}_r\left[\mathcal{H}_{\text{s-r}}^{(I)}(t'), \left[\mathcal{H}_{\text{s-r}}^{(I)}(t''), \rho^{(I)}(t'')\right]\right]. \tag{2.25}$$

Here we have used the fact that $\mathrm{Tr}_r\left[\mathcal{H}_{\text{s-r}}^{(I)}(t'), \rho^{(I)}(0)\right] = 0$. In order to prove this, we first have to assume that the LP and the reservoir are initially uncorrelated, such that the density matrix can be written as a product,

$$\rho^{(I)}(0) = \rho_{\mathrm{r}}^{(I)}(0) \otimes \rho_{\mathrm{LP}}^{(I)}(0). \tag{2.26}$$

The partial trace, therefore, contains terms such as

$$g_c\hat{\psi}^\dagger(t')\rho_{\mathrm{LP}}^{(I)}(0)\mathrm{Tr}_{\mathrm{r}}\left(\hat{\phi}^\dagger(t')\hat{\phi}(t')\hat{\phi}(t')\rho_{\mathrm{r}}^{(I)}(0)\right), \tag{2.27}$$

where the number of $\hat{\phi}, \hat{\phi}^\dagger$ operators in the product is imbalanced, and such a process would not conserve the total particle number, hence its expectation value is zero. This allows us to select the terms that contribute to the partial trace in Eq. (2.25). In particular, it can be seen from Eq. (2.19) that the only nonvanishing partial traces contain the following products

$$\mathrm{Tr}_r\left(H_{\text{gain / loss}}H_{\text{loss / gain}}\rho^{(I)}\right), \tag{2.28}$$

such that the numbers of annihilation/creation operators acting on the subspace of the reservoir balance out. In order to proceed, we extend the previous assumption Eq. (2.26) to be valid for any time, and hence the LP can be unraveled from the reservoir. This is because the coupling among the two subsystems is considered to be small, and the "environment" is generally thought of as being statistically independent from the "system" [151, 152]. A nonzero term contributing to $\rho_{\mathrm{LP}}^{(I)}$, in the spirit of Eq. (2.28),

reads

$$R_1 = g_c^2 \int_{t',t''} \int_{x',x''} \mathrm{Tr}_r \left[\left(\hat{\phi}^\dagger(t') \hat{\phi}(t') \hat{\phi}(t') \hat{\psi}^\dagger(t') \right) \left(\hat{\phi}^\dagger(t'') \hat{\phi}^\dagger(t'') \hat{\phi}(t'') \hat{\psi}(t'') \right) \rho^{(I)} \right]$$
$$\simeq g_c^2 \int_{t_{\mathrm{rel}},T_{\mathrm{cm}}} \int_{x_{\mathrm{rel}},X_{\mathrm{cm}}} \Pi_f(t_{\mathrm{rel}}, T_{\mathrm{cm}}, x_{\mathrm{rel}}, X_{\mathrm{cm}})$$
$$\times \left(\hat{\psi}^\dagger(T_{\mathrm{cm}} + t_{\mathrm{rel}}/2, X_{\mathrm{cm}} + x_{\mathrm{rel}}/2) \hat{\psi}(T_{\mathrm{cm}} - t_{\mathrm{rel}}/2, X_{\mathrm{cm}} - x_{\mathrm{rel}}/2) \rho_{\mathrm{LP}}^{(I)} \right) , \tag{2.29}$$

where center-of-mass and relative coordinates have been introduced,

$$X_{\mathrm{cm}} = \frac{x' + x''}{2} \qquad x_{\mathrm{rel}} = x' - x''$$
$$T_{\mathrm{cm}} = \frac{t' + t''}{2} \qquad t_{\mathrm{rel}} = t' - t''. \tag{2.30}$$

The prefactor $\Pi_f(t_{\mathrm{rel}}, T_{\mathrm{cm}}, x_{\mathrm{rel}}, X_{\mathrm{cm}})$ encodes information related to the exchange of energy via scattering which involves 3 particles. It can be written in the following form [141]

$$\Pi_f = \frac{1}{\Omega^3} \sum_{k_1,k_2,k_3} e^{i(x_{\mathrm{rel}}\Delta k - t_{\mathrm{rel}}\Delta\epsilon)} f(T_{\mathrm{cm}}, X_{\mathrm{cm}}, k_1)[f(T_{\mathrm{cm}}, X_{\mathrm{cm}}, k_2) + 1][f(T_{\mathrm{cm}}, X_{\mathrm{cm}}, k_3) + 1] , \tag{2.31}$$

where Ω is the relevant area of the system, k_1, k_2, k_3 the momenta of the reservoir excitons, and $\epsilon_{\mathrm{x}}(k_1), \epsilon_{\mathrm{x}}(k_2), \epsilon_{\mathrm{x}}(k_3)$ their dispersion relations. This process is shown in diagrammatic form in Fig. 2.4.

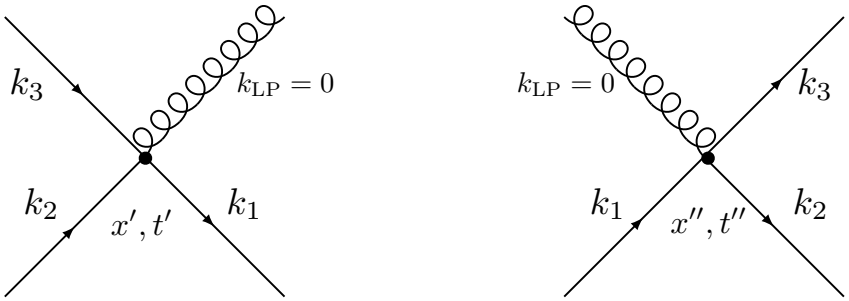

FIGURE 2.4: Interaction of LP and reservoir. At the node x'', t'', one reservoir exciton (straight line) with momentum k_1 interacts with one LP (curly line) with zero momentum, and two excitons k_2, k_3 are created. The total change in energy and momentum from Eq. (2.31) are $\Delta\epsilon = \epsilon_{\mathrm{x}}(k_2) + \epsilon_{\mathrm{x}}(k_3) - \epsilon_{\mathrm{x}}(k_1)$ and $\Delta k = k_2 + k_3 - k_1$. This is an out-scattering process, as a LP is destroyed and the reservoir gains energy. On the other hand, at the node x', t', two excitons are destroyed and one LP is created, therefore this is an in-scattering process.

Following the same logic, all the contributing terms in Eq. (2.25) can be gathered, and we find for $\rho_{\rm LP}$ after reverting back to the Schrödinger picture [141],

$$\frac{\partial \rho_{\rm LP}}{\partial t} = -i\left[\mathcal{H}_{\rm LP}, \rho_{\rm LP}\right] + K_{\rm in}(\rho_{\rm LP}) + K_{\rm out}(\rho_{\rm LP}), \tag{2.32}$$

During this process, using certain approximations and intricacies related to the system is necessary. In particular, emphasis was put in the reservoir being treated as a thermalized gas in [141], while the concept of the Markov approximation was discussed in [150]. This means that the reservoir can be thought of as being unaffected from back-action from the LP. We will return to this point at the end of this section, but for now the back-action is treated in the general case as non-zero. More explicitly, we refer to $K_{\rm in}(K_{\rm out})$ as gain (loss) induced to the LP by in(out)-scattering of high-energy excitons in the reservoir. These are written as

$$\begin{aligned} K_{\rm in}\left(\rho_{\rm LP}\right) = \frac{1}{2}\sum_{k}\int_{x_{\rm rel}} & R_{\rm in}[E_{\rm LP}(k), n_r] \\ & \times \left(e^{ikx_{\rm rel}}\hat{\psi}^{\dagger}(x_{\rm rel})\rho_{\rm LP}\hat{\psi}(k) - e^{ikx_{\rm rel}}\hat{\psi}(k)\hat{\psi}^{\dagger}(x_{\rm rel})\rho_{\rm LP} + h.c\right), \end{aligned} \tag{2.33}$$

$$\begin{aligned} K_{\rm out}\left(\rho_{\rm LP}\right) = \frac{1}{2}\sum_{k}\int_{x_{\rm rel}} & R_{\rm out}[E_{\rm LP}(k), n_r] \\ & \times \left(e^{ikx_{\rm rel}}\hat{\psi}(k)\rho_{\rm LP}\hat{\psi}^{\dagger}(x_{\rm rel}) - e^{ikx_{\rm rel}}\hat{\psi}^{\dagger}(x_{\rm rel})\hat{\psi}(k)\rho_{\rm LP} + h.c\right). \end{aligned} \tag{2.34}$$

and the operators are evaluated at the same time $T_{\rm cm}$ in center-of-mass coordinates. We note here that the peculiar coupling between operators expressed in Fourier space and operators in real space arises naturally in this formalism when taking the trace in the last term of Eq. (2.32). The rates written above are expected to have the following general forms,

$$R_{\rm in}\left[E_{\rm LP}(k), n_r\right] = n_r^2 \tilde{R}_{\rm in}\left(E_{\rm LP}(k)\right), \tag{2.35a}$$

$$R_{\rm out}\left[E_{\rm LP}(k), n_r\right] = n_r \tilde{R}_{\rm out}\left(E_{\rm LP}(k)\right) + \gamma(k), \tag{2.35b}$$

for γ being the LP loss rate defined in Eq. (2.12).

So far, we have derived a master equation Eq. (2.32) which in principle contains all the information regarding the time evolution of states in our quantum system. We now use the fact that the EP condensate is a coherent state. This means that we can attempt to map the equation of motion for $\rho_{\rm LP}$, Eq. (2.32), to an equation for the quasiprobability density of a classical field describing the coherent state [152]. In general, this can be done via a number of ways. Firstly, in the Glauber-Sudarshan P representation [153, 154],

one exploits the fact that any density matrix can be written as an ensemble over coherent states, and in this case one can show that moments of the quasiprobability density function correspond to expectation values of normal ordered products. Secondly, in the Husimi Q representation [155], one uses the fact any operator can be written as the diagonal matrix element of coherent states, which is an overcomplete basis, and in this case the moments of the quasiprobability density function correspond to expectation values of anti-normal ordered products. The prefix "quasi" refers to functions which can be negative or singular, and hence their integral can be negative in small regions. We refer the reader to [152] and references therein for a more complete accord of these representations, as well as for the Wigner representation, which we will outline in more detail below.

The Wigner representation was originally derived as a tool to obtain the joint probability of the position and momentum of quantum particles. In our case, we define the functional $P_W[\psi,\psi^*]$ on the space of complex functions $(\psi,\psi^*)\equiv(\psi(x),\psi^*(x))$,

$$P_W[\psi,\psi^*]=\frac{1}{\pi^2}\int_{\lambda,\lambda^*}e^{-\lambda\psi^*+\lambda^*\psi}\chi_W[\lambda,\lambda^*]\,, \tag{2.36}$$

where $(\lambda,\lambda^*)\equiv(\lambda(x),\lambda^*(x))$, and $\chi_W[\lambda,\lambda^*]$ is the characteristic Wigner functional

$$\chi_W[\lambda,\lambda^*]=\mathrm{Tr}\left(\rho_{\mathrm{LP}}e^{\lambda\hat{\psi}^\dagger-\lambda^*\hat{\psi}}\right)\,, \tag{2.37}$$

where the trace should be evaluated over coherent states of polaritons. We now have to map the time evolution of the density matrix of the quantum field Eq. (2.32) to an equation of motion for $P_W\equiv P_W[\psi,\psi^*]$, as a tool in order to arrive to a stochastic partial differential equation for a classical field, as explained in section 2.2.1. In order to proceed, the action of the operators on the density matrix can be mapped to a differential operation on P_W, namely [152]

$$\hat{\psi}\rho_{\mathrm{LP}}\leftrightarrow\left(\psi+\frac{1}{2}\frac{\partial}{\partial\psi^*}\right)P_W\,, \tag{2.38a}$$

$$\hat{\psi}^\dagger\rho_{\mathrm{LP}}\leftrightarrow\left(\psi^*-\frac{1}{2}\frac{\partial}{\partial\psi}\right)P_W\,, \tag{2.38b}$$

$$\rho_{\mathrm{LP}}\hat{\psi}^\dagger\leftrightarrow\left(\psi^*+\frac{1}{2}\frac{\partial}{\partial\psi}\right)P_W\,, \tag{2.38c}$$

$$\rho_{\mathrm{LP}}\hat{\psi}\leftrightarrow\left(\psi-\frac{1}{2}\frac{\partial}{\partial\psi^*}\right)P_W \tag{2.38d}$$

With these relations, the commutator in Eq. (2.32) can be decomposed via Eq. (2.18a),

$$\begin{aligned}\int_x -i\left[\hat{\psi}^\dagger \mathcal{F}^{-1}[E_{\rm LP}(k)]\hat{\psi}, \rho_{\rm LP}\right] \to \int_x i\left(\frac{\partial}{\partial\psi}\mathcal{F}^{-1}[E_{\rm LP}(k)]\psi - \frac{\partial}{\partial\psi^*}\mathcal{F}^{-1}[E_{\rm LP}(k)]\psi^*\right) P_W\,,\\ \int_x -i\frac{g}{2}\left[\hat{\psi}^\dagger\hat{\psi}^\dagger\hat{\psi}\hat{\psi}, \rho_{\rm LP}\right] \to \int_x i\Bigg\{\left(g\frac{\partial}{\partial\psi}\left|\psi\right|^2\psi - g\frac{\partial}{\partial\psi^*}\left|\psi\right|^2\psi^*\right)\\ + \left[\frac{g}{4}\frac{\partial}{\partial\psi}\frac{\partial}{\partial\psi^*}\left(\frac{\partial}{\partial\psi^*}\psi^* - \frac{\partial}{\partial\psi}\psi\right)\right]\Bigg\}P_W.\end{aligned} \tag{2.39}$$

The term related to in-scattering transforms in the following way,

$$K_{\rm in}(\rho_{\rm LP}) \to \int_x \frac{1}{2}\left[-\frac{\partial}{\partial\psi(x)}\hat{\mathcal{R}}_{\rm in}\psi(x) - \frac{\partial}{\partial\psi^*(x)}\hat{\mathcal{R}}^*_{\rm in}\psi^*(x) + \hat{\mathcal{R}}_{\rm in}\frac{\partial^2}{\partial\psi(x)\partial\psi^*(x)}\right]P_W. \tag{2.40}$$

and similarly does the one for out-scattering. Here we have defined the convolution operator

$$\hat{\mathcal{R}}_{\rm in}f(x) = \sum_k \int_{x'} R_{\rm in}e^{iq(x-x')}f(x') \equiv \mathcal{R}_{\rm in}f(x)\,, \tag{2.41}$$

where $R_{\rm in}$ is given by Eq. (2.35a). By gathering all the terms, we finally obtain the equation of motion for the Wigner function, under the assumption that $\partial\rho_{\rm LP}/\partial t$ corresponds to $\partial P_W/\partial t$,

$$\begin{aligned}\frac{\partial P_W}{\partial t} = \int_x \Bigg[-\frac{\partial}{\partial\psi(x)}F_{\rm det} - \frac{\partial}{\partial\psi^*(x)}F^*_{\rm det} + \frac{1}{2}\left(\mathcal{R}_{\rm in} + \mathcal{R}_{\rm out} + \mathcal{F}^{-1}[\gamma(k)]\right)\frac{\partial^2}{\partial\psi(x)\partial\psi^*(x)}\\ + i\frac{g}{4}\frac{\partial}{\partial\psi(x)}\frac{\partial}{\partial\psi^*(x)}\left(\frac{\partial}{\partial\psi^*(x)}\psi^*(x) - \frac{\partial}{\partial\psi(x)}\psi(x)\right)\Bigg]P_W,\end{aligned} \tag{2.42}$$

where we have defined the deterministic force acting on the LP field at position x, $F_{\rm det} \equiv F_{\rm det}|_x$,

$$F_{\rm det} = -i\left[\mathcal{F}^{-1}[E_{\rm LP}(k)] + \frac{i}{2}\left(R_{\rm in} - R_{\rm out} - \mathcal{F}^{-1}[\gamma(k)\right) + g\left|\psi(x)\right|^2\right]\psi(x). \tag{2.43}$$

It is instructive to look now at what is the strength of small fluctuations of the field if one implements the Wigner representation on a $d-$dimensional grid of N sites and elementary volume $\Delta V = (N/l)^d$. The field carries dimensions $\Delta V^{-1/2}$, hence $\Delta\psi = \Delta V^{-1/2}$. Under the assumption that $\Delta P_W/\Delta\psi \sim \Delta\psi$, one can readily deduce the strength of the terms containing second- and third-order derivatives in Eq. (2.42). This is a crucial point, since it allows us to neglect the latter given the "diluteness" condition, which constitutes the Truncated Wigner Approximation (TWA),

$$\gamma_0 \gg \frac{g}{\Delta V}. \tag{2.44}$$

In this case, the equation of motion can be approximated by a true Fokker-Planck equation in the case where the coefficient of the second-order derivative in Eq. (2.42) is positive-definite. This is a stochastic differential equation for the field $\psi(t,x)$ [44],

$$d\psi(t,x) = F_{\rm det}(t,x)dt + dW(t,x), \tag{2.45}$$

where dW is a complex Gaussian random increment with zero mean and a covariance which corresponds to twice the aforementioned coefficient,

$$\langle dW(t,x)\rangle = 0\,, \tag{2.46a}$$

$$\left\langle dW(t,x)dW^*(t,x')\right\rangle = (R_{\rm in}+R_{\rm out}+\gamma_0)\frac{\delta_{x,x'}}{\Delta V}dt. \tag{2.46b}$$

We note here that in Eqs. (2.44, 2.46b) the zeroth order contribution to the LP loss rate γ_0 has been kept as an approximation with regards to the noise strength, but we shall see that the full momentum dependence plays a crucial role in the deterministic term.

From now on we will define the total amplification term $R[n_r, E_{\rm LP}] = R_{\rm in} - R_{\rm out}$. While the quadratic (linear) behavior of $R_{\rm in}(R_{\rm out})$ in Eqs. (2.35a, 2.35b) were motivated by treating the reservoir as essentially a thermalized gas, this is not always the case for incoherent pumping; all that we need is an irreversible process which stimulates the LP [28]. In a generic manner, this is written as $R[n_r]$ which is monotonically growing, and under the assumption that condensation happens almost exclusively in the $k=0$ mode, we can write $R[n_r, E_{\rm LP}] = Rn_r$ for $R \equiv R[E_{\rm LP}(0)]$. Moreover, the Markovian approximation was found to be appropriate for most experimental conditions, as the Rabi splitting and k_BT are well separated, $\Omega_R \gg k_BT$. Therefore, from now on, we will consider $R_{\rm out} = 0$. One can now readily compare the deterministic part of the Langevin equation Eq. (2.45) with the MF model Eq. (2.10a), after properly restoring the units. The term proportional to $g_r n_r$ is generated if $H_{\rm MF}$ is included in the analysis. In that case, there is an extra contribution to Eq. (2.25) since $\mathrm{Tr}_r[H^{(I)}_{\rm MF}, \rho^{(\rm I)}] \neq 0$, and the second order term corresponds to a scattering process that involves only 2 reservoir excitons after computing the partial trace of products such as $\mathrm{Tr}_r\left(H_{\rm MF}H_{\rm MF}\rho^{(I)}\right)$.

Lastly, we emphasize that the complex field $\psi(t,x)$ entered in our analysis as a parameter of the Wigner function. Physical observables related to the system, however, should be thought of as expectation values of $\hat{\psi}$ in the quantum mechanical picture. While, as we mentioned above, expectation values of normal (anti-normal) products of creation and annihilation operators can be directly accessed in the P (Q) representations, it can be proven that symmetrized products correspond to computing moments of P_W [152], for

example

$$\frac{1}{2}\langle\hat{\psi}\hat{\psi}^\dagger+\hat{\psi}^\dagger\hat{\psi}\rangle=\langle\psi\psi^*\rangle_W\equiv\int_{\psi,\psi^*}\psi\psi^*P_W[\psi,\psi^*]\,, \tag{2.47}$$

and we can easily generalize to expectation value of any power of the operators. This allows us to extract observables by sampling from the Wigner distribution. In particular, for local observables in space, this introduces small corrections, as seen for example in computing the density of the LP,

$$\langle|\psi|^2\rangle_W=\langle\hat{\psi}^\dagger\hat{\psi}\rangle+\frac{1}{2\Delta V}, \tag{2.48}$$

where we have used that the commutator of the LP operators is $\left[\hat{\psi},\hat{\psi}^\dagger\right]=\delta_{x,x'}/\Delta V$. This type of corrections shows us that a well-defined discretization of the system is necessary in order to regularize physical observables, such that no divergences can appear in the continuous limit $\Delta V\to 0$.

2.3 Dynamics of phase fluctuations and mapping to KPZ equation

We have proven that indeed the complex LP field ψ obeys a stochastic partial differential equation, in which the noise has the appropriate strength given the diluteness condition. We now switch back to continuous space, such that $\delta_{x,x'}/\Delta x^d=\delta^d(x-x')$. Eq. (2.14) now reads

$$\begin{aligned}i\hbar\frac{\partial\psi}{\partial t}=\Bigg[&\left(-\frac{\hbar^2}{2m_{\rm LP}}\nabla^2+i\hbar\frac{\gamma_2}{2}\nabla^2\right)+\frac{i\hbar\gamma_0}{2}\left(\frac{p}{1+\frac{|\psi|^2}{n_s}}-1\right)\\&+g\,|\psi|^2+2g_r\frac{P}{\gamma_r\left(1+\frac{|\psi|^2}{n_s}\right)}\Bigg]\psi+\hbar\xi'\,,\end{aligned} \tag{2.49}$$

where the stochastic contribution comes from the random function ξ'. It can be shown that the integral of such a function corresponds to the Wiener process [44],

$$\int_0^t\xi(t')dt'=W(t). \tag{2.50}$$

Note that this type of integral naturally occurs during the integration of stochastic differential equations such as Eq. (2.45) and is mathematically well-defined, therefore we are allowed to define $dW(t)\equiv W(t+dt)-W(t)=\xi'(t)dt$, despite the fact that the Wiener process itself is non-differentiable. Returning to Eq. (2.49), we explicitly write

the units of energy and density in d dimensions,

$$\epsilon_0 = \hbar/\tau_0 \qquad\qquad \rho_0 = 1/l_0^d\,, \tag{2.51}$$

where τ_0, l_0 are the units for time and space, respectively. The various parameters of our system can be expressed as

$$\begin{aligned} \gamma_0 &= \tilde{\gamma}_0/\tau_0 & \gamma_r &= \tilde{\gamma}_r/\tau_0 & \gamma_2 &= \tilde{\gamma}_2 l_0^2/\tau_0 \\ \psi &= \sqrt{\rho_0}\tilde{\psi} & n_s &= \rho_0 \tilde{n}_s & P &= \tilde{P}/\tau_0 l_0^2 \\ R &= \tilde{R} l_0^2/\tau_0 & g &= \tilde{g}\epsilon_0/\rho_0 & g_r &= \tilde{g}_r \epsilon_0/\rho_0. \end{aligned} \tag{2.52}$$

The dimensions of the noise can be extracted from its covariance Eq. (2.46b), where we have in continuous space

$$\left\langle \xi'(t,x)\xi'^*(t',x')\right\rangle = 2\frac{Rn_r+\gamma_0}{2}\delta^d(x-x')\delta(t-t') = 2\sigma\delta^d(x-x')\delta(t-t')\,, \tag{2.53}$$

where $\sigma = \tilde{\gamma}_0(p+1)/2$ is the noise strength. We can now define a new stochastic variable,

$$\tilde{\xi} = \frac{\xi'}{\sqrt{\sigma/l_0^d\tau_0^2}}, \text{ such that } \langle\tilde{\xi}(t,x)\tilde{\xi}^*(t,x')\rangle = 2\delta^d(\tilde{x}-\tilde{x}')\delta(\tilde{t}-\tilde{t}')\,, \tag{2.54}$$

and henceforth we omit the tildes, as we work exclusively in dimensionless units. We further define $K_c = \frac{\hbar^2}{2m_{\rm LP}\epsilon_0 l_0^2}, K_d = \frac{\gamma_2}{2}$ and the threshold reservoir density $n_{r,\rm th} = P/\gamma_r$ for convenience. Our equation finally reads

$$i\frac{\partial\psi}{\partial t} = \left[-(K_c - iK_d)\nabla^2 + \frac{i\gamma_0}{2}\left(\frac{p}{1+\frac{|\psi|^2}{n_s}} - 1\right) + g|\psi|^2 + 2g_r\frac{n_{r,\rm th}}{\left(1+\frac{|\psi|^2}{n_s}\right)}\right]\psi + \sqrt{\sigma}\xi\,, \tag{2.55}$$

We are now interested in studying the statistical fluctuations induced by the noise. We work in the density-phase representation, which consists of expressing the field as $\psi(t,x) = \sqrt{n(t,x)}e^{i\theta(t,x)}$. The spatial and temporal derivatives are expressed as

$$\frac{\partial\psi}{\partial t} = \psi\left(\frac{1}{2n}\frac{\partial n}{\partial t} + i\frac{\partial\theta}{\partial t}\right)\,, \tag{2.56a}$$

$$\nabla^2\psi = \psi\left(-\frac{1}{4n^2}(\nabla n)^2 + \frac{1}{2n}\nabla^2 n + \frac{i}{n}\nabla n\nabla\theta + i\nabla^2\theta - (\nabla\theta)^2\right). \tag{2.56b}$$

By substituting into Eq. (2.55), we have for the real and imaginary parts, respectively,

$$\begin{aligned} -\frac{\partial\theta}{\partial t} &= K_c\left(\frac{1}{4n^2}(\nabla n)^2 - \frac{1}{2n}\nabla^2 n + (\nabla\theta)^2\right) + K_d\left(-\frac{1}{n}\nabla n\nabla\theta - \nabla^2\theta\right) \\ &\quad + gn + 2g_r\frac{n_{r,\mathrm{th}}}{1+n/n_s} + \sqrt{\frac{\sigma}{n}}\mathrm{Re}\left(e^{-i\theta}\xi\right), \end{aligned} \tag{2.57}$$

$$\begin{aligned} \frac{1}{2n}\frac{\partial n}{\partial t} &= K_c\left(-\frac{1}{n}\nabla n\nabla\theta - \nabla^2\theta\right) + K_d\left(-\frac{1}{4n^2}(\nabla n)^2 + \frac{1}{2n}\nabla^2 n - (\nabla\theta)^2\right) \\ &\quad + \frac{\gamma_0}{2}\left(\frac{p}{1+n/n_s} - 1\right) + \sqrt{\frac{\sigma}{n}}\mathrm{Im}\left(e^{-i\theta}\xi\right). \end{aligned} \tag{2.58}$$

We now expand around the homogeneous MF solutions,

$$n = n_0 + \delta n(t,x)\,, \tag{2.59a}$$

$$\theta = \theta_0(t) + \delta\theta(t,x), \tag{2.59b}$$

such that the zeroth order equations correspond to Eqs. (2.15a, 2.15b). Under the assumption that the statistical density fluctuations are smooth and stationary, as well as much smaller than the steady state density n_0, namely

$$\nabla\delta n \simeq 0\,, \qquad \frac{\partial\delta n}{\partial t} \simeq 0\,, \qquad \frac{\delta n}{n_0} \ll 1\,, \tag{2.60}$$

we can derive an equation valid up to first order in δn. To this order, we can straightforwardly solve Eq. (2.58) for δn, after using the zeroth order result for the steady state MF density Eq. (2.16),

$$\delta n = \left[-K_c\nabla^2\delta\theta - K_d(\nabla\delta\theta)^2 + \sqrt{\frac{\sigma}{n_0}}\mathrm{Im}\left(e^{-i\theta_0}\xi\right)\right]\frac{2pn_s}{\gamma_0}, \tag{2.61}$$

where the contribution of the fluctuations to the noise is expected to be negligible. Under these assumptions, substituting Eq. (2.61) in Eq. (2.57) leads to a KPZ equation for the phase fluctuations,

$$\frac{\partial\delta\theta}{\partial t} = \nu\nabla^2\delta\theta + \frac{\lambda}{2}(\nabla\delta\theta)^2 + \sqrt{D}\eta\,, \tag{2.62}$$

where the parameters ν, λ, D are fixed by the microscopic parameters of the gGPe,

$$\nu = K_d + aK_c\,, \tag{2.63a}$$

$$\lambda = -2(K_c - aK_d)\,, \tag{2.63b}$$

$$D = \frac{\sigma}{2n_0}(1+a^2),\,, \tag{2.63c}$$

with

$$a = \frac{2pgn_s}{\gamma_0}\left(1 - \frac{2g_r n_{r,\mathrm{th}}}{p^2 g n_s}\right). \tag{2.64}$$

We note here that the real and imaginary parts of the noise ξ, have the following correlations,

$$\left\langle \mathrm{Re}(\xi(t,x))\mathrm{Re}(\xi^*(t',x'))\right\rangle = \left\langle \mathrm{Im}(\xi(t,x))\mathrm{Im}(\xi^*(t',x'))\right\rangle = \delta(x-x')\delta(t-t')\,, \tag{2.65a}$$

$$\left\langle \mathrm{Re}(\xi(t,x))\mathrm{Im}(\xi^*(t',x'))\right\rangle = 0. \tag{2.65b}$$

The real noise η has unit variance $\langle \eta(t,x)\eta(t',x')\rangle = 2\delta(x-x')\delta(t-t')$ and is defined as

$$\begin{aligned}\eta &= -\sqrt{\frac{\sigma}{n_0}}\left[\mathrm{Re}\left(e^{-i\theta_0}\xi\right) + a\mathrm{Im}\left(e^{-i\theta_0}\xi\right)\right] \\ &= -\sqrt{\frac{\sigma}{n_0}}\left[\mathrm{Re}\left(\xi\right)\cos\theta_0 - a\mathrm{Re}\left(\xi\right)\sin\theta_0 + \mathrm{Im}\left(\xi\right)\sin\theta_0 + a\mathrm{Im}\left(\xi\right)\cos\theta_0\right].\end{aligned} \tag{2.66}$$

Therefore, we have conclusively proven that the dynamics of fluctuations of the phase of the condensate wavefunction for the LP can be mapped to a KPZ equation, when the system is not subject to confinement. We will treat the latter case separately in chapter 3, and highlight its differences from the homogeneous case.

Chapter 3

Signatures of KPZ universality sub-classes in the phase of $1d$ exciton polaritons

The connection between KPZ universality and the Bose-Einstein condensate of exciton polaritons became apparent in recent years, and the dynamics of the phase of the polariton condensate was proven to be mapped onto a KPZ equation [156–158]. This has profound implications, as it shows that the nature of polariton condensates is very different from their equilibrium counterparts. In $1d$, there have been some works confirming this mapping, from the point-of-view of scaling of spatio-temporal correlations [158], as well as in terms of distribution of phase fluctuations [159] for experimentally-relevant parameters. Moreover, the conclusive experimental demonstration of KPZ scaling in a $1d$ polariton condensate was provided in Ref. [148], thus promoting it to a compelling experimental platform to probe KPZ universality.

In this chapter, we will discuss how the curved universality sub-class associated with the KPZ growth in a "droplet" geometry can be accessed in exciton polaritons in $1d$, adding to the previous results concerning the flat and stationary sub-classes [159]. From the point-of-view of numerical simulations, we propose a protocol in which the system is subjected to an external confining potential. This makes the system inhomogeneous, and we will show that the phase at the boundaries of the system propagates in time faster than the phase at the bulk, effectively leading to a bending of the phase profile. We compute the first order correlation function of the condensate wavefunction in space and time, which can be mapped to the correlation function of the condensate phase, under some approximations and a cumulant expansion. Moreover, we will compute certain

observables which rely on extracting the phase of the condensate directly. In both cases, the sensitivity to the growth geometry is directly visible.

3.1 Model for EP under external confinement

We consider the following gGPe for the EP system under an external confining potential $V(x)$,

$$i\hbar\frac{\partial\psi}{\partial t} = \left[\left(-\frac{\hbar^2}{2m_{\mathrm{LP}}}\nabla^2 - \frac{\hbar^4}{8\Omega_R m_{\mathrm{LP}}}\nabla^4 + \epsilon + V(x) + i\hbar\frac{\gamma_2}{2}\nabla^2\right) + \frac{i\hbar\gamma_0}{2}\left(\frac{p}{1+\frac{|\psi|^2}{n_s}} - 1\right) + g\,|\psi|^2\right]\psi + \hbar\xi'. \tag{3.1}$$

Here, we use the adiabatic approximation for eliminating the reservoir dynamics. For the purpose of this chapter, we have included the expansion of the dispersion relation for the EP in the LP branch to fourth order, as written in Eq. (2.11), and the polariton-reservoir interaction has been assumed to be neglibible, $g_r \simeq 0$. Furthermore, the complex noise ξ' has the same properties as the one introduced in Eq. (2.53). We choose the following units $\tau_0, \epsilon_0, l_0, \rho_0$ for time, energy, space, and density of the wavefunction,

$$\tau_0 = \gamma_0^{-1} \qquad \epsilon_0 = \hbar\gamma_0 \qquad l_0 = \sqrt{\frac{\hbar}{2m_{\mathrm{LP}}\gamma_0}} \qquad \rho_0 = \frac{\gamma_r(p-1)}{Rp}\,, \tag{3.2}$$

in order to rescale the gGPe (3.1). Moreover, under the assumption that the condensate amplitude is small, $|\psi|^2 \ll n_s$, we can expand the denominators in Eq. (3.1), and for the choice of units Eq. (3.2) we arrive at the following dimensionless equation,

$$i\frac{\partial\tilde{\psi}}{\partial\tilde{t}} = \left[-(K_c - iK_d)\partial_{\tilde{x}}^2 - K_c^{(2)}\partial_{\tilde{x}}^4 - (r_c(\tilde{x}) - ir_d) + (u_c - iu_d)|\tilde{\psi}|^2\right]\tilde{\psi} + \sqrt{\sigma'}\tilde{\xi}\,, \tag{3.3}$$

where the dimensionless noise $\tilde{\xi}$ has covariance $\left\langle\tilde{\xi}(t,x)\tilde{\xi}(t',x')\right\rangle = 2\delta(\tilde{x}-\tilde{x}')\delta(\tilde{t}-\tilde{t}')$. All the parameters in Eq. (3.3) are expressed with respect to the microscopic ones from Eq. (3.1) via

$$\begin{aligned} K_c &= 1 & K_d &= \frac{m\gamma_{l,2}}{\hbar} & K_c^{(2)} &= \frac{\gamma_{l,0}}{2\Omega} \\ r_c &= -\frac{\epsilon + V(x)}{\hbar\gamma_0} & r_d &= \frac{p-1}{2} & u_c &= \frac{g}{\hbar\gamma_0}n_0 \\ u_d &= \frac{pR}{2\gamma_r}\rho_0 & \sigma' &= \sigma\frac{\tau_0}{\rho_0 l_0}. \end{aligned} \tag{3.4}$$

For the entirety of this chapter we will omit the tildes, and we will work exclusively under this choice of units.

3.2 Numerical simulations

Our analysis consists of numerically integrating Eq. (3.1) by using the second-order split-step Fourier method. The parameters of the equation were taken to be compatible with typical experiments conducted in Institut Néel in Grenoble with CdTe samples, in the group of Maxime Richard [147, 160]. In particular, we used the following values: $m = 4 \times 10^{-5} \mathrm{m}_e$, $\gamma_0 = 0.5\ ps^{-1}$, $\gamma_r = \gamma_0/25$, $g = 0.4996\ \mu eV \times \mu m$, $\gamma_{l,2} = 1.3\ \mu m^2 \times ps^{-1}$, $\Omega_R = 100\ ps^{-1}$, $p = 1.6$, $n_s = 50\ \mu m^{-1}$. The system size was taken to be $L = 2^{10} l_0$. We record the wavefunction $\psi(t, x)$ during the time evolution and extract its phase $\theta(t, x) \in (-\pi, \pi]$. Our study is performed in the low-noise regime, where we confirmed that there are no topological defects, such as solitons or phase slips, and in this case, the phase can be safely unwrapped, $\theta(t, x) \to \theta_{\mathrm{unw}}(t, x) \in (-\infty, \infty)$. In our numerical simulations, the unwrapping is achieved by constraining the phase such that the difference between neighouring space-time points is less than $\kappa \cdot 2\pi$, where the factor $\kappa \simeq 1$ is chosen empirically in order to take into account unwinding errors due to space and time discretization. Henceforth, in our numerical results we refer to the phase as the unwrapped field θ_{unw}.

3.3 Mapping to the inhomogeneous KPZ equation

Starting from Eq. (3.3), we express the wavefunction in the density-phase representation. The density and phase fields are now decomposed in the following way

$$n(t, x) = n_0(t, x) + \delta n(t, x)\,, \qquad \theta(t, x) = \theta_0(t, x) + \delta\theta(t, x)\,, \tag{3.5}$$

where (n_0, θ_0) are defined as the zeroth-order solutions, and $(\delta n, \delta\theta)$ are small fluctuations around these solutions. We first focus on the former, and we note that, due to the confining potential, an explicit space dependence should be included in n_0 and θ_0, in contrast to the analysis of section 2.3. We obtain these quantities by averaging Eq. (3.3) over the noise fluctuations

$$\begin{aligned}
\partial_t n_0 =& - K_d \frac{(\partial_x n_0)^2}{2n_0} + K_d \partial_x^2 n_0 - 2n_0 K_d (\partial_x \theta_0)^2 - 2K_c (\partial_x n_0)(\partial_x \theta_0) - 2n_0 K_c \partial_x^2 \theta_0 \\
&+ 2n_0 r_d - 2n_0^2 u_d\,, \\
\partial_t \theta_0 =& - K_c \frac{(\partial_x n_0)^2}{4n_0^2} + K_c \frac{\partial_x^2 n_0}{2n_0} - K_c (\partial_x \theta_0)^2 + K_d \frac{(\partial_x n_0)(\partial_x \theta_0)}{n_0} + K_d \partial_x^2 \theta_0 + r_c(x) \\
&- u_c n_0\,.
\end{aligned}$$

Under the assumption that $\partial_t n_0 \simeq 0$, meaning that the density reaches a steady state, and moreover that the density fluctuations are smooth and sufficiently stationary, such that $\partial_t \delta n \simeq 0$ and $\partial_x^{(n)} \delta n \simeq 0$, we can analyse the fluctuations, as defined in Eq. (3.5). In particular, the time evolution for $\delta\theta$ is governed by

$$\begin{aligned}\partial_t \delta\theta = K_d \partial_x^2 \delta\theta - K_c (\partial_x \delta\theta)^2 + \partial_x \delta\theta \left(K_d \frac{\partial_x n_0}{n_0} - 2K_c \partial_x \theta_0 \right) \\ + \delta n \left[K_c \frac{(\partial_x n_0)^2}{2n_0^3} - K_c \frac{\partial_x^2 n_0}{2n_0^2} - K_d \frac{(\partial_x n_0)(\partial_x \theta_0)}{n_0^2} - u_c \right] - \sqrt{\frac{\sigma'}{n_0}} \mathrm{Re}[\xi e^{-\theta_0}] \,, \end{aligned} \tag{3.6}$$

where the density fluctuations $\delta n \equiv \delta n(x)$ are expressed as

$$\delta n = \frac{2n_0 K_d \left[2(\partial_x \theta_0)(\partial_x \delta\theta) + (\partial_x \delta\theta)^2 \right] + 2K_c \left[(\partial_x n_0)(\partial_x \delta\theta) + n_0 \partial_x^2 \delta\theta \right] - 2\sqrt{\sigma' n_0}\, \mathrm{Im}[\xi e^{-i\theta_0}]}{2r_d - 4n_0 u_d + K_d \frac{(\partial_x n_0)^2}{2n_0^2} - 2K_d (\partial_x \theta_0)^2 - 2K_c \partial_x^2 \theta_0} \,. \tag{3.7}$$

In this calculation, we used the generic fact that the mean phase grows linearly with time, whereas the fluctuations grow with the KPZ exponent $t^{1/3}$ in $1d$, and therefore $\delta\theta \ll \theta_0$, as well as $\partial_x^{(n)} \delta\theta \ll \partial_x^{(n)} \theta_0$. We now substitute Eq. (3.7) into Eq. (3.6), and we arrive at an inhomogeneous KPZ equation, which reads

$$\partial_t \delta\theta = \nu(x) \partial_x^2 \delta\theta + \frac{\lambda(x)}{2} (\partial_x \delta\theta)^2 + \sqrt{D(x)} \eta(t,x) + \tilde{v}(x) \partial_x \delta\theta. \tag{3.8}$$

The KPZ parameters are given by

$$\nu(x) = K_d + 2n_0 K_c \tilde{u}(x), \qquad \lambda(x) = 2[-K_c + 2n_0 K_d \tilde{u}(x)] \,, \tag{3.9}$$

where the function $\tilde{u}(x)$ is defined as

$$\tilde{u}(x) = \frac{K_c \left[\frac{(\partial_x n_0)^2}{2n_0^3} - \frac{\partial_x^2 n_0}{2n_0^2} \right] - K_d \frac{(\partial_x n_0)(\partial_x \theta_0)}{n_0^2} - u_c}{K_d \left[\frac{(\partial_x n_0)^2}{2n_0^2} - 2(\partial_x \theta_0)^2 \right] - 2K_c \partial_x^2 \theta_0 + 2r_d - 4u_d n_0}. \tag{3.10}$$

The noise in Eq. (3.8) is defined as $\eta = \zeta / \sqrt{D(x)}$, where ζ is a function of the real and imaginary parts of the complex noise of the gGPe ξ, namely

$$\zeta(t,x) \equiv -2\sqrt{\sigma' n_0}\, \tilde{u}(x) \mathrm{Im}(\xi e^{-i\theta_0}) - \sqrt{\frac{\sigma'}{n_0}} \mathrm{Re}(\xi e^{-i\theta_0}). \tag{3.11}$$

We find $\langle \zeta(t,x) \rangle = 0$, while the noise strength $D(x)$ can be computed from the covariance $\langle \zeta(t,x) \zeta(t',x') \rangle$, under the assumption that

$$\begin{aligned} &\big\langle \mathrm{Re}(\xi(t,x)) \mathrm{Re}(\xi(t',x')) \big\rangle = \big\langle \mathrm{Im}(\xi(t,x)) \mathrm{Im}(\xi(t',x')) \big\rangle = \delta(x-x') \delta(t-t') \\ &\big\langle \mathrm{Re}(\xi(t,x)) \mathrm{Im}(\xi(t',x')) \big\rangle = 0 \,. \end{aligned} \tag{3.12}$$

One finds $\langle\zeta(t,x)\zeta(t',x')\rangle = 2D(x)\delta(x-x')\delta(t-t')$ with

$$D(x) = \frac{\sigma'}{2n_0}\left(1+4\tilde{u}^2(x)n_0^2\right) \tag{3.13}$$

One should note here the presence of an extra term $\tilde{v}(x)\nabla\delta\theta$ in Eq. (3.8), with

$$\tilde{v}(x) = -2K_c\partial_x\theta_0 + 4n_0K_d\tilde{u}(x)\partial_x\theta_0 + K_d\frac{\partial_x n_0}{n_0} + 2K_c\tilde{u}(x)\partial_x n_0\,, \tag{3.14}$$

however, we argue that this term is zero due to the parity symmetry of the confinement potentials used in our analysis. More explicitly, since $V(x)$ is symmetric under $x\to -x$, it follows that $\theta(t,x)$ and $n(t,x)$ are both even functions of x. It follows from Eq. (3.14) then, that the function $\tilde{v}(x)$ is an odd function of x. We are interested in the behavior of the phase profile around the central tip at $x=0$, since away from it the profile is more strongly influenced by the drag at the boundaries and is not expected to follow the KPZ dynamics. Thus, around the central tip at $x\simeq 0, \tilde{v}(x)\simeq 0$ (odd function) and the extra term $\tilde{v}(x)\partial_x\delta\theta$ can be neglected in Eq. (3.8). One finally recovers the KPZ equation with x-dependent coefficients.

3.4 Influence of the confinement potential

In order to test the robustness of our proposal to engineer a curved phase profile, we investigate the influence of the precise shape of the confining potential by studying two different potentials: a harmonic potential, as well as Gaussian walls,

$$V_H(x) = \frac{1}{2}m\omega_0^2x^2\,, \tag{3.15a}$$

$$V_G(x) = \frac{V_0}{\ell}\left(e^{-(\frac{x-L/2}{\ell})^2}+e^{-(\frac{x+L/2}{\ell})^2}\right). \tag{3.15b}$$

The trap frequency ω_0 in V_H is adjustable, and we found that the most favorable conditions for studying KPZ universal properties are achieved when the potential is a very shallow parabola, and we set $\omega_0\simeq 4\times 10^{-4}\gamma_0$. Regarding V_G, it can be seen that it interpolates, for a given strength V_0, between a hard-wall potential $V_{G,1}$ for $\ell\to 0$ and a smooth-wall potential $V_{G,2}$ for $\ell\gg 0$, as illustrated in Fig. 3.1. Note that in the simulations, since ℓ is expressed in units of the characteristic length l_0, $\ell<1$ effectively corresponds to the $\ell\to 0$ limit. Typical phase profiles obtained for the hard-wall potential $V_{G,1}$ ($\ell=0.01$), the smooth Gaussian walls $V_{G,2}$ ($\ell=100$), the shallow harmonic potential, and without any confinement, are shown in Fig. 3.2. The hard-wall potential initially only affects the boundaries and then slowly bends the phase profile. For larger values of ℓ, a larger portion of the phase profile immediately feels the potential, and the

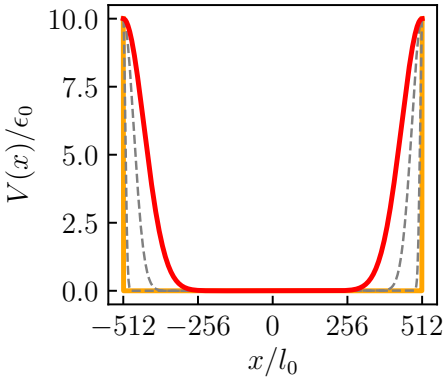

FIGURE 3.1: Gaussian walls potential for different values of the parameter $\ell = 0.01, 10, 50, 100$, which interpolates between hard walls ($\ell = 0.01$, yellow) and smooth walls ($\ell = 100$, red). The ratio $V_0/\ell = 10$ is kept constant.

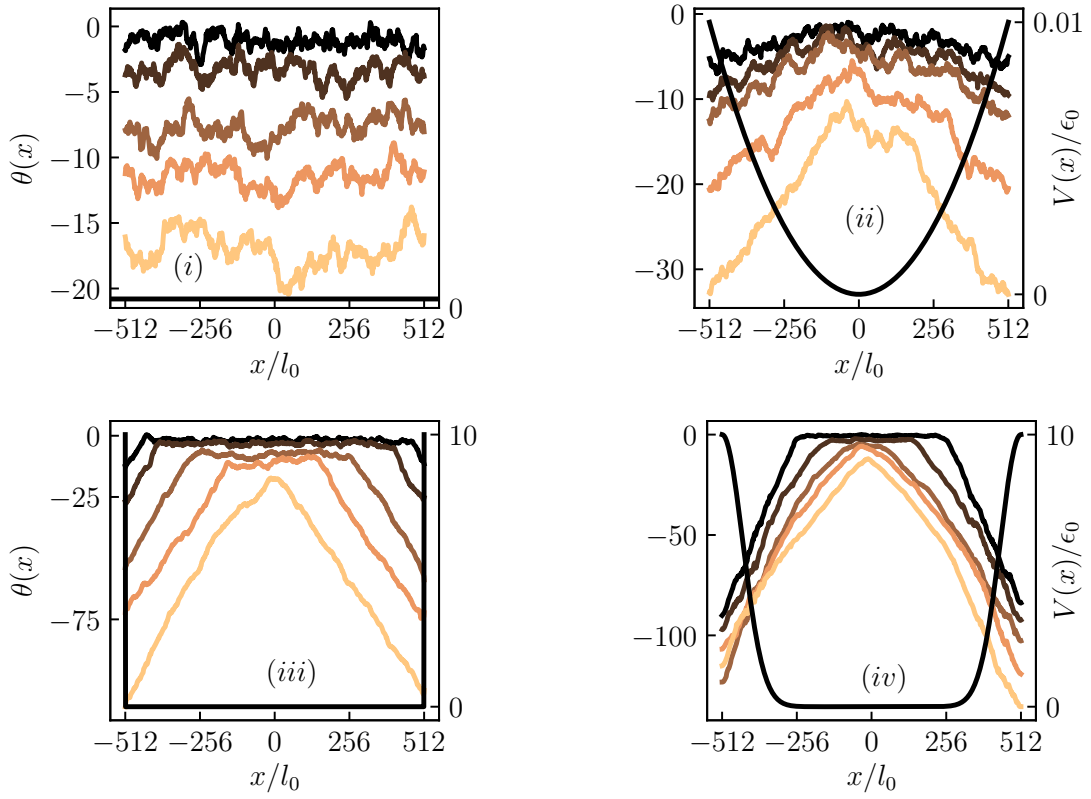

FIGURE 3.2: Typical phase profiles at different times during the evolution, with lighter colours corresponding to larger times, together with the relevant potentials (black smooth curves). (i) Absence of confining potential, leading to a flat profile, (ii) presence of the parabolic confining potential V_H, (iii) $V_{G,1}$ ($\ell = 0.01$), and (iv) $V_{G,2}$ ($\ell = 100$). Note that for the latter we averaged over 6 realizations of the noise in order to stabilize the profile, leading to a profile which displays gradual bending due to the effective drag at the boundaries, as explained in the text.

bending occurs more rapidly. With this potential, the phase profile displays a smoother curvature around the central tip at short times. However, for all values of ℓ, at late

times, a cusp forms at the central tip and the phase is no longer smoothly curved, which is also true for the harmonic potential. The KPZ regime is thus expected to develop only at intermediate times for both types of confining potentials, and not necessarily in the asymptotic limit of very large times, as we will illustrate below.

3.4.1 Scaling of the variance

In order to assert the presence of the KPZ regime, we first study the scaling of the variance of the phase profile $\langle \Delta\theta(t, x_0)^2 \rangle$ at various space points x_0, with

$$\Delta\theta(t, x = x_0) = \theta(t, x_0) - \langle \theta(t, x_0) \rangle \ , \tag{3.16}$$

and where $\langle ... \rangle$ denotes the average over noise realisations. This quantity is expected to behave as $\left\langle \Delta\theta(t, x_0)^2 \right\rangle \sim t^{2/3}$ if the dynamics is in a KPZ regime. Our results are displayed in Fig. 3.3 for both $V_{G,2}, V_H$. For the former, one observes a KPZ dynamics

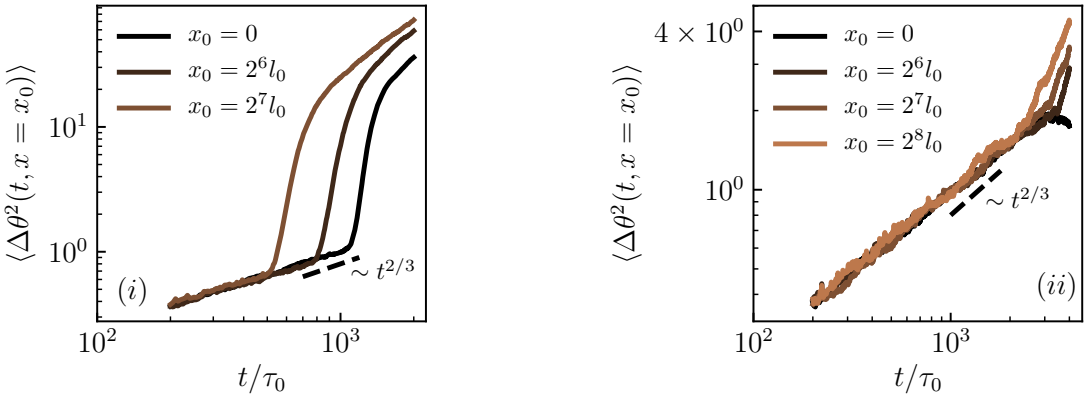

FIGURE 3.3: Variance of the phase computed at different x_0 for the evolution with (i) $V_{G,2}$ and (ii) V_H. The KPZ scaling persists for longer times around the central tip for the latter potential.

at short and intermediate time, before a sharp crossover occurs to another regime at long times. The time of the crossover depends on the location on the phase profile. It corresponds at $x = 0$ to the time where the cusp is formed, and this is where the KPZ regime is the most extended in time. It is also clear that the KPZ scaling extends over a longer time for the parabolic potential, thus deeming it more favorable to study the KPZ dynamics. However, we found that even with Gaussian walls, the KPZ advanced statistics can still be precisely observed, as shown below. We focus in the following on the central tip $x = 0$ (for one-point statistics), and hence omit the arguments.

3.4.2 Results for shallow harmonic potential

3.4.2.1 Validity of the mapping to the inhomogeneous KPZ equation

In the case where $V(x) = 0$, one recovers the standard mapping to the homogeneous KPZ equation where the KPZ parameters Eqs. (3.9, 3.13) are constant. With a non-vanishing potential V_H, these parameters continuously vary with space. Such a variation crucially affects the dynamics, since the average velocity of the phase $\frac{\partial \langle\theta\rangle}{\partial t}$ is proportional to the KPZ non-linearity λ. Qualitatively, when $V \neq 0$, the non-linearity is larger where the potential is stronger. Therefore, we expect that the condensate phase profile will be effectively dragged, as was already seen in Fig. 3.2. Let us note that for such a shallow potential, the spatial variation of the KPZ parameters in Eqs. (3.9, 3.13) is small, and in the vicinity of $x = 0$ one finds $\nu(x) \simeq \nu_{\text{flat}}, \lambda(x) \simeq \lambda_{\text{flat}}, D(x) \simeq D_{\text{flat}}$, as shown in Fig. 3.4.

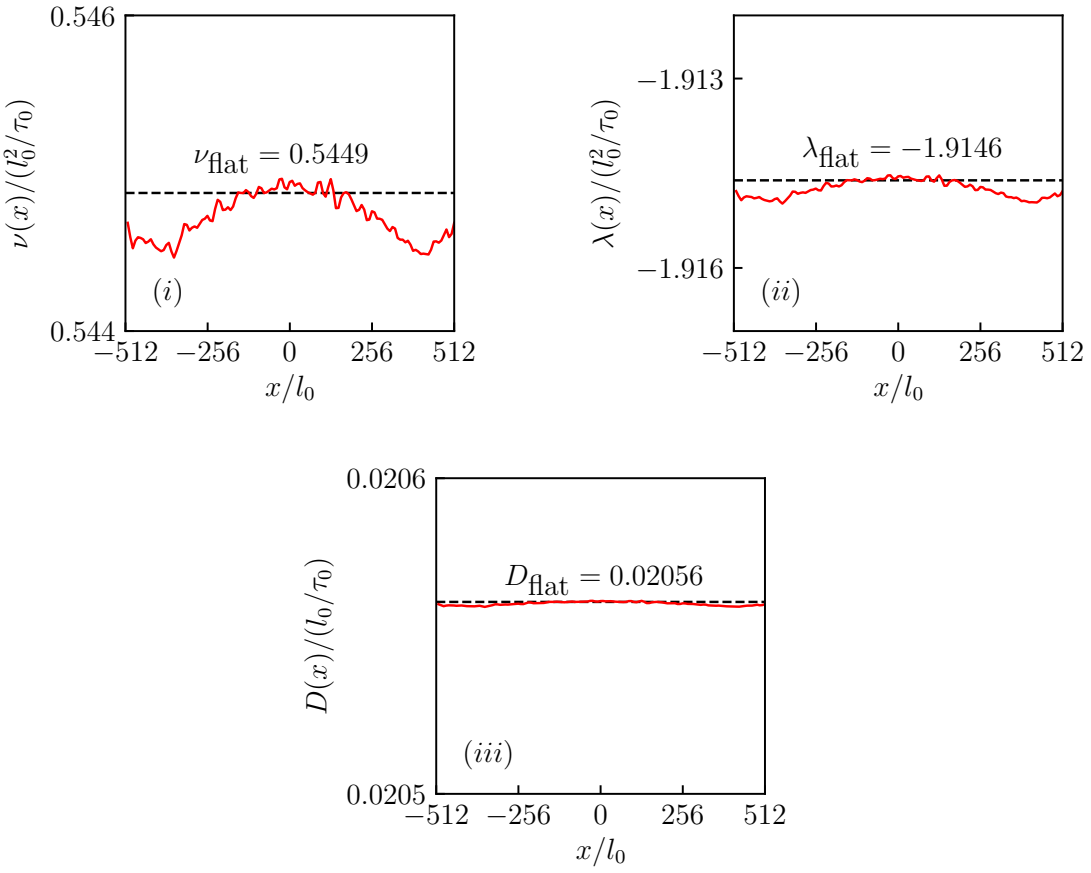

FIGURE 3.4: KPZ parameters $\nu(x), \lambda(x), D(x)$ obtained for the harmonic potential V_H after performing the average within the KPZ time window (see text), denoted by the overline bar, after restoring the original units. Their spatial variation is very smooth for this choice of confining potential and their values in the vicinity of the central point are very close to the homogeneous ones.

We now assess whether the assumptions underlying the calculation in section 3.3 are fulfilled for this type of potential. To this end, we compute the spatial profiles of the zeroth-order solutions for the EP system (n_0, θ_0), the density fluctuations δn, the first spatial derivatives $\partial_x \overline{n_0}, \partial_x \overline{\delta n}, \partial_x \overline{\theta_0}$ (with the bars denoting time averages) and the curvature of the phase $\partial_x^2 \overline{\theta_0}$. The zeroth-order solutions are obtained as $n_0(t,x) = \langle n(t,x) \rangle$ and $\theta_0(t,x) = \langle \theta(t,x) \rangle$ at any given t. The density fluctuations are then defined as $\delta n(t,x) = n(t,x) - n_0(t,x)$, and the spatial derivatives are computed numerically. Typical results are displayed in Fig. 3.5 for the density, and Fig. 3.6 for the spatial derivatives and the curvature. These results demonstrate that the time dependence of n_0, θ_0 is neg-

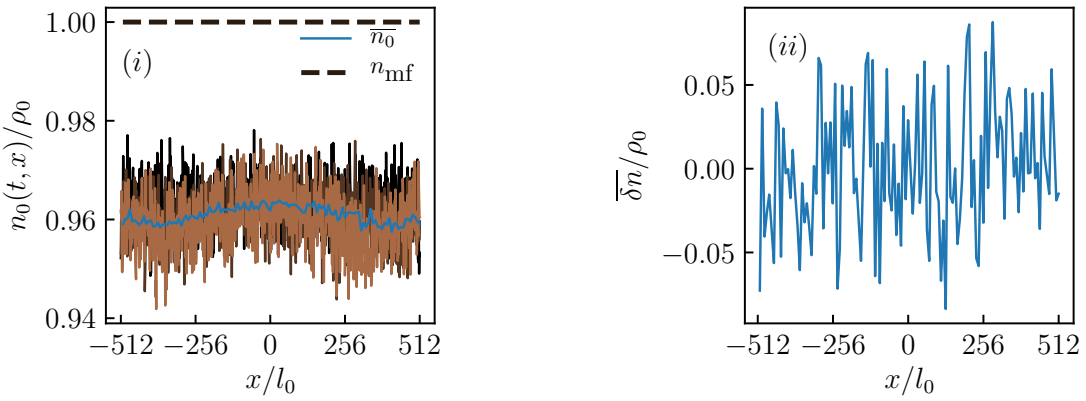

FIGURE 3.5: (i) Zeroth-order spatial density profile $n_0(t,x)$ for $t/\tau_0 = 200, 1400, 2000$ with lighter colours corresponding to larger times, together with the theoretical prediction $n_{\mathrm{mf}} = \rho_0 r_d / u_d$ obtained in the homogeneous case for the same parameters (dashed) and the time average $\overline{n_0}$ (blue) in the time window in which we observe KPZ dynamics (see section 3.4.2.3), which extends approximately from $t/\tau_0 = 1400$ until $t/\tau_0 = 1600$. (ii) Time averaged spatial density fluctuations $\overline{\delta n}$ in the same window.

ligible near $x = 0$ for the relevant time window in which KPZ behavior is observed, which we will show in sections 3.4.2.2, 3.4.2.3, 3.4.2.4, hence it is justified to perform a time average of θ_0 recorded in this window, denoted by the overline bar. The curvature is then found to be a negative constant near $x = 0$ as expected. Lastly, $\delta n \ll n_0$ and $\partial_x \delta n \simeq 0$, hence our assumptions are consistent.

3.4.2.2 Scaling of the first-order correlation function of the condensate wavefunction

The KPZ scaling properties can be studied directly from the first-order correlation function of the EP condensate wavefunction,

$$g_1(\Delta t, \Delta x) = \frac{|\langle \psi^*(t+\Delta t, x+\Delta x)\psi(t,x)\rangle|}{\left\langle \sqrt{n(t+\Delta t, x+\Delta x)n(t,x)} \right\rangle}, \tag{3.17}$$

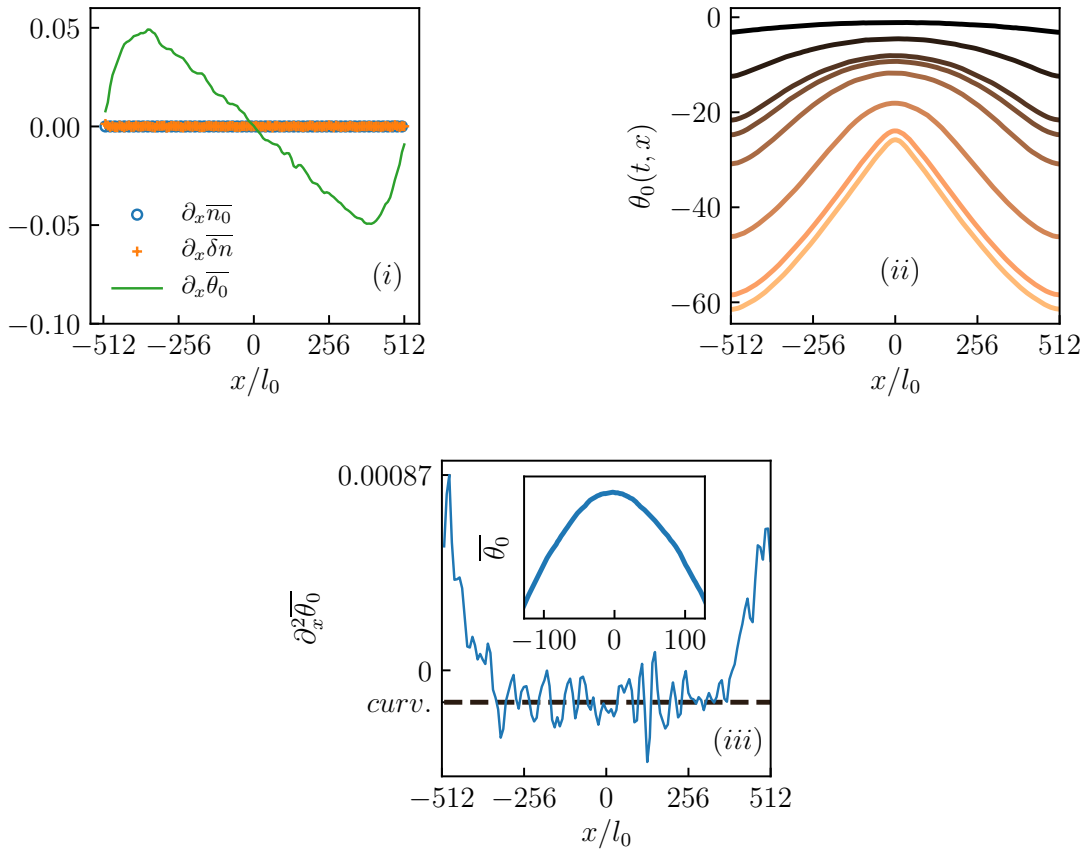

FIGURE 3.6: (*i*) Comparison of spatial derivatives $\partial_x\overline{n_0}, \partial_x\overline{\delta n}, \partial_x\overline{\theta_0}$. For the shallow harmonic potential, $\overline{n_0}$ turns out to be very close to n_{mf} and its spatial derivative can be neglected. (*ii*) Zeroth-order phase profile $\theta_0(t,x)$ for $t/\tau_0 = 200, 800, 1400, 1600, 2000, 3000, 3800, 4000$, with lighter colours corresponding to later times, demonstrating very slow time dependence in the vicinity of $x = 0$ within the KPZ time window, and (*iii*) its curvature after performing a time average in the KPZ window. By fitting the data near $x = 0$, we estimate the curvature to be approximately equal to 1.4×10^{-4} (dashed line).

Note that the first-order coherence g_1 is routinely measured in EP experiments, rendering the following analysis easily accessible. By neglecting the density-phase correlations and performing a cumulant expansion, one can relate g_1 to the connected correlation function of the phase C, obtaining to first order

$$-2\ln\left[g_1(\Delta t,\Delta x)\right] = \left\langle\left[\theta(t+\Delta t,x+\Delta x)-\theta(t,x)\right]^2\right\rangle - \left\langle\theta(t+\Delta t,x+\Delta x)-\theta(t,x)\right\rangle^2 \equiv C(\Delta t,\Delta x)\,. \tag{3.18}$$

If the phase follows the $1d$ KPZ dynamics, it should endow the Family-Vicsek scaling form [38]

$$C(\Delta t,\Delta x) = C_0\Delta t^{2/3}F_{1d}\left(y_0\frac{\Delta x}{\Delta t^{2/3}}\right)\,, \tag{3.19}$$

where $F_{1d}(y)$ is a universal scaling function and C_0, y_0 are non-universal normalisation parameters defined as

$$y_0 = (2A\lambda^2)^{-1/3},\ C_0 = \Gamma^{2/3},\ \text{where } A = \frac{D}{\nu},\ \Gamma = \frac{\lambda}{2}A^2\,, \tag{3.20}$$

where the numerical prefactors are conventional. The precise form of the scaling function $F_{1d}(y)$ is known exactly only for the stationary interface [79]. However, the scaling function satisfies the same asymptotics in all sub-classes

$$F_{1d}(y) \overset{y\to 0}{\longrightarrow} F_{1d,0}\,,\quad F_{1d}(y) \overset{y\to\infty}{\sim} 2y\,, \tag{3.21}$$

where $F_{1d,0}$ is a universal constant that depends on the geometrical sub-class, and whose values are known exactly. Therefore, one expects similar behavior for the scaling functions in the three sub-classes, apart from small vertical shifts reflecting the differences in $F_{1d,0}$ and thus small changes in the intermediate crossover region between the two asymptotic limits. In our simulations, we determined $C(\Delta x, \Delta t)$ from the wavefunction correlation function g_1 using Eq. (3.18). We first estimated the KPZ scaling exponents with and without the confining potential by studying the equal-time and equal-space correlation functions, which, according to Eqs. (3.19, 3.21), should behave as

$$C(\Delta t = 0, \Delta x) \sim A\Delta x^{2\chi}, \tag{3.22a}$$

$$C(\Delta t, \Delta x = 0) \sim F_{1d,0}\Gamma^{2/3}\Delta t^{2\beta}\,, \tag{3.22b}$$

with $\chi = 1/2$ and $\beta = 1/3$ the $1d$ KPZ roughness and growth critical exponents. We found $\chi = 0.49 \pm 0.01$ and $\beta = 0.30 \pm 0.01$ in both the flat and the curved cases for the purely spatial and purely temporal correlations, see Fig. 3.7. The value of the growth exponent β slightly differs from the theoretical one but it is comparable with values reported in previous studies of EP condensate for this system size [159] for the flat geometry. Furthermore, one can extract the value of the parameter A defined in Eq. (3.22a) from the spatial correlation. We find

$$A \simeq \begin{cases} 0.032 l_0^{-1}, & \text{curved geometry} \\ 0.035 l_0^{-1}, & \text{flat geometry.} \end{cases} \tag{3.23}$$

These values can be compared with the theoretical one $A_{\text{th}} \equiv D/\nu$. For the flat case, D and ν are related to the microscopic parameters through Eqs. (3.9, 3.13) with $\partial_x\theta_0 = 0$ and $n_0 = n_{\text{mf}} = \rho_0 r_d/u_d$. One finds $A_{\text{th}} \simeq 0.0377 l_0^{-1}$, which is in very close agreement with the value extracted from the spatial correlation. For the curved case, we focus on spatial points around the central tip. As shown in Fig. 3.4, although the parameters D and ν depend on x, they are nearly constant in the vicinity of $x = 0$ and very close to

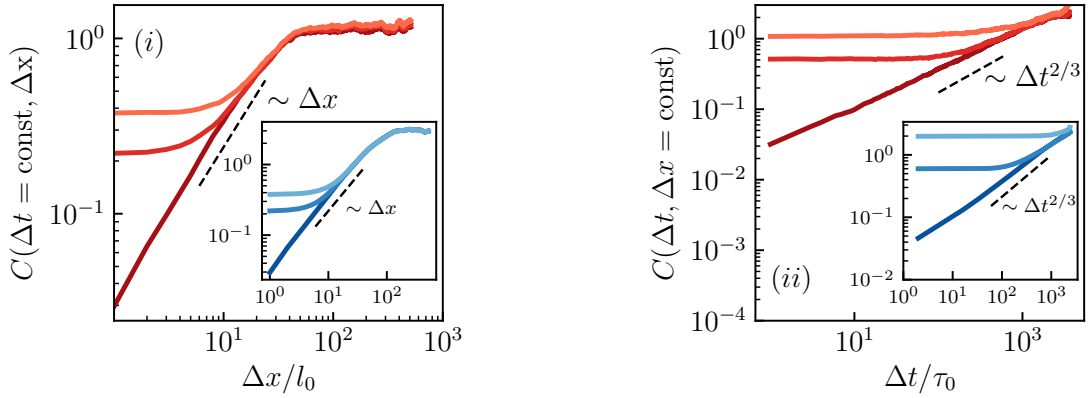

FIGURE 3.7: (i) Purely spatial and (ii) purely temporal correlation functions, with the scaling laws as guide to the eye for each case (dashed lines), for the curved (main plots) and flat (insets) geometries. We display three curves which correspond to different fixed values of temporal and spatial separation, $\Delta t/\tau_0 = 0, 40, 100$ and $\Delta x/l_0 = 0, 16, 64$ (darker to lighter shades).

the values for the flat case, hence one finds $A(x) \simeq A(x=0) \simeq A_{\text{flat}}$. The procedure we followed for determining the parameter Γ is outlined in Appendix A.

Let us now construct the universal scaling function $F_{1d}(y)$ defined in Eq. (3.19). For this, we first selected all the data points lying in the correct scaling regime by filtering out the points differing by more than small cutoffs ϵ_x, ϵ_t from the expected scaling laws in Eqs. (3.22a, 3.22b) for each value of spatial and temporal separation. The scaling function is then obtained by plotting $C(\Delta t, \Delta x)/(C_0 \Delta t^{2/3})$ as a function of $y_0 \Delta x/\Delta t^{2/3}$. The results are displayed in Fig. 3.8 together with the theoretical curve $F_{1d,\text{stat}}(y)$ for the stationary case [79]. For both the flat and the curved cases, we observe a reasonable collapse of all the data points onto a single function F_{1d}, which demonstrates that C indeed takes a scaling form. Additionally, we confirm that the scaling functions F_{1d} are quite similar for the three cases. However, it is not a perfectly one-dimensional curve, it has a finite (small) thickness, and the numerical values for $F_{1d,0} = F_{1d}(0)$ differ of about $\sim 40\%$ from the theoretical exact values in both the flat and curved cases ($F^{\text{num}}_{1d,\text{flat}}(0) \simeq 0.95$ vs $F^{\text{th}}_{1d,\text{flat}}(0) = 0.63805...$, $F^{\text{num}}_{1d,\text{curved}}(0) \simeq 1.23$ vs $F^{\text{th}}_{1d,\text{curved}}(0) = 0.8132...$). These discrepancies may originate from the fact that the actual growth exponent is slightly smaller than the theoretical one, and also from the fact that the g_1 function includes other contributions beside the phase correlations, even if they are assumed to be small (higher-order cumulants of the phase or density-phase correlations). However, we emphasise that the values of these constants are clearly distinct in the two cases, and their ratio (or relative difference) turns out to be within 3% accuracy with the theoretical ratio (or relative difference). This indicates that the

mapping from the Gross-Pitaevskii to the KPZ equation is well-grounded, and that both the flat and the curved universality sub-classes can be probed in EP systems.

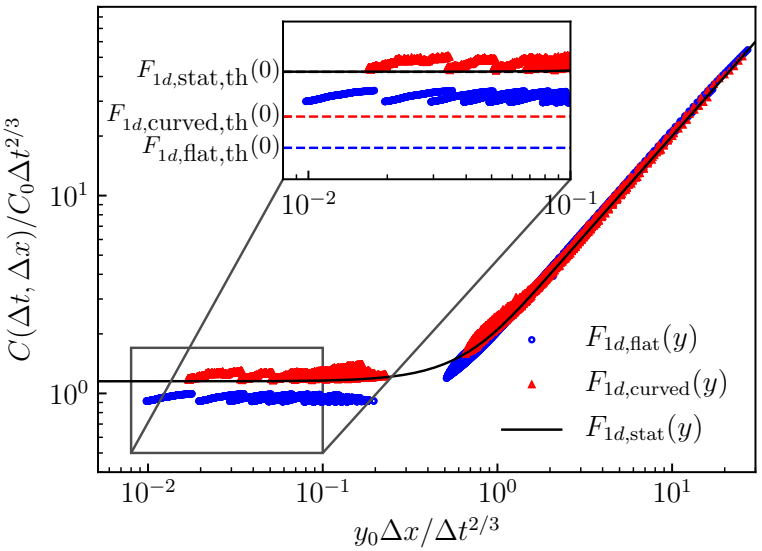

FIGURE 3.8: Universal scaling function $F_{1d}(y)$ for the flat (blue dots) and curved (red triangles) phase profiles. The theoretical result for the stationary interface $F_{1d,\mathrm{stat}}(y)$ is shown for comparison (solid line). The theoretical values $F^{\mathrm{th}}_{1d,\mathrm{flat}}(0) = 0.63805...$, $F^{\mathrm{th}}_{1d,\mathrm{curved}}(0) = 0.8132...$, $F^{\mathrm{th}}_{1d,\mathrm{stat}}(0) = 1.15039...$ are indicated in the inset, together with the two numerical curves for $y_0\Delta x/\Delta t^{2/3} \to 0$.

3.4.2.3 One-point statistics of the phase fluctuations

As we discussed in section 1.3.2, the global geometry of the growth influences various statistical properties, thus partitioning the KPZ universality class into distinct sub-classes which share the same critical exponents. In particular, we saw that the statistics of rescaled height fluctuations at a fixed space point x_0 in the long-time limit correspond to the TW-GOE, or to the TW-GUE distribution, if the interface is flat, or circular, respectively. We now probe this in the context of EP, in which we saw that the roughening interface is the phase profile. More precisely, as the phase profile propagates linearly in time with fluctuations growing as $t^{1/3}$, one introduces the rescaled fluctuation field χ, defined from the long time behavior of the phase in $1d$,

$$\theta(t,x) \to \omega_\infty t + (\Gamma t)^\beta \, \chi(t,\zeta)\,, \tag{3.24}$$

where ω_∞ is the asymptotic frequency of the phase, which has a non-trivial dependence on the KPZ parameters [161], and ζ is the spatial coordinate rescaled by the correlation length of fluctuations $\zeta \equiv x/\xi(t)$ with $\xi(t) = (\Gamma t)^{2/3}\frac{2}{A}$ [162]. We focus on the universal statistical properties of the centered unwound phase $\Delta\theta(t,x_0) = \theta(t,x_0) - \langle\theta(t,x_0)\rangle$.

This corresponds to the statistical properties of the field $\chi(t, x_0/\xi(t))$.

We first perform a study of the higher-order cumulants of $\Delta\theta(t, x_0)$. This is because, in order to compare the probability distribution of the rescaled phase fluctuations and their correlation function to the theoretical ones, the normalisations must be fixed, which involve Γ. We computed Γ in Appendix A, by choosing the value of $\mathrm{Var}(\chi)$, whether the GOE or the GUE one, and thus to guess a priori which of the sub-class is realised. However, let us emphasise that the sub-class can be determined without any prior knowledge by computing universal ratios of cumulants, which are independent of the normalisations. More specifically, we compute the third and fourth order cumulants of the centered phase $\langle\Delta\theta^3\rangle_c \equiv \langle\Delta\theta^3\rangle$ and $\langle\Delta\theta^4\rangle_c \equiv \langle\Delta\theta^4\rangle - 3\langle\Delta\theta^2\rangle^2$. From them, one can construct the skewness $\mathrm{sk}(\Delta\theta) = \langle\Delta\theta^3\rangle_c / \langle\Delta\theta^2\rangle^{3/2}$ and excess kurtosis $\mathrm{ku}(\Delta\theta) = \langle\Delta\theta^4\rangle_c / \langle\Delta\theta^2\rangle^2$, which are universal. They can be compared with the theoretical values for $\mathrm{sk}(\chi)$ and $\mathrm{ku}(\chi)$ which are known exactly for both the GOE and GUE distributions [76] and do not depend on the non-universal parameters ω_∞ or Γ. Our

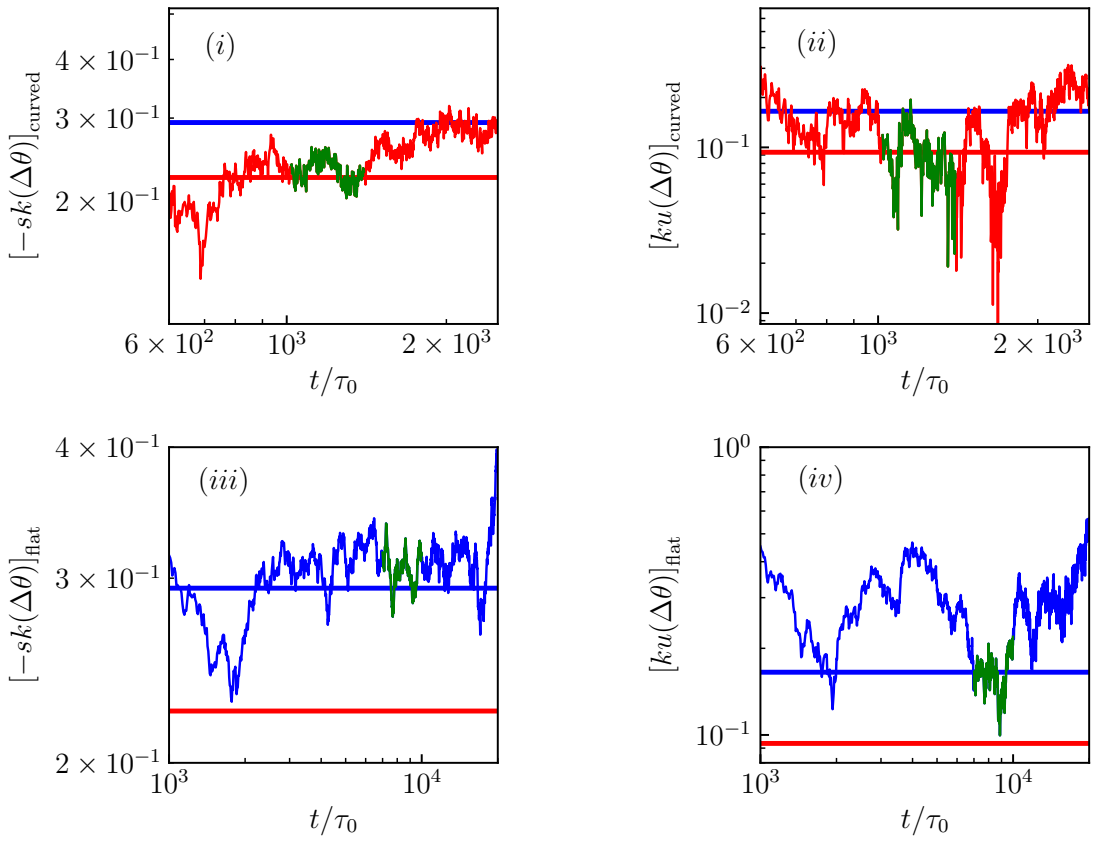

FIGURE 3.9: Skewness and excess kurtosis of the centered unwound phase field of the condensate in the (i, ii) curved and (iii, iv) flat geometries, together with the theoretical values corresponding to the TW-GOE (blue) and TW-GUE distribution (red). We also display the universal plateaus reached for each geometry (green).

results are presented in Fig. 3.9 for both geometries, where the curved one corresponds to evolution under the shallow harmonic potential V_H from Eq. (3.15a). Let us note that the sign of the skewness $sk(\Delta\theta)$ corresponds to the sign of the KPZ non-linearity λ, which is negative for our choice of experimental parameters.

For the flat geometry, since the profiles are homogeneous, we performed an additional spatial average in order to accumulate statistics. We find convergence to the anticipated values for both cases, in particular for the skewness, in the same time windows as for the variance corresponding to the KPZ regime. For the curved geometry, we observe at large times a departure from the stationary plateaus which correspond to KPZ universality, in line with previous observations. The excess kurtosis, which involves the determination of the fourth-order cumulant, is naturally less statistically tame, even for the case of the curved geometry where averaging over 10.000 independent realisations of the noise has been performed at the chosen space point $x = 0$.

These results are an independent confirmation that the fluctuations of the phase with or without confinement follow two different distributions, and their skewness and excess kurtosis coincide with the ones expected for a curved or flat geometry respectively. This justifies a posteriori the choice of $\mathrm{Var}(\chi)$ in section 3.4.2.2. Let us emphasise that these quantities may be easier to measure experimentally and could be used as a direct probe of the strong non-Gaussianity of the distributions, and also of the existence of different universality sub-classes for these distributions.

We now compute the rescaled fluctuation field χ from $\Delta\theta$ following Eq. (3.24), at the plateaus shown in Fig. 3.9. Note that for the flat case, we conform to the standard definition of the TW-GOE random variable found in the literature, and further rescale χ as $\chi \to 2^{-2/3}\chi$. We construct the histograms of χ both for the flat case without confinement and for the curved case with the confining potential V_H from Eq. (3.15a). The resulting distributions are displayed in Fig. 3.10, where they are compared with the theoretical distributions. We note that the negative sign of the non-linearity λ implies that the comparison should be against the mirror distributions $P_{\text{TW-GOE}}(-\chi)$ and $P_{\text{TW-GUE}}(-\chi)$. One observes a clear distinction between the two cases, and moreover the distribution for the curved case is in excellent agreement with the TW-GUE distribution, thus demonstrating that one can indeed tune the KPZ geometrical sub-class realised in the EP system.

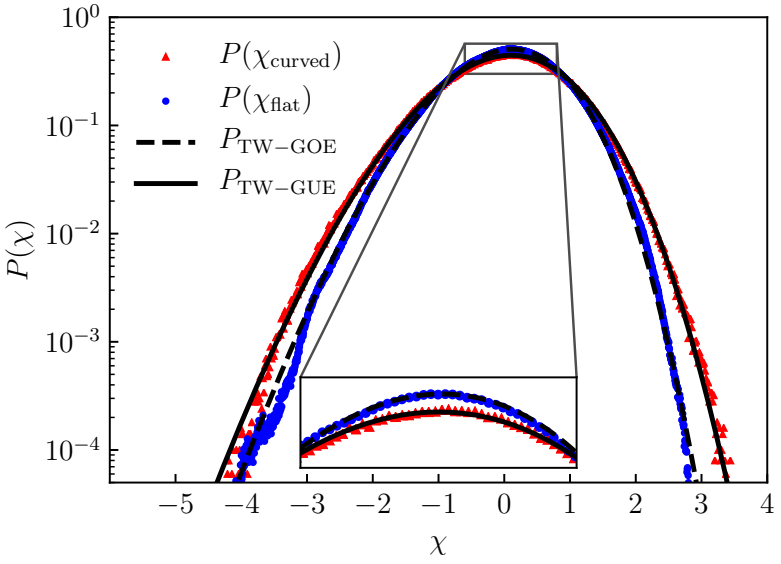

FIGURE 3.10: Centered distribution of the rescaled phase fluctuations χ sampled at $x = 0$, for flat (blue dots) and curved (red triangles) phase profiles, together with the theoretical TW-GOE and TW-GUE distributions.

3.4.2.4 Two-point statistics of the phase fluctuations

After establishing a clear distinction in terms of one-point statistics of the phase fluctuations in the two geometries, manifesting in a very good agreement with the Tracy-Widom distributions, we now study the two-point statistics of the phase fluctuations, where the curved geometry is again realised by V_H.

In our simulations, we computed the correlation function of the rescaled phase fluctuations, in a similar manner as is done for the height fluctuations in Eqs. (1.25, 1.26). More specifically, we have

$$C_\chi(\Delta\zeta) = \frac{\langle \Delta\theta(t,x)\Delta\theta(t,x+\Delta x)\rangle}{(\Gamma t)^{2/3}} \,. \tag{3.25}$$

As we discussed in section 1.3.2.2, for a KPZ interface, these correlations correspond to the time correlation function of the Airy_1, respectively Airy_2 process in the asymptotic limit, in the flat, respectively curved geometry

$$C_\chi(\Delta\zeta) = \mathcal{G}_i(\Delta\zeta) = \left\langle \mathcal{A}_i(t'+\Delta\zeta)\mathcal{A}_i(t')\right\rangle \,, \tag{3.26}$$

where $i = 1, 2$ stands for Airy_1, respectively Airy_2, processes. The results we obtained for the two geometries are presented in Fig. 3.11. We note that in line with the rescaling

of χ in the flat case mentioned in section 3.4.2.3, we also perform in this case the following rescaling $t \to t/2^{-2/3}$ and $\mathcal{G}_1 \to \mathcal{G}_1/2^{-2/3}$ to conform to the standard definition of the Airy$_1$ process [63] and compare with the theoretical results from [85]. Furthermore, in the curved geometry, the limit stochastic process is shown to be $\chi_{\text{curved}}(\zeta, t) \xrightarrow{d} \mathcal{A}_2 - \zeta^2$, where $-\zeta^2$ reflects the influence of the mean profile [78], which is automatically subtracted in our case since we consider the connected function. For the flat case, we

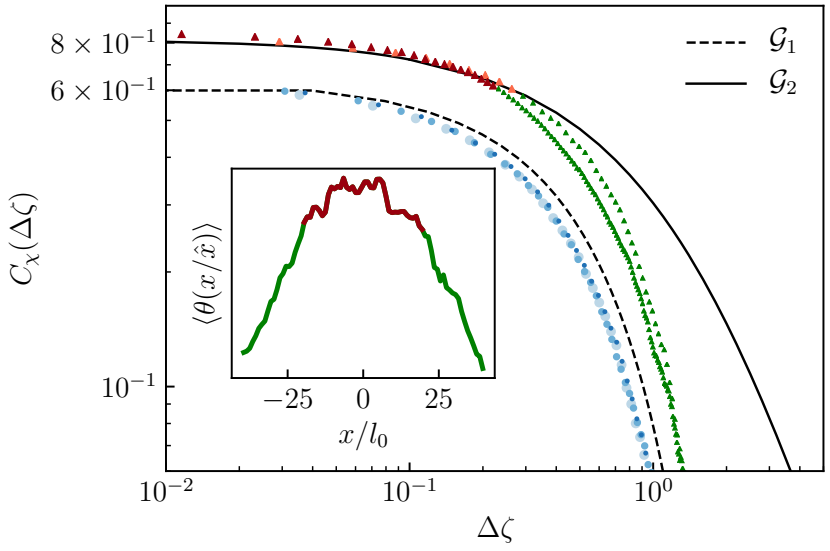

FIGURE 3.11: Correlation function C_χ of the rescaled phase fluctuations as a function of the rescaled length $\Delta\zeta$ for different times for the flat case (blue dots) and for the curved case (green and orange triangles), together with the theoretical results for the correlation of the Airy$_1$ $\mathcal{G}_1(\Delta\zeta)$ (dashed line) and Airy$_2$ $\mathcal{G}_2(\Delta\zeta)$ (solid line) processes presented in [85, 163, 164]. For the flat phase profile, data corresponding to times $t/\tau_0 = 7.5 \times 10^3, 8.125 \times 10^3, 1 \times 10^4$ is shown, and for the curved phase profile, data corresponding to $t/\tau_0 = 4 \times 10^2, 1.6 \times 10^3$ is shown (lighter to darker colors correspond to increasing times). For the curved case, the red shades correspond to the small $\Delta\zeta$ regime where the phase profile is locally curved, while green correspond to large $\Delta\zeta$, where the profile is shaped by the effective drag – see inset.

observe that the correlation function is stable in time, from $t/\tau_0 = 7 \times 10^3$ to, approximately, $t/\tau_0 = 1 \times 10^4$ and we find a good agreement with the theoretical Airy$_1$ correlations $\mathcal{G}_1(\Delta\zeta)$, even for large ζ. The small shift visible in the figure can be traced back to the fact that the parameter Γ in Eq. (3.25) is extracted from the numerical simulations and is found to be a bit larger than the theoretical value (see Appendix A).

For the curved case, the correlation function is stable over a time window from $t/\tau_0 = 4 \times 10^2$ until $t/\tau_0 = 1.6 \times 10^3$ where the KPZ scaling regime is observed. We focus on the small$-\Delta\zeta$ limit, corresponding to small spatial separation around $x = 0$. Indeed, we expect a local curvature only around the central tip, since the profile near the boundaries is affected by the effective drag ensuing from the confining potential. The

phase correlations are found to behave as an Airy_2 process only over this limited range of space, but the agreement with the theoretical Airy_2 correlations $\mathcal{G}_2(\Delta\zeta)$ on this range is extremely satisfactory.

3.4.3 Results for smooth Gaussian walls

We computed the probability distribution and the correlation of the rescaled height fluctuation field χ for the smooth Gaussian walls $V_{G,2}$, in the same spirit as sections 3.4.2.3 and 3.4.2.4, respectively. The results are displayed in Figs. 3.12 and 3.13, to be compared with the corresponding Figs. 3.10 and 3.11, where the curvature was achieved by using the shallow parabolic potential V_H. We note here that the parameter Γ was computed separately for this case, following the procedure outlined in Appendix A, but the parameter was taken to correspond to the theoretical prediction $A = A_{\text{th}} = D/\nu$. One

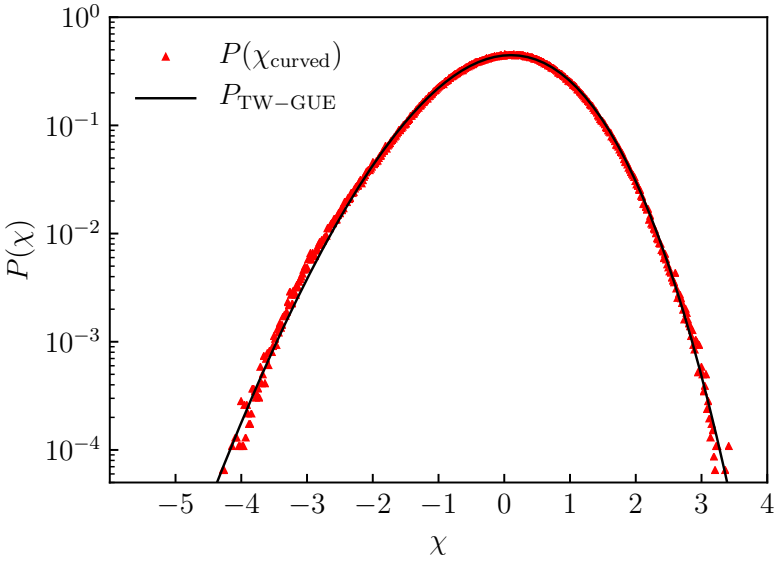

FIGURE 3.12: Centered distribution of the rescaled phase fluctuations χ sampled at $x = 0$, for the curved phase profile with $V_{G,2}$, together with the theoretical TW-GUE distribution.

observes that the probability distribution still follows with great accuracy a TW-GUE distribution, as for the parabolic potential, although the time window of the KPZ dynamics is shorter. We also computed the probability distribution of the rescaled phase fluctuations for the hard-wall potential $V_{G,1}$, and the agreement is as remarkable, the two curves being in fact superimposed. For the two-point statistics, the agreement with the theoretical curve for the Airy_2 process is still satisfactory for small $\Delta\zeta$. As for V_H, the phase acquires a smooth curvature only around the central point, such that the spatial region where the universal properties of the KPZ curved sub-class can be observed has a limited extension.

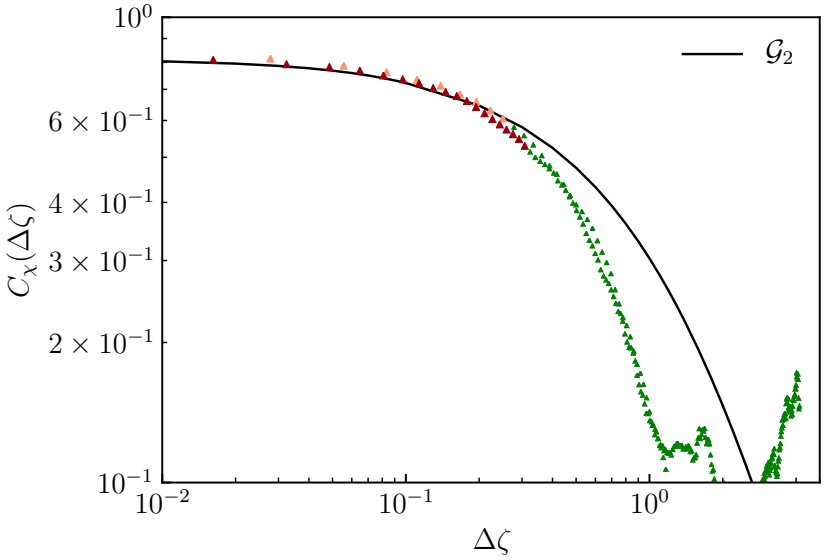

FIGURE 3.13: Correlation function C_χ of the rescaled phase fluctuations as a function of the rescaled length $\Delta\zeta$ for the curved phase with $V_{G,2}$, together with the theoretical results for the correlation $\mathcal{G}_2(\Delta\zeta)$ of the Airy_2 process. Data corresponding to times $t/\tau_0 = 4 \times 10^2$ (orange triangles), 9×10^2 (red triangles) is shown. The red shades roughly correspond to the small $\Delta\zeta$ regime where the phase profile is locally curved, while green correspond to large $\Delta\zeta$, where the profile is shaped by the effective drag, in the same spirit as for Fig. 3.11.

3.5 Conclusions

In this chapter, we have shown that by engineering the confining potential of $1d$ exciton polaritons one can tune the geometry of the phase of the condensate and thus access both the flat and curved KPZ universality sub-classes. In particular, we have found excellent agreement with the theoretical exact results, not only for the scaling properties, but also at the level of one-point statistics (probability distributions). Additionally, we performed the very first analysis of a very fine statistical quantity, for both the flat and the curved phase geometry: We probed the reduced correlations, which are the subleading behavior emerging once the dominant scaling one (studied in section 3.4.2.2) has been subtracted. In this respect, the agreement found with the theoretical results for the Airy processes is remarkable, albeit only locally for the curved case since the condensate phase is only curved on a limited range by the confining potential. The results presented here strongly confirm the relevance of KPZ dynamics for the EP system, as KPZ universal properties emerge from the microscopic Gross-Pitaevskii model in all levels we explored.

We note that the KPZ statistics related to the curved geometry are found to be nearly

insensitive to the precise form of the confining potential, thus highlighting the robustness of our protocol. Therefore, our findings pave the way for stimulating new protocols for investigating KPZ universality in experiments, since the KPZ sub-classes can be accessed through simple engineering of the EP system. In particular, harmonic confinement can be implemented by a suitable engineering of the pumping mechanism [165]. Whereas probing the scaling properties is readily accessible from the measurement of the first-order correlation function, the experimental determination of the probability distributions may be more challenging as it involves the measurement of the time and space resolved phase of the condensate. This requires the development of specific interferometric techniques capable of resolving very small times. On the other hand, higher-order correlations have been measured in [166, 167] for the case of ultracold atoms. Similar techniques could be implemented in the EP system, leading to the possibility of accessing universal ratios of cumulants, and thus enabling the demonstration of the typical non-gaussian shape of the TW-GOE and TW-GUE probability distributions and the characterization of universality sub-classes.

Chapter 4

KPZ universality in discrete $2d$ driven-dissipative exciton polariton condensates

The $2d$ polariton condensate appears to be significantly different from its $1d$ counterpart, which was studied in chapter 3, in terms of the emergence of KPZ dynamics. We note that we will discuss here the case of *incoherent pumping*, and refer the reader to, for example, [139, 168, 169] for works related to coherent driving, and in particular the Optical Parametric Oscillation (OPO) regime, where the possibility of observing KPZ-like behavior was recently highlighted [138], as well as related to the newly-proposed quadratic driving [170].

4.1 The fate of off-diagonal long-range order in $2d$

In $2d$, bosonic quantum fluids at equilibrium undergo a Beresinskii-Kosterlitz-Thouless (BKT) transition associated to vortex-antivortex unbinding. The deviation from equilibrium, which is determined mainly from the polariton lifetime – larger lifetimes corresponding to equilibrium-like conditions, appears to drastically affect the behavior of vortices. More specifically, for systems out of equilibrium, the attractive vortex-antivortex interaction is dramatically dampened at large distances, and can even change sign to become repulsive [171, 172], hindering their annihilation. Moreover, in more extreme non-equilibrium conditions, the vortex motion can be self-accelerated, leading to the creation of new vortex pairs.

Concerning the emergence of KPZ universality, from the study of anisotropic [173] or compact [174, 175] versions of the KPZ equation and RG arguments, it was suggested that the presence of vortices hinders the KPZ behavior. More specifically, it was claimed that in a weakly anisotropic system, when the KPZ non-linearity λ is large, vortex-anti-vortex pairs always unbind, and the proliferation of vortices, which happens at spatial scale L_v, spoils the stretched exponential decay of coherence with the KPZ universal critical exponents predicted to occur at $L_{\mathrm{KPZ}} \gg L_v$ if topological defects were absent [173]. On the other hand, when a strong anisotropy is imposed, or $\lambda \simeq 0$, the behavior of the system is associated with a BKT phase transition. Several studies, based on both experiments and numerical simulations, have reported BKT-like types of behaviors in $2d$, with scattered results. In particular, spatial and temporal power laws decays of first order correlation functions, with respective exponents α_s and α_t, were found numerically with unequal values $\alpha_s = 2\alpha_t > 1/4$ in moderately non-equilibrium conditions and pump values close to condensation threshold [176], in quantitative agreement with theoretical calculations [149] and experiments [177]. On the other hand, $\alpha_s = \alpha_t < 1/4$ were measured in an experiment where the polaritons have a remarkably high lifetime, of the order of $100ps$ [178]. To summarize the above considerations, the emerging consensus in the community is that the physics of $2d$ polariton systems is dominated by vortices and BKT behaviors, or its non-equilibrium analogue, where the exponents of the power law in the decay of spatial and temporal coherence in the ordered phase can be different.

Two important points should be emphasized, however. Firstly, as can be seen from Eq. (2.49), there are many parameters in the model which can be tuned in numerical simulations, and to a certain extent also in experiments, in principle leading to a multitude of possible regimes. For example, in the case of incoherent pumping, the momentum-dependent relaxation to the minimum of the lower polariton branch is not well understood experimentally, and this plays an important role in the magnitude of the KPZ non-linearity λ, and hence in the realizability of a KPZ regime for experimentally relevant system sizes. Secondly, the majority of the theoretical arguments outlined above are based on perturbative RG analysis [179–181]. However, as we discussed in section 1.4.2, it was shown in the late nineties [113] that such a scheme fails to capture the strong-coupling fixed point associated with the KPZ rough phase in $2d$, which renders any arguments based on perturbative flow equations fragile.

Indeed, first signatures of KPZ universality were reported [182] in the scaling of spatio-temporal correlation functions in some region of the parameter space, and regimes of absence of topological defects were accessed numerically in the limit of low-noise. Still, it was unclear whether this could be extended via further tuning of the parameters to

the nominal regime, in which the noise strength is fixed by the pump and losses, as in Eqs. (2.46b, 2.53). In this chapter, we demonstrate the existence of a KPZ regime for the phase dynamics of polariton condensates in $2d$ for realistic parameters, which place the system in highly non-equilibrium conditions. In particular, we show that topological defects such as vortices are absent for these parameters and moderately high pump, allowing us to uncover the KPZ scaling in the spatio-temporal correlation function of the condensate wavefunction. Furthermore, we compare the obtained scaling function with the one predicted for KPZ by NPRG approaches, finding an excellent agreement. Finally, we present the first analysis of the fluctuations of the phase of the condensate, via the calculation of the probability distribution function and its universal cumulants, and show that they are compatible with results from large-scale numerical simulations of KPZ systems [104, 109].

4.2 Model

Our starting point is again Eq. (2.49) for $\psi \equiv \psi(t, \vec{r})$, as it was introduced in section 2.2.2.1, which we rewrite for clarity,

$$i\hbar\frac{\partial\psi}{\partial t} = \left[\left(-\frac{\hbar^2}{2m_{\mathrm{LP}}}\nabla^2 + \epsilon + i\hbar\frac{\gamma_2}{2}\nabla^2\right) + \frac{i\hbar\gamma_0}{2}\left(\frac{p}{1+\frac{|\psi|^2}{n_s}} - 1\right) + \hbar g\,|\psi|^2\right]\psi + \hbar\xi'. \tag{4.1}$$

We used the adiabatic approximation for eliminating the reservoir dynamics, as was done in chapter 3, and the interaction between the polaritons and the reservoir excitons has again been assumed to be negligible $g_r \simeq 0$. For the kinetic term, we only include the approximation of the dispersion relation for the EP near the bottom of the LP branch, which reads

$$E_{\mathrm{LP}}(k) = \epsilon + \hbar^2 k^2/2m_{\mathrm{LP}} \tag{4.2}$$

according to Eq. (2.11), where $\epsilon = \hbar\omega_{\mathrm{LP}}$. The complex noise ξ' has zero mean and covariance $\langle\xi'(\vec{r},t)\xi'^*(\vec{r}',t')\rangle = 2\sigma\delta^2(\vec{r}-\vec{r}')\delta(t-t')$, where the noise nevel is $\sigma = \gamma_0(p+1)/4$. Let us note that in $2d$, there is an extra factor of 2 in the denominator according to the literature, when compared to the noise nevel for the $1d$ system from Eq. (2.53). Furthermore, we do not include the confinement potential $V(x)$ in our analysis, thus we place the system in a flat spatial geometry.

4.3 Numerical simulations

We numerically integrate the gGPe (4.1) using a split-step procedure in Python3 for each noise realization. We use a $2d$ grid with spacing $\alpha = 2.83\mu m$, which consists of $N = 64$ points for the analysis of the correlation functions (sections 4.4 and 4.5) and we perform a finite-size analysis for systems consisting of $N = 32, 64, 128$ points for the study of the distribution of fluctuations (section 4.6). Note that a finite dx of a few μ m can model experimental systems where the polariton condensate forms on a lattice of micro-pillars, which corresponds to the configuration where 1D KPZ was observed [148]. The system parameters are chosen as $m = 8 \times 10^{-5} m_e$, where m_e is the mass of the electron, $\gamma_0 = 0.3125 ps^{-1}$, $\gamma_r = \gamma_0/10$, $\gamma_{l,2} = 0.1\ \mu m^2 ps^{-1}$, $n_s = 3.75 \mu m^{-2}$. We note that the value considered for γ_0 corresponds to a polariton lifetime $\tau = 3.2ps$, which indeed places the system in highly out-of-equilibrium conditions. Moreover, throughout this chapter, we consider a non-interacting system, where the polariton-polariton interaction is set to zero, $g = 0$.

Let us note that by appropriate rescaling of the field and time, the KPZ equation (1.12) can be expressed in term of a single parameter $g_{\mathrm{KPZ}} = \lambda^2 D/\nu^3$, which is dimensionless for $d = 2$. For our choice of parameters outlined above, we find $g_{\mathrm{KPZ}} \simeq 10^5$, thus paving the road for observing KPZ universal properties for small system sizes of relevance to polariton experiments. Moreover, let us mention that several works introduce some anisotropy in the polariton effective mass $(m_\parallel, m_\perp)$, which leads through a similar mapping to the anisotropic extension of the KPZ equation [173]. However, as long as the product $m_\parallel m_\perp$ remains positive, the anisotropy is irrelevant and the universal properties of the anisotropic KPZ dynamics are controlled by the isotropic fixed point. In the case where $m_\parallel m_\perp < 0$, the non-linearity g_{KPZ} becomes irrelevant and the effective properties of the system are governed by the anisotropic Edwards-Wilkinson (Gaussian) fixed point [179, 180, 183]. Since we are interested in the nonlinear KPZ regime, we consider an isotropic polariton dispersion and thus neglect any anisotropy effect.

The numerical integration is performed with a time step of $dt = 0.16ps$ for the results of section 4.4, and down to $dt = 0.0016ps$ for the results of section 4.6. This finer discretization ensures that the phase at a given point on the $2d$ plane can be uniquely unwrapped in time $\theta(t) \in (-\pi, \pi] \to (-\infty, \infty)$ in the absence of vortices, by constraining the phase difference between two consecutive times to be less than $f \times 2\pi$. This procedure is robust, as long as $f \geq 0.5$. Realizing this is crucial, since a compact field can feature topological defects, such as phase jumps or vortices, which lead to the existence of various regimes. Whereas a compact version of the KPZ equation turns out to be

relevant in some systems such as driven vortex lattices in disordered superconductors [184] or polar "active smectic" phases [181], we show that the behavior of the phase in the regime studied in this work belongs to the non-compact KPZ universality class.

In order to tentatively locate the KPZ regime, we first investigate the density of topological defects, which are either purely spatial vortices in the (x, y) plane, or space-time vortices which have a non-vanishing projection of their vorticity in the (t, x) and/or (t, y) planes. The latter were shown to play an important role in $1d$ [148, 158]. Maintaining the other parameters fixed, we vary the reduced pump p from low $p \simeq 1$ (close to threshold) to moderately high $p = 2$. For each value of p, we determine the density of purely spatial and space-time vortices, which is shown in Fig. 4.1, with typical phase configurations in the (x, y) plane (similar maps are obtained in the (t, x) and (t, y) planes). The numerical procedure to detect the vortices and compute their density is detailed in Appendix B. We find that the number of vortices drastically decreases when increasing the pump power, and for $p \gtrsim 1.6$, very few spatial vortices are present, in agreement with Ref. [176], and also very few space-time vortices. Both appear only by pairs of nearby vortex and anti-vortex. We hence focus in the following on the highest value of the pump $p = 2$, which appears as more favorable for observing KPZ dynamics. We show in section 4.5 that the KPZ regime is robust, to a certain extent, against decreasing the pump power.

The presence of topological defects turn out to be also sensitive to the discreteness of space, and we find that the presence of a lattice (modeled by the grid with finite dx) is favorable to observe the KPZ regime since the density of such defects is suppressed when increasing the lattice spacing dx, as shown in Fig. 4.2. For $dx \gtrsim 1\mu m$, the emergence of space-time vortices is rare and very short-lived. In the following, we choose $dx = 2.83\mu m$, which is close to the spacing in experimental micro-pillar lattices [148], and for which the number of both spatial and space-time vortices is very small and does not spoil the KPZ universal properties.

4.4 KPZ scaling in spatio-temporal correlation functions

Using our numerical simulations we calculate the first-order correlation function $g_{1,\psi}$ of the condensate wavefunction, which is defined as

$$g_{1,\psi}(\Delta t, \Delta r) = \frac{|\langle \psi^*(t_0, \vec{r}_0)\psi(t_0 + \Delta t, \vec{r}_0 + \Delta\vec{r}\rangle|}{\sqrt{\langle n(t_0, \vec{r}_0)\rangle \langle n(t_0 + \Delta t, \vec{r}_0 + \Delta\vec{r})\rangle}}, \tag{4.3}$$

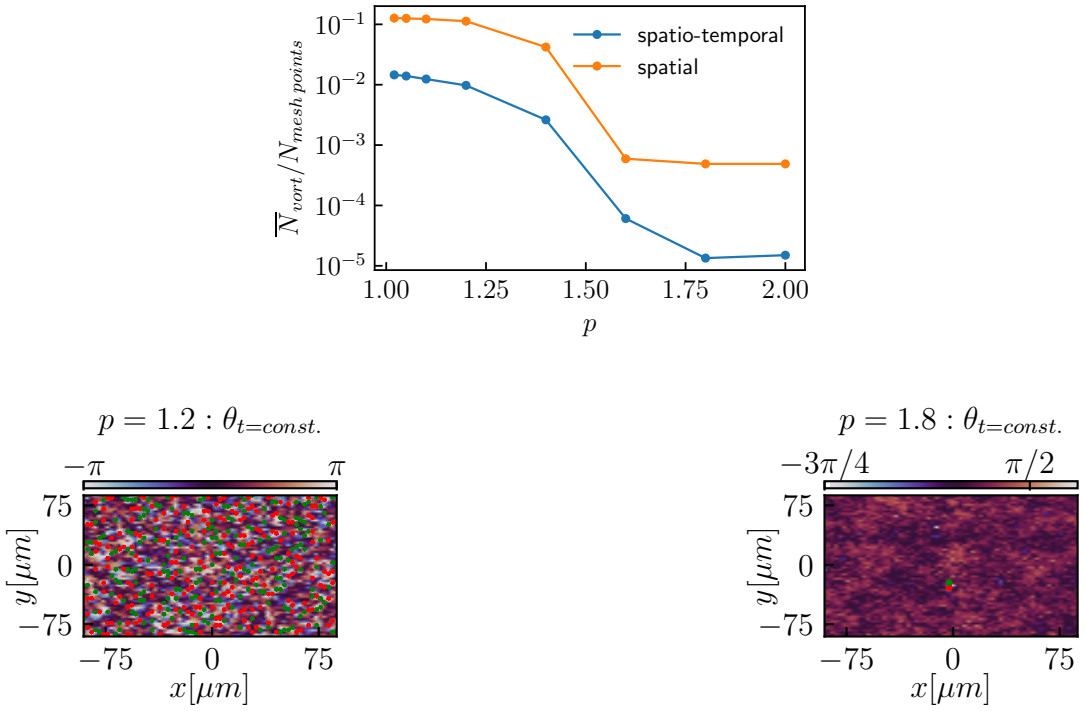

FIGURE 4.1: Density of purely spatial and space-time vortices as a function of the pump power p, with typical phase configurations in the (x, y) plane (vortex - green, anti-vortex - red) shown for $p = 1.2$ (left) and $p = 1.8$ (right) for a grid spacing of $dx = 2.83\mu m$.

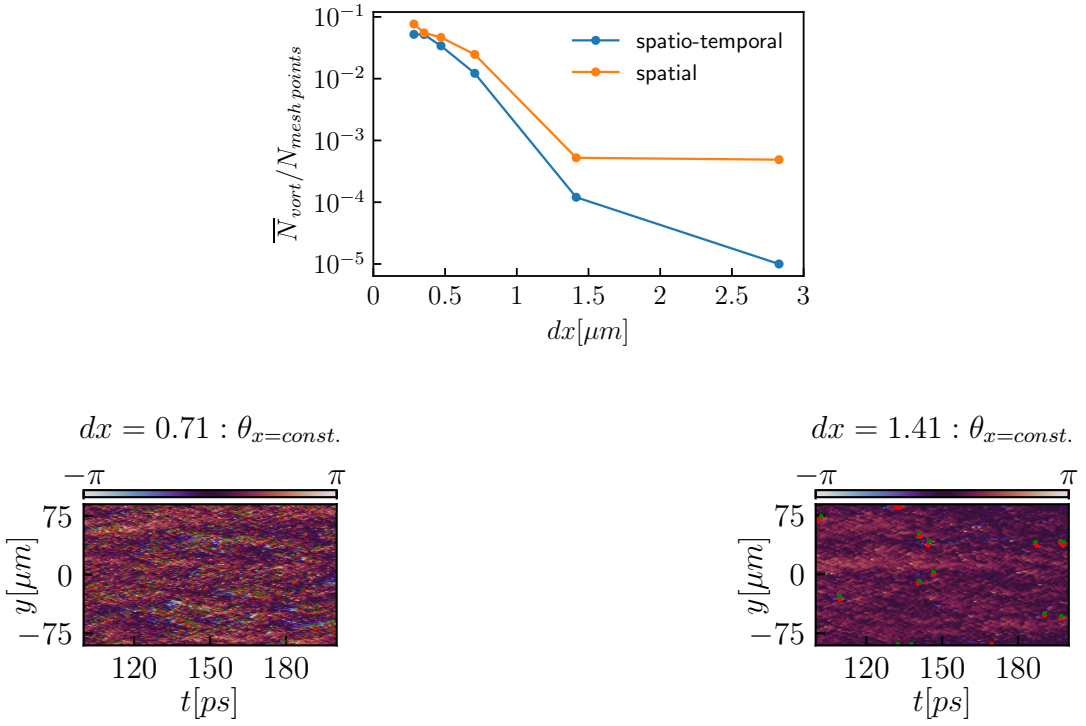

FIGURE 4.2: Density of purely spatial and space-time vortices as a function of the lattice spacing, with typical phase configurations in the (t, y) plane (vortex - green, anti-vortex - red) shown for a grid spacing of $dx = 0.71\mu m$ (left) and $dx = 1.41\mu m$ (right), for a fixed pump power $p = 2$.

Because of isotropy, $g_{1,\psi}$ only depends on the modulus $\Delta r = |\Delta\vec{r}|$, therefore we also average the data over spherical shells of radius Δr around $\vec{r}_0$, and we choose here $\vec{r}_0 = \vec{0}$.

Under the assumption that the density-phase and density-density correlations are both negligible, the expression of $g_{1,\psi}$ becomes

$$g_{1,\psi}(\Delta t, \Delta r) \simeq \left\langle e^{i\Delta\theta} \right\rangle , \tag{4.4}$$

where $\Delta\theta \equiv \theta(t_0 + \Delta t, \vec{r}_0 + \Delta\vec{r}) - \theta(t_0, \vec{r}_0)$. As was discussed for the case of $1d$, see for example Eq. (3.18), upon performing a cumulant expansion of $g_{1,\psi}$ to lowest order, one deduces that it is related to the connected correlation function C of the phase as

$$-2\ln\left[g_{1,\psi}(\Delta t, \Delta r)\right] = \left\langle \Delta\theta^2 \right\rangle - \left\langle \Delta\theta \right\rangle^2 \equiv C(\Delta\vec{r}, \Delta t)\,. \tag{4.5}$$

where C conforms to the equivalent definition for the interface,

$$C(\Delta t, \Delta\vec{r}) = \langle h(t + \Delta t, \vec{r} + \Delta\vec{r}) h(t, \vec{r})\rangle - \langle h(t + \Delta t, \vec{r} + \Delta\vec{r})\rangle\langle h(t, \vec{r})\rangle. \tag{4.6}$$

Let us note that Eq. (4.6) also takes a scaling form, defined as

$$C(\Delta t, \Delta\vec{r}) = C_0 \Delta t^{2\beta} F_{2d}\left(y_0 \frac{\Delta\vec{r}}{\Delta t^{1/z}}\right) , \tag{4.7}$$

where the universal scaling function F_{2d} is computed in Appendix C. One deduces that the scaling function F_{2d} has the predicted asymptotics,

$$F_{2d}(y) \overset{y\to 0}{\longrightarrow} F_{2d,0}\,, \quad F_{2d}(y) \overset{y\to\infty}{\sim} F_{2d,\infty} y^{2\chi}\,, \tag{4.8}$$

Note that $g_{1,\psi}$ constitutes a reliable observable to access the scaling behavior of the phase only provided the previous assumptions are verified. This is not guaranteed a priori and has to be assessed, but we stress that it was shown to be the case in $1d$ in the experimental conditions where the KPZ regime was evidenced [148]. They are also satisfied in our study, as shown in section. 4.5. We first study the equal-time and equal-space correlation functions. If the phase follows the KPZ dynamics in $2d$, then according to Eqs. (4.7, 4.8), $-2\ln|g_{1,\psi}|$ should exhibit the power-law behavior

$$-2\ln|g_{1,\psi}(\Delta t = 0, \Delta r)| \sim \Delta r^{2\chi}\,, \tag{4.9a}$$

$$-2\ln|g_{1,\psi}(\Delta t, \Delta r = 0)| \sim \Delta t^{2\beta}\,, \tag{4.9b}$$

with $\chi \simeq 0.39, \beta \simeq 0.24$. We observe the expected scaling behavior both in space and time, as shown in Fig. 4.3. For temporal correlations, the KPZ scaling extends for

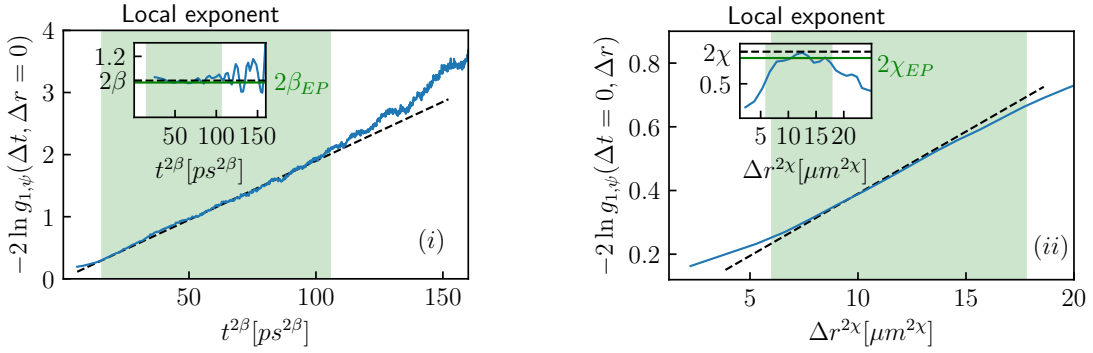

FIGURE 4.3: (i) Equal-space and (ii) equal-time correlation functions (blue plain lines) evaluated from $g_{1,\psi}$ as explained in the text, compared with the KPZ scaling laws (black dashed lines). The numerical data follow the KPZ scaling for an extended range of time and space separations (indicated by the green shade). The local exponents, which are computed from Eqs. (4.10a, 4.10b) are shown in the inset in both cases, together with their fits by a constant in the green region (solid green lines, denoted $2\beta_{EP}$ and $2\chi_{EP}$) and the values from KPZ numerical simulations (black dashed line, denoted 2β and 2β). Note that a running average has been used in order to smoothen the equal-space correlation function (i) before using Eq. (4.10b).

time differences spanning over a decade, from $3 \times 10^2 - 1.5 \times 10^4 ps$, whereas for spatial correlations, the KPZ scaling is observed over a range from $10 - 40 \mu m$. The limited space range is related to the relatively small size of our system, with a condensate of approximately $90 \mu m$ radius. Note that the polariton interaction with the reservoir g_r was set to zero here, but it is likely to play a role on the typical space and time scales where KPZ dynamics dominates, as observed in $1d$ [148].

In order to provide a quantitative estimate of the critical exponents χ and β, we compute the local exponent, given by the following logarithmic derivative

$$\frac{d}{d\ln \Delta r}\left[\ln\Big(-2\ln|g_{1,\psi}(\Delta t = 0, \Delta r)|\Big)\right] \sim 2\chi\,, \tag{4.10a}$$

$$\frac{d}{d\ln \Delta t}\left[\ln\Big(-2\ln|g_{1,\psi}(\Delta t, \Delta r = 0)|\Big)\right] \sim 2\beta\,. \tag{4.10b}$$

The result is shown in the insets of Fig. 4.3. We fit the obtained local exponents by a constant in the appropriate spatial and temporal windows, which yields the values of the universal exponents $\beta_{EP} \simeq 0.22 \pm 0.06$ and $\chi_{EP} \simeq 0.36 \pm 0.04$. These values are well in agreement with the results from numerical simulations for the $2d$ KPZ universality class.

We now study the scaling properties of the spatio-temporal correlations over the whole relevant domain $(\Delta t, \Delta r)$. For this, we first select the data lying within the scaling regime, indicated in the inset of Fig 4.4. We then construct the scaling function $F_{2d}(y)$ defined in Eq. (4.7). The normalizations C_0, y_0 are determined from fitting the equal-time and equal-space correlation functions with the power-laws Eqs. (4.9a, 4.9b) in the

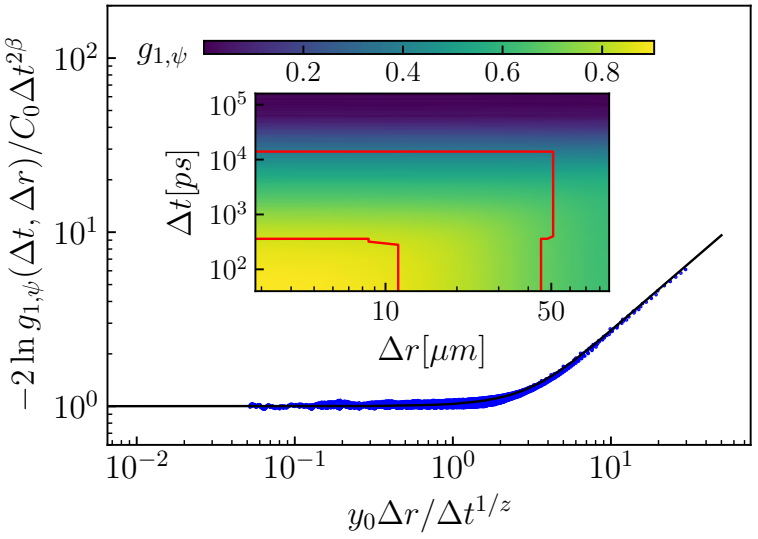

FIGURE 4.4: Universal scaling function $F_{2d}(y)$, from our numerical data (blue dots) and from the FRG calculation (solid line). Inset: Space-time map of $g_{1,\psi}$, with the red contour delimiting the scaling region where data are selected to construct $F_{2d}(y)$.

appropriate ranges. The corresponding fitting coefficients b_r, b_t are related to C_0, y_0 by $b_r = C_0 y_0^{2\chi} F_{2d,\infty}$ and $b_t = C_0 F_{2d,0}$, and $F_{2d,0}$ and $F_{2d,\infty}$ are given in Appendix C. Our results are shown in Fig. 4.4, together with the theoretical scaling function calculated from FRG. We observe a collapse of the data onto a single curve, which matches with the theoretical one with impressive accuracy. This result shows that the phase of the two-dimensional polariton condensate follows a KPZ effective dynamics over extended length and time scales for our choice of parameters.

4.5 Robustness of the KPZ regime

In order to test the robustness of the KPZ regime, we compute the correlation function $g_{1,\psi}$ for different values of p. The equal-time and equal-space correlations, compensated by the KPZ power-laws, are displayed in Fig. 4.5. We find that the temporal scaling is very robust, as plateaus for time delays spanning approximately $10^3 - 10^4 ps$ are clearly identified for all values of the pump. The spatial scaling turns out to be more sensitive to the pump variations, and plateaus for spatial separations approximately $10 - 40\mu m$ are apparent for $p \gtrsim 1.8$, but not for lower values of the pump. The progressive departure from the KPZ regime, manifest in the spatial scaling, can be attributed to the increasing effect of density-phase correlations, as shown below. To conclude, we find a robust KPZ scaling for the correlation functions in the moderately-high pump regime,

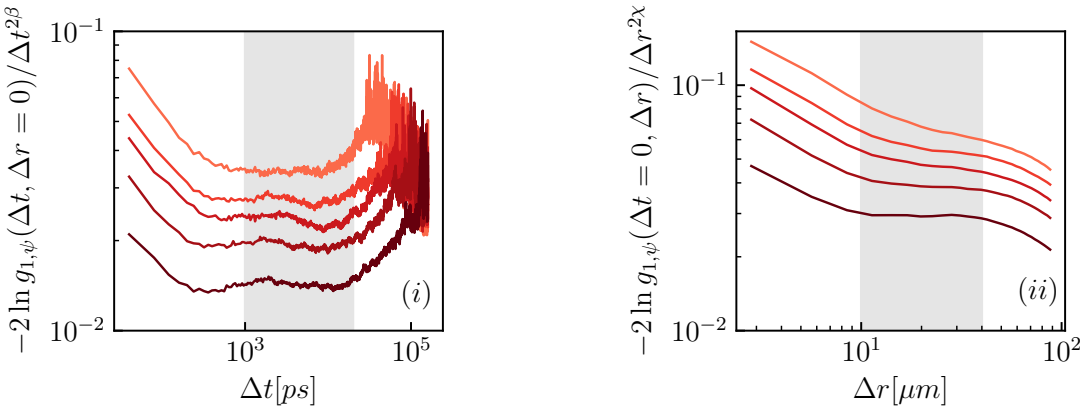

FIGURE 4.5: (i) Equal-space and (ii) equal-time correlation functions $g_{1,\psi}$, with darker colours corresponding to larger values of the pump parameter, $p = 1.6, 1.7, 1.8, 2, 2.5$. The correlations are compensated by the appropriate KPZ power laws, such that the corresponding data appear as plateaus in the KPZ spatial and temporal ranges, which are highlighted in gray.

which is especially stable for the temporal behavior.

As explained in section 4.4, the connection between the correlations of the condensate field ψ and the correlations of the phase field θ itself relies on some assumptions. In order to check their validity, we extract from the condensate field its density $n(t, \vec{r})$ and phase $\theta(t, \vec{r})$, and compute separately the contributions in $g_{1,\psi}$ of the density

$$g_{1,n}(\Delta t, \Delta r) = \frac{\left\langle \sqrt{n(t_0, \vec{r}_0) n(t_0 + \Delta t, \vec{r}_0 + \Delta \vec{r})} \right\rangle}{\sqrt{\langle n(t_0, \vec{r}_0) \rangle \langle n(t_0 + \Delta t, \vec{r}_0 + \Delta \vec{r}) \rangle}} \tag{4.11}$$

and the one of the phase

$$g_{1,\theta}(\Delta t, \Delta r) = \left\langle e^{i(\theta(t_0 + \Delta t, \vec{r}_0 + \Delta \vec{r}) - \theta(t_0, \vec{r}_0))} \right\rangle . \tag{4.12}$$

The results for $p = 2$ and $p = 1.6$ are displayed in Fig. 4.6. We observe that $g_{1,n}$ is very close to unity over the whole KPZ spatial and temporal ranges for both pump powers, and is constant for $p = 2$, while it develops a finite (but small) slope for $p = 1.6$. Thus, the role of density-density correlations is indeed small, and in particular, it is neglibible for larger pump powers. The density-phase time correlations are almost vanishing, since $g_{1,\psi}(\Delta t, 0)$ and $g_{1,\theta}(\Delta t, 0)$ almost perfectly coincide over the whole KPZ time range, as shown in panel (i) of Fig. 4.6. The density-phase space correlations are more important, and their effect increases while decreasing the pump. One observes in panel (ii) of Fig. 4.6 that for $p = 2$, they do not change the scaling behavior of $g_{1,\psi}(0, \Delta r)$ as they just amount to a global multiplicative factor as compared with $g_{1,\theta}(0, \Delta r)$, whereas for

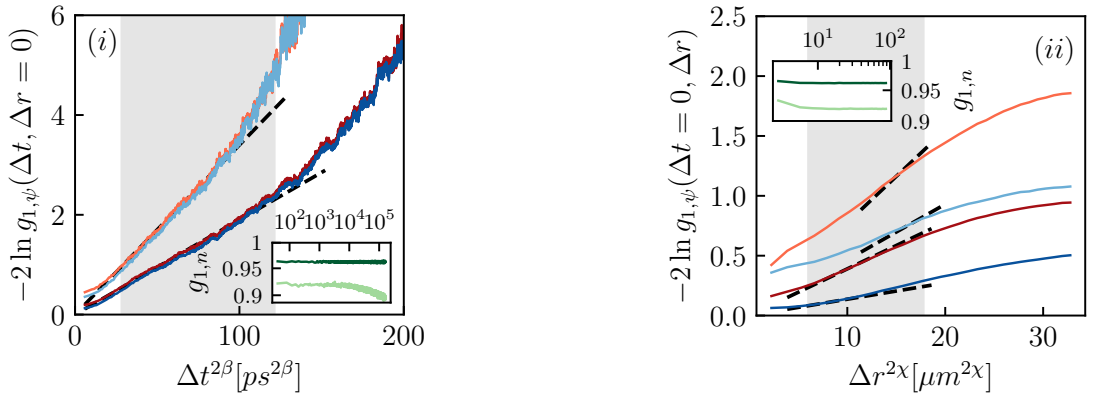

FIGURE 4.6: (i) Equal-space and (ii) equal-time correlation functions $g_{1,\psi}$ (darker) and $g_{1,\theta}$ (lighter), for $p = 1.6$ (blue colors) and $p = 2$ (red colors). The dashed lines indicate the corresponding stretched exponentials with KPZ exponents and the KPZ regime is highlighted as in Fig. 4.5. In panel (ii), the lighter shades are shifted upwards after multiplying by a factor of 1.25 in order to avoid overlapping with the darker shades. Inset: Density-density correlation $g_{1,n}$ for these values of the pump.

$p = 1.6$, $g_{1,\theta}(0, \Delta r)$ no longer follows the KPZ stretched exponential behavior. Thus, one concludes that for $p = 2$, the behavior of the correlations $g_{1,\psi}$ indeed reflects the KPZ scaling of the phase itself, both in space and time, whereas for $p = 1.6$, the density-phase space correlations also contribute to the behavior of the $g_{1,\psi}$, and the KPZ regime no longer exists.

4.6 One-point statistics of the phase fluctuations

We now study the probability distribution of the rescaled fluctuations of the unwrapped phase $\theta \equiv \theta(t, \vec{r}_0)$ at a fixed space point $\vec{r}_0$. For the classical interface in $1d$ described by a height field h, the distribution of the reduced height fluctuations defined as $\chi = (h - v_\infty t)/(\Gamma t)^{1/3}$, with v_∞ and Γ non-universal parameters, is known exactly. As we discussed in section 1.3.2.1, the distribution was shown to be sensitive to the global geometry of the growth, thereby defining three main universality sub-classes. For flat, curved, or stationary geometries, the probability distribution is given by Tracy-Widom GOE (Gaussian Orthogonal Ensemble), Tracy-Widom GUE (Gaussian Unitary Ensemble) or Baik-Rains distributions, respectively [76]. Strikingly, these universality sub-classes can also be realized in the polariton condensate in $1d$ [159], where the role of global geometry can be emulated by appropriate external potentials [185]. These results were discussed in depth in chapter 3.

In $2d$, the only available theoretical results regarding the distribution of the reduced height fluctuations are from numerical simulations [104, 106, 109]. As in $1d$, the height

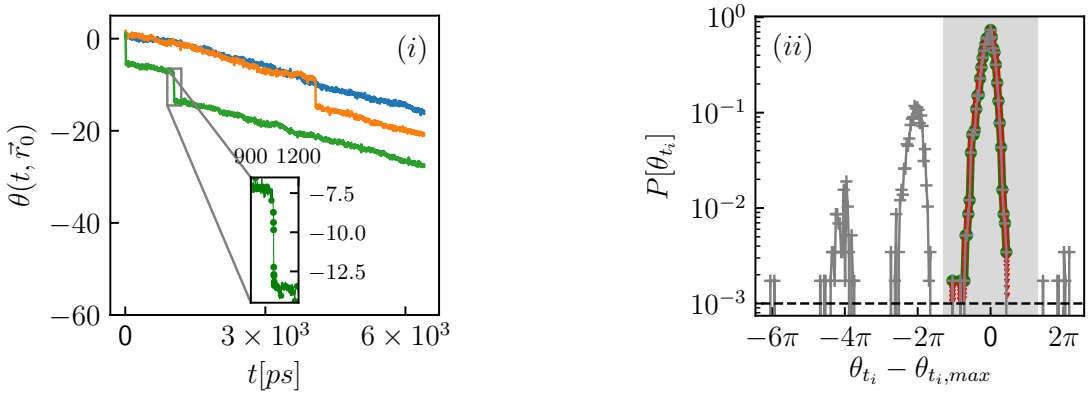

FIGURE 4.7: (*i*) Three typical unwrapped phase trajectories, displaying zero, one, or two phase jumps. (*ii*) $P[\theta(t_i)]$ for a given t_i (gray symbols). We first select the data for which $|\theta_{t_i}-\theta_{t_i,\max}|<\epsilon$, which we highlight in gray, and then we perform a secondary selection for $P[\theta_{t_i}]>P_{\min}$, where $P_{\min}$ is shown as a dashed black line. We highlight the data which satisfy both criteria (green dots), as well as the extrapolated data (red V symbols).

field exhibits a linear growth in time, with average velocity v_∞, over which fluctuations develop with a t^β scaling. All numerical works find that the distribution of the reduced fluctuations χ are non-Gaussian, and suggest the existence of different geometry-dependent universality sub-classes as in $1d$. However, we stress that there is no known analytical form for these distributions, in analogy to the Tracy-Widom or Baik-Rains distributions in $1d$, and therefore, we will rely on a comparison of the first universal cumulants of the phase, namely the skewness and excess kurtosis, which are defined as

$$sk(\delta\theta)=\mu_3/\mu_2^{3/2}\,,\qquad\qquad ku(\delta\theta)=\mu_4/\mu_2^2-3\,, \tag{4.13}$$

where $\mu_n=\langle\delta\theta^n\rangle$ correspond to the $n-$th moments of the height fluctuations $\delta\theta=\theta-\mu_1$. Due to the absence of analytical results, various attempts have been made to fit the resulting distribution to the Pearson or the generalized Gumbel distributions, due to their relevance to other non-equilibrium problems, see for example [186], however these distributions ultimately fail to capture the behavior of rare events of relevance to the $2d$ KPZ growth problem.

To investigate the statistical properties of the phase fluctuations, we record, for $p=2$, 5120 independent realisations of the time evolution of ψ, from which we extract the phase. Typical unwrapped phase trajectories are shown in panel (*i*) of Fig. 4.7. One observes that in our strong out-of-equilibrium conditions, phase jumps occur. As illustrated in the inset, these are rapid changes of the phase on a very short time scale of the order of $10ps$. We stress that these jumps are present even after *carefully* unwrapping the phase in time at a given space point $\vec{r}_0$, as discussed in section 4.3, by compensating

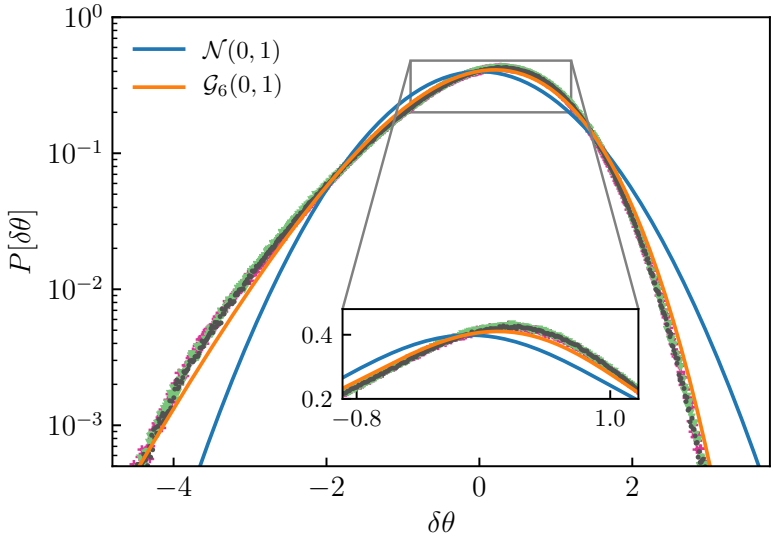

FIGURE 4.8: Histogram of the centered and rescaled phase fluctuations $\delta\theta$ in the appropriate time window for different system sizes $L = 90.5\mu m, 181\mu m, 362\mu m$ (fuchsia, light green, dark gray symbols, respectively). Each curve (and hence the analysis concerning each system size) comprises of approximately 8×10^6 data. The Gaussian distribution $\mathcal{N}$ is also shown, together with the generalized Gumbel distribution with scaling parameter $\kappa = 6$, $\mathcal{G}_6$ [104]. The probability density function is clearly non-Gaussian even near the center, as shown in the inset, and resembles the generalized Gumbel distribution.

for the instantaneous 2π shifts due to definition of the phase modulo 2π which happen in one discrete time step as small as $0.0016ps$. The existence of these jumps disrupts the leading linear behavior in time, and thus prevents from consistently defining the reduced fluctuations as $\delta\theta \propto (\theta - \langle\theta\rangle)/t^\beta$.

In order to circumvent this issue, we resort to a similar analysis performed in $1d$ and reported in [148]. We first compute the probability density function $P[\theta_{t_i}]$ for each discrete time instant t_i in the KPZ window. An example of such a distribution is shown in panel (ii) of Fig. 4.7. The occurrence of a phase jump results in a shift of approximately 2π in the values of the phase. Hence, the fluctuations of the realization where no, one, two, ... jumps occurred populate the distribution in the first, second, third, ... peak, where the different peaks are separated by approximately 2π. These peaks have a similar shape, which shows that the dynamics is in fact piece-wise KPZ in between the jumps. To study the shape of the distribution with more accuracy, we select the fluctuations in the first peak for each time instant, by requiring $|\theta_{t_i} - \theta_{t_i,\max}| < \epsilon$, where $\theta_{t_i,\max}$ is the point for which $P[\theta_{t_i,\max}] = \max(P[\theta_{t_i}])$, and we focus on the subset of them where $P[\theta_{t_i}] > P_{\min}$. For each time instant, the corresponding distribution is centered at zero, by subtracting the first moment of the selected data, $\delta\theta_{t_i} = \theta_{t_i} - \mu_{1,t_i}$, and normalized

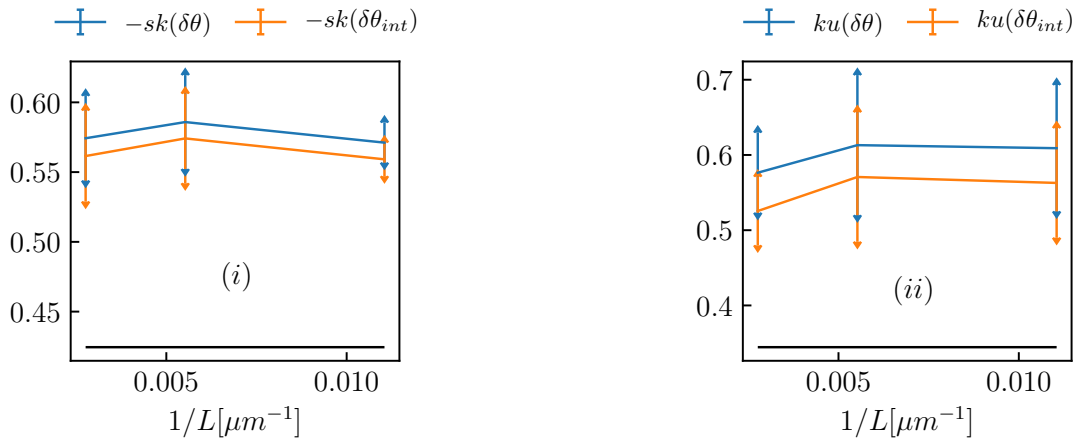

FIGURE 4.9: Finite size analysis for the (i) skewness and (ii) excess kurtosis of the phase fluctuations $\delta\theta$, with error bars corresponding to the standard deviation found after performing the computation at four distinct space points $\vec{r}_i$ with $i = 1..4$, as well as of the interpolated data $\delta\theta_{int}$ as explained in the text, with their respective error bars. We also show the universal values for the generalized Gumbel distribution with scaling parameter $\kappa = 6$ used in Ref. [104] (black) in order to compare to large-scale numerical simulations pertaining to the growth regime in flat geometry for the $2d$ KPZ universality class.

to unit variance. We then sum the fluctuations of the first peaks, properly normalized, for all time instants in the appropriate time window where cumulants reach stationary values. The obtained distribution is shown in Fig. 4.8.

We stress that both ϵ and $P_{\min}$ are selected empirically. This leads to unavoidable errors in the computation of cumulants from Eq. (4.13), due to the small number of discrete bins for given t_i. We attempt to counter the effect of such errors by interpolating in order to create a new data set $\delta\theta_{int}$, and we quantify their effect by computing the skewness and excess kurtosis of both data sets. Our results are shown in Fig. 4.9. In particular, we display the mean values for the skewness and excess kurtosis for plateaus corresponding to stationary behavior found in a time window $\Delta t_i = (1.1 \times 10^3 ps, 1.6 \times 10^3 ps)$. These values are larger by 25% to 40% for both quantities compared with the numerical results from simulations of KPZ systems, but we emphasize that our system is much smaller that the systems simulated in Refs. [104, 109].

4.7 Conclusions

In this chapter, we have shown, using numerical simulations of the discrete stochastic generalised Gross-Pitaevskii equation, that a KPZ regime can be achieved in discrete $2d$

driven-dissipative exciton polariton condensates under incoherent pumping. We have obtained the condensate spatio-temporal first-order correlation function, and shown that, for the parameters studied, it exhibits stretched exponential behavior, both in space and time, with critical exponents characteristic of the 2D KPZ universality class. This scaling persists in a finite region of pump strength and lattice spacing. Moreover, the associated scaling function accurately matches with the KPZ theoretical scaling function given by FRG methods. We have also obtained the distribution of the phase fluctuations, which is highly non-Gaussian and very close to the distribution computed in numerical simulations of KPZ interfaces. This is a compelling evidence that the phase fluctuations behave as the KPZ stochastic process.

Our findings open promising perspectives. On the theoretical side, it would be desirable to obtain a consistent description of the phase diagram of a polariton condensate in $2d$, with a clear understanding of the interplay between the various possible regimes such as non-equilibrium BKT and KPZ. This remains a challenge, as the parameter space to explore is multi-dimensional. This means that, in principle, various parameters of the model (*e.g.* polariton-polariton interaction strength, polariton loss rate, saturation density) can be tuned. On the experimental side, the evidence of a KPZ regime in $2d$ polaritons would constitute a major breakthrough, especially since a convincing realization of KPZ universality class in $2d$ is still missing and actively sought for. Note that the experimental demonstration of the KPZ scaling in $1d$ polariton condensates is very recent [148], and similar techniques could be used in $2d$.

Chapter 5

Conclusions & Perspectives

In this thesis, we studied universal properties related to the KPZ universality class, which arise when studying an inherently out-of-equilibrium system, an exciton polariton condensate.

In $1d$, we proposed a simple protocol in order to test whether the system is versatile enough in order to access different KPZ universality sub-classes. By introducing a confining potential to the system, we achieve the bending of the phase front, due to the propagation velocity being inhomogeneous, and in fact being proportional to the confining potential strength. We employed extensive numerical simulations of the EP system in presence of the confinement, which proved that the boundaries of the phase front indeed propagate faster than the bulk, thus leading to the gradual bending of the front, followed by uniform propagation after a finite time. We showed that a given point on the front follows the KPZ dynamics until a certain time when the drag induced by the potential reaches it. We computed the scaling function for the system, with and without the confinement potential, and we report excellent agreement with the analytical result [79]. Its asymptotic value when the argument tends to zero corresponds to the variance of the distribution of the rescaled fluctuations, thus deeming a detailed study of their statistics necessary in order to distinguish between the sub-classes. Furthermore, we have found that the probability distrbution of rescaled phase fluctuations is markedly different, depending on whether the potential is present or not. In particular, it corresponds to the theoretical prediction for the circular and flat sub-class, the TW-GUE and TW-GOE distribution, respectively. Moreover, the spatial correlation function of the rescaled fluctuations was found to match with the corresponding prediction in the two cases, the covariance of the Airy_2 and Airy_1 stochastic process, with the only limitation being the limited spatial range in which smooth curvature is achieved in the phase front

when the confinement is present.

In $2d$, we explored whether the KPZ universality is present in the system, without the confinement potential. In this case, topological defects are expected to be more prominent, thus rendering the extraction and the unwinding of the phase more subtle. In the literature, it was theoretically argued that the KPZ regime may be hindered by the presence of vortices, and a non-equilibrium BKT behaviour was reported close to the condensation threshold. However, the numerical simulations have been conflicting so far, and no widely approved concensus has been reached regarding the complete phase diagram. We have shed some further light on this debate, by performing numerical simulations for polariton condensates, using certain parameter values realistic in experiment, such as the pump relative to threshold, and the noise level. Furthermore, we have found that the discreteness of space is crucial for the onset of KPZ universal dynamics. The latter is very much achievable experimentally, *e.g.* in a lattice of coupled micropillars. Lastly, we considered an extremely non-equilibrium system, due to the high loss rate of polaritons from the cavity. As our main result, we have found that, the condensate spatio-temporal first-order correlation function, for the parameters studied, exhibits stretched exponential behavior, both in space and time, with critical exponents characteristic of the 2D KPZ universality class. This scaling persists in a finite region of pump strength. The scaling function of the system was found to match with the FRG predictions from Ref. [116], one of the few analytical results available for the $2d$ KPZ universality class. Furthermore, we have performed the first study of the phase of a $2d$ non-equilibrium polariton system. We reported on various difficulties that arise due to phase jumps induced by the large noise nevel, but nonetheless, we have computed the probability distribution of rescaled fluctuations and universal ratios of high order cumulants, namely the skewness and excess kurtosis. We have found that both are compatible with the reported values from large-scale numerics of discrete systems in the $2d$ KPZ universality class, although the cumulants display differences of about 20% to 40% with respect to the numerical results for a $2d$ classical interface.

These results naturally call for experimental verification. Based on accurate measurement of the first order correlation function, a recent study [148] proved that the KPZ physics is dominant in $1d$, thus demonstrating the non-equilibrium character of the exciton polariton system. A similar experimental test of our confinement protocol would readily promote the system to a strong rival to turbulent liquid crystals [61, 62], when it comes to a high-precision platform for studying KPZ physics in depth. However, the measurement of the phase up to very small times would be needed in order to conclusively distinguish between the Tracy-Widom distributions, but such a technique is

currently missing. More recently, however, correlations of arbitrarily high order have been measured for ultracold atoms, paving the way of accessing higher order cumulants, provided they can also be applied in EP systems.

In $2d$, plenty of interesting questions arise from our findings. Focusing on the case of EP systems under incoherent pumping, the precise role of the saturation density and the polariton linewidth on the enhancement of the visibility of KPZ scaling, as well as on the proliferation of vortices, require further study. On that front, it is particularly important to also understand the role of polariton-polariton interactions. On one hand, their presence is not fundamental for the existence of a KPZ regime, since the mapping still holds at vanishing interactions, as can be seen from Eqs. (2.63a, 2.63b, 2.63c, 2.64), provided that there is a momentum-dependent loss-rate. Furthermore, the study reported in Ref. [182] suggests that the development of the KPZ regime is favored by weak interactions. We note that such conditions can be accessed experimentally in polariton condensates by appropriate tuning of Feshbach resonances [187]. However, on the other hand, we emphasize that it is unclear how the apparent favor of weak polariton-polariton interactions in terms of the KPZ universality can be reconciled with the findings of [171, 172] discussed in Sec. 4.1, according to which, the ratio γ_0/gn_s strongly influences the vortex dynamics.

From the above, it is clear that further extensive numerical analysis of the system is warranted, which would consist of tuning separately the polariton-polariton interaction strength, the saturation density, as well as polariton loss rate, in order to carefully assess their effect on the extent of the spatial and temporal windows where the KPZ scaling is present in the system, and moreover, whether the study of the phase fluctuations can amount to even more accurate predictions related to the skewness and excess kurtosis. Moreover, it is important to introduce a non-uniform pump in order to better mimic the experimental conditions. Furthermore, alternative pumping schemes could be considered from an experimental point-of-view, such as the introduction of a quadratic drive [170], which has shown great promise in enhancing the visibility of KPZ scaling theoretically. Lastly, after drawing inspiration from the study we performed in $1d$, it would be interesting to explore the effect of a confinement potential to the $2d$ system.

Appendix A

Numerical estimation of Γ

Let us discuss about the value of the numerical parameter Γ, which is used to rescale the first-order correlation function of the EP wavefunction in chapter 3, in order to extract the universal scaling function $F_{1D}(y)$ via Eqs. (3.19, 3.20).

For our choice of parameter values (corresponding to Grenoble experiments), we obtain $\Gamma_{\text{th}} = \frac{\lambda A^2}{2} \simeq 0.00136\tau_0^{-1}$. However, this parameter can be extracted from our simulations from the definition of the long-time ansatz Eq. (1.20), as well as from the purely temporal correlation Eq. (3.22b). We choose the former, as it directly involves the phase. From this definition, it follows that the variance of the phase is related to the variance of the rescaled fluctuations χ as

$$\left\langle \Delta\theta^2 \right\rangle = (\Gamma t)^{2/3} \text{Var}(\chi)\,, \tag{A.1}$$

where the value of $\text{Var}(\chi)$ is known exactly in both geometries [76]. We stress that, at this stage, we *assume* that the flat and circular sub-classes are realized in our system if the geometry of the growth is tuned via the external confinement potential. However, as we show in section 3.4.2.3 via a detailed study of the skewness and excess kurtosis of the phase fluctuations, convergence to the universal values for the Tracy-Widom distributions is observed, thus justifying our assumption.

In order to extract Γ, we compute $\left\langle \Delta\theta^2 \right\rangle / t^{2/3}$, average over the plateaus reached in the appropriate time windows corresponding to the KPZ regime and divide by $\text{Var}(\chi)$. The values obtained before the rescaling by the variance are illustrated on Fig. A.1 where these plateaus are shown. We obtain

$$\Gamma \simeq \begin{cases} 0.0013\tau_0^{-1}, \text{ curved geometry} \\ 0.002\tau_0^{-1}, \text{ flat geometry.} \end{cases} \tag{A.2}$$

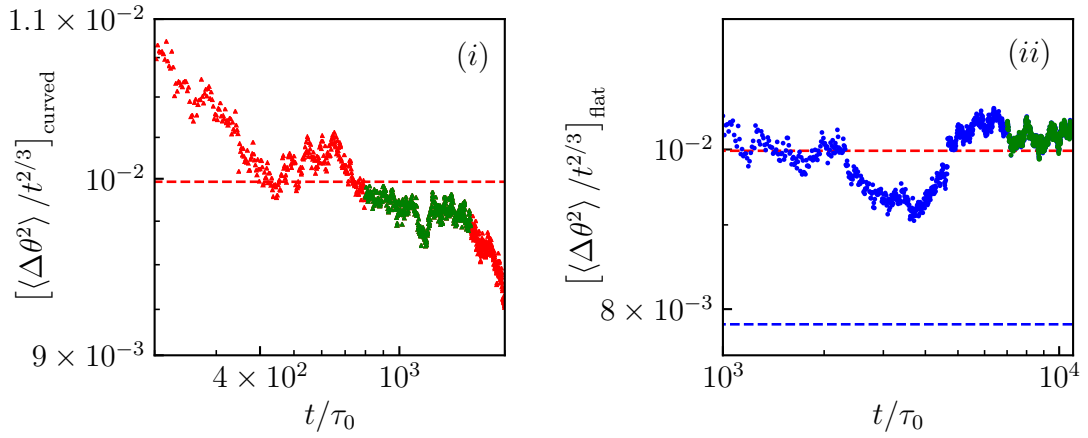

FIGURE A.1: Determination of the Γ parameter in the (i) curved and (ii) flat geometry, together with the theoretical values for $\Gamma^{2/3}\mathrm{Var}(\chi)$ (red and blue dashed lines) obtained from the microscopic parameters with the theoretical value of $\mathrm{Var}(\chi)$ for the identified distribution in each case. The rescaled variance $\langle \Delta\theta^2 \rangle / t^{2/3}$ is averaged over the plateaus in the green time windows and then divided by $\mathrm{Var}(\chi)$, which yields the values listed in Eq. (A.2).

These values are in agreement with the theoretical estimate Γ_{th}. Even though Γ depends on x in the curved case, it is almost constant if one restricts to a small space region around the central point $x = 0$. We observe that while the data for the curved phase lies very close to the corresponding theoretical prediction (before the departure from KPZ universality for large times), the value for the flat phase differs by about 30% from the theoretical one. We are, at present, unable to explain this small discrepancy, but nevertheless we take it into account in our work by using in the normalisations the actual numerical values of Γ.

Appendix B

Vortex detection

In order to search for vortices in the phase of the condensate and locate their cores, one usually computes the circulation $I = \oint_C \vec{\nabla}\theta \cdot d\vec{l}$ around closed contours C enclosing each point of the 2D grid. If a quantized vortex is present at a point, then $I = \kappa 2\pi$, where κ is the vortex charge, else $I = 0$ [188]. The closed contour C should be defined such that it encloses a small part of the fluid containing up to one vortex core, in which case the circulation does not depend on the precise form of the contour.

However, this method quickly becomes intractable when applied to each point in a grid consisting of many points, such as a space grid with fine spatial discretization, or a space-time grid, defined by selecting one spatial direction and time. In the latter case, the time discretization is typically chosen as much finer than the spatial one, thus requiring an extremely large number of points in order to study the dynamics of the condensate until some time after the steady state has been reached. We circumvent this issue by computing the curl of the gradient of the phase of the condensate, $\vec{\nabla} \times \vec{\nabla}\theta$. By definition, the projection of this quantity in each of the three directions, the two spatial and the temporal ones, is related to the infinitesimal circulation of the gradient of the phase around each point of the grid,

$$\vec{\nabla} \times \vec{\nabla}\theta \cdot \vec{S} \to I \,, \tag{B.1}$$

where $\vec{S}$ is the normal vector,

$$\vec{S} = dx^2 \hat{t} + dxdt\hat{x} + dxdt\hat{y} \,, \tag{B.2}$$

where dx is the unit length, which is chosen to be the same for both the x and y directions, and dt is the unit time.

From our numerical simulations, we extract the phase of the condensate in the (x, y) plane in an appropriate time window in the steady state, thus creating an (effectively)

$3d$ dataset. We then compute the components of the gradient numerically along each direction separately, once the phase has been unwrapped in that direction. Finally, we compute each of the components of the curl straightforwardly. Overall, this procedure allows us to identify, in a particularly efficient manner, both the spatial vortices, as well as the space-time topological defects, by mapping the $2+1$-dimensional problem to three distinct 2-dimensional ones.

In order to compute the vortex density, we study each component of the curl separately. More specifically, for each component $i = \{x, y, t\}$, we count the number of non-zero values of each curl component for each distinct "slice" $\{x_i, y_i, t_i\}$. This allows us to compute the mean number of defects,

$$\overline{N}_{\text{vort},xy} = \frac{1}{\#t_i} \sum_{t_i \in \Delta t} \text{count}_{\text{vort}}(t_i)\,, \tag{B.3a}$$

$$\overline{N}_{\text{vort},xt} = \frac{1}{\#y_i} \sum_{y_i} \text{count}_{\text{vort}}(y_i)\,, \tag{B.3b}$$

$$\overline{N}_{\text{vort},yt} = \frac{1}{\#x_i} \sum_{x_i} \text{count}_{\text{vort}}(x_i)\,, \tag{B.3c}$$

where $\Delta t = 100ps$ starting from an initial sampling time $t_0 = 100ps$, for which the steady state of the system has already been reached for our choice of parameters. We then normalize our result by dividing with the total number of points in the $2d$ grid, and we present our results for the mean occupation of our grid by topological defects in Figs. 4.1 and 4.2.

Appendix C

Scaling function for KPZ growth in $2d$

As we already discussed in section 1.4.2, analytical results pertaining to the KPZ universality class in $2d$ are notoriously hard to come by. In particular, the KPZ rough phase is described by a genuinely strong-coupling fixed-point in $d \geq 2$. Indeed, it was shown in [113] that the perturbative RG flow equation for the effective KPZ coupling g_{KPZ} can be resummed exactly, yielding an expression valid to all orders in perturbation theory in the vicinity of $d = 2$. However, g_{KPZ} flows to infinity, and not to a finite fixed point associated with the KPZ rough phase. Therefore, any RG calculation based on perturbative techniques fails to qualitatively capture the strong-coupling fixed-point, and one cannot extract any sound information about the KPZ fixed-point in $2d$ or higher dimensions from the resulting flow equation.

A non-perturbative RG calculation was devised using the inherently non-perturbative Functional Renormalisation group (FRG) in Refs. [114–116], which allows one to access the strong-coupling KPZ fixed-point in all dimensions. It shows that the KPZ fixed-point is not connected to the Gaussian Edwards-Wilkinson fixed-point in any dimension, which explains the failure of perturbation theory, even resummed at all orders. The universal scaling function associated with the two-point correlation function in $2d$ was calculated in [116], which provides the scaling function $\mathring{F}_{2d}$ defined as

$$\bar{C}(\omega, \vec{p}) = \frac{2}{p^{d+2+\chi}} \bar{C}_0 \mathring{F}_{2d} \left(\bar{y}_0 \frac{\omega}{p^z} \right) , \tag{C.1}$$

where $\bar{C}_0$, $\bar{y}_0$ are non-universal normalization constants, and $\bar{C}(\vec{p}, \omega)$ is the Fourier transform of the connected two-point correlation function Eq. (4.6). More specifically, for

arbitrary values of time and space separation $(t, \vec{r})$, the Fourier transform reads

$$C(t,\vec{r}) = \int_{-\infty}^{\infty} \frac{d\omega}{2\pi} \int \frac{d^d\vec{p}}{(2\pi)^d} \left(e^{-i(\omega t - \vec{p}\cdot\vec{r})} - 1 \right) \bar{C}(\omega,\vec{p}). \tag{C.2}$$

By replacing $\bar{C}(\omega,\vec{p})$ by its scaling form (C.1), switching to polar coordinates, and finally changing frequency variable to $\tau = \bar{y}_0\omega/p^z$, one obtains in $2d$

$$C(t,\vec{r}) = \frac{\bar{C}_0}{\bar{y}_0} \frac{1}{2\pi^2} \int_0^{\infty} d\tau \mathring{F}_{2d}(\tau) \int_0^{\infty} \frac{dp}{p^{3+\chi-z}} \left[\cos(p^z\tau t/\bar{y}_0)\mathcal{B}_J(0,pr) - 1 \right] \tag{C.3}$$

where $\mathcal{B}_J$ is a Bessel function, and the parity of $\mathring{F}_{2d}$ has been used. By changing momentum variable to $u = p^z\tau t/\bar{y}_0$, one finally obtains

$$\begin{aligned} C(t,\vec{r}) &= C_0 t^{2\chi/z} F_{2d}(y_0 x/t^{1/z}) \\ F_{2d}(y) &= \int_0^{\infty} d\tau \mathring{F}_{2d}(\tau)\tau^{2\chi/z} \int_0^{\infty} \frac{du}{u^{2\chi/z}} \left[\cos(u)\mathcal{B}_J(0,(u/\tau)^{1/z}y) - 1 \right] \qquad \text{(C.4)} \\ C_0 &= \frac{\bar{C}_0}{(2\pi^2) z \bar{y}_0^{1+2\chi}} \\ y_0 &= \bar{y}_0{}^{1/z} \qquad \text{(C.5)} \end{aligned}$$

We stress that the normalization constants C_0 and y_0 are not universal, and have to be prescribed. In this appendix, we fix C_0 and y_0 such that $F_{2d,0} = 1$ and $F_{2d,\infty} = 0.45$. We note that this was not the case in $1d$, where $F_{1d,\infty} = 2$ in Eq. (3.21), and C_0, y_0 were fixed by the KPZ parameters ν, λ, D according to Eq. (3.20). Those particular normalizations are fixed historically, and amount to directly comparing $F_{1d,0}$ with the theoretical results pertaining to the Tracy-Widom and Baik-Rains distributions, namely their variance. Such results are not available in $2d$, hence the precise normalizations are not important.

The integrals in (C.4) were computed numerically, using the tabulated data for $\mathring{F}_{2d}$ from Ref. [116]. In chapter 4, we use the function F_{2d} computed from FRG as the theoretical reference for the scaling function of the $2d$ KPZ universality class.

Appendix D

Remarks on the space discretization

For the entirety of this thesis, the numerical simulation of the time evolution was performed using the NumPy and SciPy libraries of Python, as well as the framework for parallel calculations offered by the QuTiP package [189, 190].

The most important ramification of simulating a continuous system, is the fact that one has to pay attention to discretize the space and time, as the notion of the continuum does not exist for the computer. By doing that, during the course of the analysis presented in chapter 4, we came across extremely interesting physical phenomena which seem to directly influence the appearance of KPZ universal properties, in the context of a condensate of exciton polaritons in $2d$.

More specifically, we have found that, by increasing the number of grid sites N and decreasing the discretization length scale dx of our $2d$ grid, in a way that the total length of the system $L = Ndx$ remains constant, more and more vortices seem to populate the system, as seen in Fig. 4.2. Whereas in the continuum limit $dx \to 0$ the vortex density seems to converge to a stationary value, we have found that the majority of the vortices are still localized in one pixel of the space-time grid defined by the two grid spacings (dx, dt). Albeit counter-intuitive, this means that, the KPZ phase dynamics can only be visible (in this parameter regime) in systems which are engineered to be discrete, in order to dampen the proliferation of hybrid space-time vortices. We have found that, for our choice of system parameters detailed in section 4.3, this can be achieved for a spatial grid spacing of $dx \gtrsim 1.5\mu m$. For less discrete systems, the proliferation of vortices overruns the system, and coherence is lost immediately. Furthermore, we have

found that the numerical stability of the time evolution is achieved for $dt \leq 2 \times 10^{-1} ps$ for our split-step solver.

Bibliography

[1] A. Dragulescu and V. M. Yakovenko. Statistical mechanics of money. *The European Physical Journal B - Condensed Matter and Complex Systems*, 17(4): 723–729, 2000. https://doi.org/10.1007/s100510070114.

[2] C. Castellano, S. Fortunato, and V. Loreto. Statistical physics of social dynamics. *Rev. Mod. Phys.*, 81(2):591–646, 2009. https://link.aps.org/doi/10.1103/RevModPhys.81.591.

[3] M. J. Spivey, S. E. Anderson, and R. Dale. The phase transition in human cognition. *New Mathematics and Natural Computation (NMNC)*, 5(01):197–220, 2009. https://ideas.repec.org/a/wsi/nmncxx/v05y2009i01ns1793005709001234.html.

[4] N. Goldenfeld. *Lectures on phase transitions and the renormalization group*. CRC Press, 1972. https://doi.org/10.1201/9780429493492.

[5] L. P. Kadanoff. Scaling laws for Ising models near T_c. *Physics Physique Fizika*, 2:263–272, 1966. https://link.aps.org/doi/10.1103/PhysicsPhysiqueFizika.2.263.

[6] K. G. Wilson. The renormalization group and critical phenomena. *Rev. Mod. Phys.*, 55:583–600, 1983. https://link.aps.org/doi/10.1103/RevModPhys.55.583.

[7] M. Henkel. *Conformal invariance and critical phenomena*. Springer, 1999. https://doi.org/10.1007/978-3-662-03937-3_2.

[8] H. E. Stanley and T. A. Kaplan. High-temperature expansions-the classical Heisenberg model. *Phys. Rev. Lett.*, 16:981–983, 1966. https://link.aps.org/doi/10.1103/PhysRevLett.16.981.

[9] H. E. Stanley and T. A. Kaplan. Possibility of a phase transition for the two-dimensional Heisenberg model. *Phys. Rev. Lett.*, 17:913–915, 1966. https://link.aps.org/doi/10.1103/PhysRevLett.17.913.

[10] N. D. Mermin and H. Wagner. Absence of ferromagnetism or antiferromagnetism in one- or two-dimensional isotropic Heisenberg models. *Phys. Rev. Lett.*, 17: 1133–1136, 1966. https://link.aps.org/doi/10.1103/PhysRevLett.17.1133.

[11] J. M. Kosterlitz and D. J. Thouless. Ordering, metastability and phase transitions in two-dimensional systems. *Journal of Physics C: Solid State Physics*, 6(7):1181–1203, 1973. https://doi.org/10.1088/0022-3719/6/7/010.

[12] S. N. Bose. Plancks gesetz und lichtquantenhypothese. *Zeitschrift für Physik*, 26 (1):178–181, 1924. https://doi.org/10.1007/BF01327326.

[13] E. Pérez and T. Sauer. Einstein's quantum theory of the monatomic ideal gas: Non-statistical arguments for a new statistics. *Archive for History of Exact Sciences*, 64(5):561–612, 2010. https://doi.org/10.1007/s00407-010-0066-x.

[14] C. J. Pethick and H. Smith. Bose–Einstein condensation in dilute gases, 2nd ed. *Contemporary Physics*, 51(5), 2010. https://doi.org/10.1080/00107510903404374.

[15] D. S. Petrov and G. V. Shlyapnikov. Interatomic collisions in a tightly confined Bose gas. *Phys. Rev. A*, 64:012706, 2001. https://link.aps.org/doi/10.1103/PhysRevA.64.012706.

[16] W. H. Keesom and A. P. Keesom. New measurements on the specific heat of liquid Helium. *Physica*, 2(1):557–572, 1935. https://ui.adsabs.harvard.edu/abs/1935Phy.....2..557K.

[17] W. H. Keesom and M. Wolfke. *Communications from the Physical Laboratory at the University of Leiden*, 190:17, 1927.

[18] P. Kapitza. Viscosity of liquid Helium below the λ-point. *Nature*, 141(3558): 74–74, 1938. https://doi.org/10.1038/141074a0.

[19] J. F. Allen and A. D. Misener. Flow of liquid Helium II. *Nature*, 141(3558): 75–75, 1938. https://doi.org/10.1038/141075a0.

[20] F. London. The λ-phenomenon of liquid helium and the Bose-Einstein degeneracy. *Nature*, 141(3571):643–644, 1938. https://doi.org/10.1038/141643a0.

[21] M. H. Anderson, J. R. Ensher, M. R. Matthews, C. E. Wieman, and E. A. Cornell. Observation of Bose-Einstein condensation in a dilute atomic vapor. *Science*, 269(5221):198–201, 1995. ISSN 0036-8075. https://science.sciencemag.org/content/269/5221/198.

[22] K. B. Davis, M. O. Mewes, M. R. Andrews, N. J. van Druten, D. S. Durfee, D. M. Kurn, and W. Ketterle. Bose-Einstein condensation in a gas of Sodium atoms. *Phys. Rev. Lett.*, 75:3969–3973, 1995. https://link.aps.org/doi/10.1103/PhysRevLett.75.3969.

[23] P. C. Martin, E. D. Siggia, and H. A. Rose. Statistical dynamics of classical systems. *Phys. Rev. A*, 8:423–437, 1973. https://link.aps.org/doi/10.1103/PhysRevA.8.423.

[24] H-K. Janssen. On a Lagrangean for classical field dynamics and renormalization group calculations of dynamical critical properties. *Zeitschrift für Physik B Condensed Matter*, 23(4):377–380, 1976. https://doi.org/10.1007/BF01316547.

[25] C. de Dominicis. Techniques de renormalization de la théorie des champs et dynamique des phénomènes critiques. *J. Phys. Colloques*, 37(C1): C1–247–C1–253, 1976. https://doi.org/10.1051/jphyscol:1976138.

[26] C. Wetterich. Exact evolution equation for the effective potential. *Physics Letters B*, 301(1):90–94, 1993. https://www.sciencedirect.com/science/article/pii/037026939390726X.

[27] L. Canet, H. Chaté, and B. Delamotte. General framework of the non-perturbative renormalization group for non-equilibrium steady states. *Journal of Physics A: Mathematical and Theoretical*, 44(49):495001, 2011. https://doi.org/10.1088/1751-8113/44/49/495001.

[28] I. Carusotto and C. Ciuti. Quantum fluids of light. *Rev. Mod. Phys.*, 85:299–366, 2013. doi: 10.1103/RevModPhys.85.299. https://doi.org/10.1103/RevModPhys.85.299.

[29] M. Kardar, G. Parisi, and Y-C. Zhang. Dynamic scaling of growing interfaces. *Phys. Rev. Lett*, 56:889–892, 1986. https://doi.org/10.1103/PhysRevLett.56.889.

[30] T. Halpin-Healy and Y-C. Zhang. Kinetic roughening phenomena, stochastic growth, directed polymers and all that. Aspects of multidisciplinary statistical mechanics. *Physics Reports*, 254(4):215–414, 1995. https://doi.org/10.1016/0370-1573(94)00087-J.

[31] T. Kriecherbauer and J. Krug. A pedestrian's view on interacting particle systems, KPZ universality and random matrices. *Journal of Physics A: Mathematical and Theoretical*, 43(40):403001, 2010. http://dx.doi.org/10.1088/1751-8113/43/40/403001.

[32] K. A. Takeuchi. An appetizer to modern developments on the Kardar–Parisi–Zhang universality class. *Physica A: Statistical Mechanics and its Applications*, 504:77–105, 2018. ISSN 0378-4371. https://www.sciencedirect.com/science/article/pii/S0378437118303170.

[33] I. Corwin. The Kardar-Parisi-Zhang equation and universality class. *Random Matrices: Theory and Applications*, 01(01):1130001, 2012. https://doi.org/10.1142/S2010326311300014.

[34] P. Bak, C. Tang, and K. Wiesenfeld. Self-organized criticality: An explanation of the $1/f$ noise. *Phys. Rev. Lett.*, 59:381–384, 1987. https://link.aps.org/doi/10.1103/PhysRevLett.59.381.

[35] A-L. Barabási and H. E. Stanley. *Fractal concepts in surface growth*. Cambridge University Press, 1995. https://doi.org/10.1017/CBO9780511599798.

[36] J. Krug. Origins of scale invariance in growth processes. *Advances in Physics*, 46 (2):139–282, 1997. https://doi.org/10.1080/00018739700101498.

[37] P. Meakin. The growth of rough surfaces and interfaces. *Physics Reports*, 235(4): 189–289, 1993. https://www.sciencedirect.com/science/article/pii/037015739390047H.

[38] F. Family and T. Vicsek. Scaling of the active zone in the Eden process on percolation networks and the ballistic deposition model. *Journal of Physics A: Mathematical and General*, 18(2):L75–L81, 1985. http://dx.doi.org/10.1088/0305-4470/18/2/005.

[39] T. Williams and R. Bjerknes. Stochastic model for abnormal clone spread through epithelial basal layer. *Nature*, 236(5340):19–21, 1972. https://doi.org/10.1038/236019a0.

[40] H. P. Yockey, editor. *Symposium on information theory in Biology*, 1958. Pergamon Press. by Eden, M.

[41] F. Neyman, editor. *Fourth Berkeley symposium on Mathematical Statistics and Probability*, volume IV, 1961. U. C. Berkeley. by Eden, M.

[42] Y-C. Parisi, G.and Zhang. Field theories and growth models. *Journal of Statistical Physics*, 41(1):1–16, 1985. https://doi.org/10.1007/BF01020601.

[43] S. F. Edwards and D. R. Wilkinson. The surface statistics of a granular aggregate. *Proceedings of the Royal Society of London. A. Mathematical and Physical Sciences*, 381(1780):17–31, 1982. https://doi.org/10.1098/rspa.1982.0056.

[44] C. W. Gardiner. *Stochastic Methods. A handbook for the natural and social sciences*. Springer-Verlag Berlin Heidelberg, 2009. 4th edition.

[45] D. Forster, D. R. Nelson, and M. J. Stephen. Large-distance and long-time properties of a randomly stirred fluid. *Phys. Rev. A*, 16:732–749, 1977. https://link.aps.org/doi/10.1103/PhysRevA.16.732.

[46] C-H. Lam and F. G. Shin. Improved discretization of the Kardar-Parisi-Zhang equation. *Phys. Rev. E*, 58(5):5592–5595, 1998. https://link.aps.org/doi/10.1103/PhysRevE.58.5592.

[47] J. Krug, P. Meakin, and T. Halpin-Healy. Amplitude universality for driven interfaces and directed polymers in random media. *Phys. Rev. A*, 45(2):638–653, 1992. https://link.aps.org/doi/10.1103/PhysRevA.45.638.

[48] J. Baik, P. Deift, and K. Johansson. On the distribution of the length of the longest increasing subsequence of random permutations. *J. Amer. Math. Soc.*, 12:1119–1178, 1999. https://doi.org/10.1090/S0894-0347-99-00307-0.

[49] K. Johansson. Shape fluctuations and random matrices. *Communications in Mathematical Physics*, 209(2):437–476, 2000. https://doi.org/10.1007/s002200050027.

[50] G. Amir, I. Corwin, and J. Quastel. Probability distribution of the free energy of the continuum directed random polymer in 1+1 dimensions. *Communications on Pure and Applied Mathematics*, 64(4):466–537, 2011. https://doi.org/10.1002/cpa.20347.

[51] T. Sasamoto and H. Spohn. The 1 + 1-dimensional Kardar–Parisi–Zhang equation and its universality class. *Journal of Statistical Mechanics: Theory and experiment*, 2010(11):P11013, 2010. http://dx.doi.org/10.1088/1742-5468/2010/11/P11013.

[52] T. Sasamoto and H. Spohn. Exact height distributions for the KPZ equation with narrow wedge initial condition. *Nuclear Physics B*, 834(3):523–542, 2010. http://www.sciencedirect.com/science/article/pii/S0550321310001768.

[53] T. Sasamoto and H. Spohn. One-dimensional Kardar-Parisi-Zhang equation: An exact solution and its universality. *Phys. Rev. Lett*, 104(23):230602, 2010. https://link.aps.org/doi/10.1103/PhysRevLett.104.230602.

[54] T. Sasamoto and H. Spohn. The crossover regime for the weakly asymmetric simple exclusion process. *Journal of Statistical Physics*, 140(2):209–231, 2010. https://doi.org/10.1007/s10955-010-9990-z.

[55] V. Dotsenko. Bethe ansatz derivation of the Tracy-Widom distribution for one-dimensional directed polymers. *EPL (Europhysics Letters)*, 90(2):20003, 2010. http://dx.doi.org/10.1209/0295-5075/90/20003.

[56] P. Calabrese, P. Le Doussal, and A. Rosso. Free-energy distribution of the directed polymer at high temperature. *EPL (Europhysics Letters)*, 90(2):20002, 2010. http://dx.doi.org/10.1209/0295-5075/90/20002.

[57] L. Bertini and G. Giacomin. Stochastic Burgers and KPZ equations from particle systems. *Communications in Mathematical Physics*, 183(3):571–607, 1997. https://doi.org/10.1007/s002200050044.

[58] M. Hairer. Solving the KPZ equation. *Annals of Mathematics*, 178(2):559–664, 2013. http://www.jstor.org/stable/23470800.

[59] B. Derrida. An exactly soluble non-equilibrium system: The asymmetric simple exclusion process. *Physics Reports*, 301(1):65–83, 1998. ISSN 0370-1573. https://www.sciencedirect.com/science/article/pii/S0370157398000064.

[60] Olivier G. and Kirone M. The asymmetric simple exclusion process: An integrable model for non-equilibrium statistical mechanics. *Journal of Physics A: Mathematical and General*, 39(41):12679–12705, 2006. https://doi.org/10.1088/0305-4470/39/41/s03.

[61] K. A. Takeuchi and M. Sano. Universal fluctuations of growing interfaces: Evidence in turbulent liquid crystals. *Phys. Rev. Lett*, 104:230601, 2010. https://doi.org/10.1103/PhysRevLett.104.230601.

[62] K. A. Takeuchi, M. Sano, T. Sasamoto, and H. Spohn. Growing interfaces uncover universal fluctuations behind scale invariance. *Scientific Reports*, 1(1): 34, 2011. https://doi.org/10.1038/srep00034.

[63] K. A. Takeuchi and M. Sano. Evidence for geometry-dependent universal fluctuations of the Kardar-Parisi-Zhang interfaces in liquid-crystal turbulence. *Journal of Statistical Physics*, 147(5):853–890, 2012. https://doi.org/10.1007/s10955-012-0503-0.

[64] J. Baik and E. M. Rains. *Random matrix models and their applications*, volume 40. Cambridge University Press, 2001. edited by Bleher, M. Pavel and Its, Alexander R.

[65] J. Baik and E. M. Rains. The asymptotics of monotone subsequences of involutions. *Duke Math. J.*, 109(2):205–281, 2001. https://projecteuclid.org:443/euclid.dmj/1091737272.

[66] P. L. Ferrari and H. Spohn. A determinantal formula for the GOE Tracy–Widom distribution. *Journal of Physics A: Mathematical and General*, 38(33): L557–L561, 2005. http://dx.doi.org/10.1088/0305-4470/38/33/L02.

[67] T Sasamoto. Spatial correlations of the 1d KPZ surface on a flat substrate. *Journal of Physics A: Mathematical and General*, 38(33):L549–L556, 2005. http://dx.doi.org/10.1088/0305-4470/38/33/L01.

[68] P. Calabrese and P. Le Doussal. Exact solution for the Kardar-Parisi-Zhang equation with flat initial conditions. *Phys. Rev. Lett*, 105:250603, 2011. https://doi.org/10.1103/PhysRevLett.106.250603.

[69] P. Le Doussal and P. Calabrese. The KPZ equation with flat initial condition and the directed polymer with one free end. *Journal of Statistical Mechanics: Theory and Experiment*, 2012(06):P06001, 2012. http://dx.doi.org/10.1088/1742-5468/2012/06/P06001.

[70] J. Baik and E. M. Rains. Limiting distributions for a polynuclear growth model with external sources. *Journal of Statistical Physics*, 100(3):523–541, 2000. https://doi.org/10.1023/A:1018615306992.

[71] P. L. Ferrari and H. Spohn. Scaling limit for the space-time covariance of the stationary totally asymmetric simple exclusion process. *Communications in Mathematical Physics*, 265(1):1–44, 2006. https://doi.org/10.1007/s00220-006-1549-0.

[72] T. Imamura and T. Sasamoto. Exact solution for the stationary Kardar-Parisi-Zhang equation. *Phys. Rev. Lett*, 108:190603, 2012. https://doi.org/10.1103/PhysRevLett.108.190603.

[73] T. Imamura and T. Sasamoto. Stationary correlations for the 1d KPZ equation. *Journal of Statistical Physics*, 150(5):908–939, 2013. https://doi.org/10.1007/s10955-013-0710-3.

[74] M. Prähofer and H. Spohn. Statistical self-similarity of one-dimensional growth processes. *Physica A: Statistical Mechanics and its Applications*, 279(1):342–352, 2000. https://www.sciencedirect.com/science/article/pii/S0378437199005178.

[75] M. Prähofer and H. Spohn. Repository of various numerical results related to the 1D KPZ universality class, 2021. https://www-m5.ma.tum.de/KPZ.

[76] M. Prähofer and H. Spohn. Universal distributions for growth processes in $1 + 1$ dimensions and random matrices. *Phys. Rev. Lett*, 84:4882–4885, 2000. https://doi.org/10.1103/PhysRevLett.84.4882.

[77] C. A. Tracy and H. Widom. Level-spacing distributions and the Airy kernel. *Communications in Mathematical Physics*, 159(1):151–174, 1994.

[78] M. Prähofer and H. Spohn. Scale invariance of the PNG droplet and the Airy process. *Journal of Statistical Physics*, 108(5):1071–1106, 2002. https://doi.org/10.1023/A:1019791415147.

[79] M. Prähofer and H. Spohn. Exact scaling functions for one-dimensional stationary KPZ growth. *Journal of Statistical Physics*, 115(1):255–279, 2004. https://doi.org/10.1023/B:JOSS.0000019810.21828.fc.

[80] S. Prolhac and H. Spohn. Two-point generating function of the free energy for a directed polymer in a random medium. *Journal of Statistical Mechanics: Theory and Experiment*, 2011(01):P01031, 2011. http://dx.doi.org/10.1088/1742-5468/2011/01/P01031.

[81] A. Borodin, P. L. Ferrari, and T. Sasamoto. Large time asymptotics of growth models on space-like paths II: PNG and parallel TASEP. *Communications in Mathematical Physics*, 283(2):417–449, 2008. https://doi.org/10.1007/s00220-008-0515-4.

[82] J. Baik, P. L. Ferrari, and S. Péché. Limit process of stationary TASEP near the characteristic line. *Communications on Pure and Applied Mathematics*, 63(8): 1017–1070, 2010. https://doi.org/10.1002/cpa.20316.

[83] M. Mehta. *Random matrices, Pure and Applied Mathematics Series vol. 142*. Elsevier BV, Amsterdam Netherlands, 2004.

[84] K. Johansson. Discrete polynuclear growth and determinantal processes. *Communications in Mathematical Physics*, 242(1):277–329, 2003. https://doi.org/10.1007/s00220-003-0945-y.

[85] F. Bornemann, P. L. Ferrari, and M. Prähofer. The Airy_1 process is not the limit of the largest eigenvalue in GOE matrix diffusion. *Journal of Statistical Physics*, 133(3):405–415, 2008. https://doi.org/10.1007/s10955-008-9621-0.

[86] J. G. Zabolitzky and D. Stauffer. Simulation of large Eden clusters. *Phys. Rev. A*, 34(2):1523–1530, 1986. https://link.aps.org/doi/10.1103/PhysRevA.34.1523.

[87] J. Kertész and Dietrich E. Wolf. Anomalous roughening in growth processes. *Phys. Rev. Lett.*, 62(22):2571–2574, 1989. https://link.aps.org/doi/10.1103/PhysRevLett.62.2571.

[88] J. M. Kim and J. M. Kosterlitz. Growth in a restricted solid-on-solid model. *Phys. Rev. Lett.*, 62(19):2289–2292, 1989. https://link.aps.org/doi/10.1103/PhysRevLett.62.2289.

[89] B. M. Forrest and L-H. Tang. Surface roughening in a hypercube-stacking model. *Phys. Rev. Lett.*, 64(12):1405–1408, 1990. https://link.aps.org/doi/10.1103/PhysRevLett.64.1405.

[90] J. M. Kim, J. M. Kosterlitz, and T. Ala-Nissila. Surface growth and crossover behaviour in a restricted solid-on-solid model. *Journal of Physics A: Mathematical and General*, 24(23):5569–5586, 1991. http://dx.doi.org/10.1088/0305-4470/24/23/022.

[91] L-H. Tang, B. M. Forrest, and D. E. Wolf. Kinetic surface roughening. II. Hypercube-stacking models. *Phys. Rev. A*, 45(10):7162–7179, 1992. https://link.aps.org/doi/10.1103/PhysRevA.45.7162.

[92] C-S. Chin and M. den Nijs. Stationary-state skewness in two-dimensional Kardar-Parisi-Zhang type growth. *Phys. Rev. E*, 59(3):2633–2641, 1999. URL https://link.aps.org/doi/10.1103/PhysRevE.59.2633.

[93] J. Kondev, C. L. Henley, and D. G. Salinas. Nonlinear measures for characterizing rough surface morphologies. *Phys. Rev. E*, 61(1):104–125, 2000. https://link.aps.org/doi/10.1103/PhysRevE.61.104.

[94] E. Marinari, A. Pagnani, and G. Parisi. Critical exponents of the KPZ equation via multi-surface coding numerical simulations. *Journal of Physics A: Mathematical and General*, 33(46):8181–8192, 2000. http://dx.doi.org/10.1088/0305-4470/33/46/303.

[95] F. D. A. Aarão Reis. Universality and corrections to scaling in the ballistic deposition model. *Phys. Rev. E*, 63(5):056116–, 2001. https://link.aps.org/doi/10.1103/PhysRevE.63.056116.

[96] G. Ódor, B. Liedke, and K-H. Heinig. Mapping of (2+1)-dimensional Kardar-Parisi-Zhang growth onto a driven lattice gas model of dimers. *Phys. Rev. E*, 79(2):021125–, 2009. https://link.aps.org/doi/10.1103/PhysRevE.79.021125.

[97] J. Kelling and G. Ódor. Extremely large-scale simulation of a Kardar-Parisi-Zhang model using graphics cards. *Phys. Rev. E*, 84(6):061150, 2011. https://link.aps.org/doi/10.1103/PhysRevE.84.061150.

[98] J. G. Amar and F. Family. Numerical solution of a continuum equation for interface growth in 2+1 dimensions. *Phys. Rev. A*, 41(6):3399–3402, 1990. https://link.aps.org/doi/10.1103/PhysRevA.41.3399.

[99] B. Grossmann, H. Guo, and M. Grant. Kinetic roughening of interfaces in driven systems. *Phys. Rev. A*, 43(4):1727–1743, 1991. https://link.aps.org/doi/10.1103/PhysRevA.43.1727.

[100] K. Moser, J. Kertész, and D. E. Wolf. Numerical solution of the Kardar-Parisi-Zhang equation in one, two and three dimensions. *Physica A: Statistical Mechanics and its Applications*, 178(2):215–226, 1991. https://www.sciencedirect.com/science/article/pii/0378437191900177.

[101] V. G. Miranda and F. D. A. Aarão Reis. Numerical study of the Kardar-Parisi-Zhang equation. *Phys. Rev. E*, 77(3):031134–, 2008. https://link.aps.org/doi/10.1103/PhysRevE.77.031134.

[102] T. J. Newman and A. J. Bray. Strong-coupling behaviour in discrete Kardar-Parisi-Zhang equations. *Journal of Physics A: Mathematical and General*, 29(24):7917–7928, 1996. http://dx.doi.org/10.1088/0305-4470/29/24/016.

[103] A. Pagnani and G. Parisi. Numerical estimate of the Kardar-Parisi-Zhang universality class in $(2+1)$ dimensions. *Phys. Rev. E*, 92(1):010101, 2015. https://link.aps.org/doi/10.1103/PhysRevE.92.010101.

[104] T. J. Oliveira, S. G. Alves, and S. C. Ferreira. Kardar-Parisi-Zhang universality class in $(2+1)$ dimensions: Universal geometry-dependent distributions and finite-time corrections. *Phys. Rev. E*, 87:040102, 2013. https://doi.org/10.1103/PhysRevE.87.040102.

[105] F. D. A. Aarão Reis. Universality in two-dimensional Kardar-Parisi-Zhang growth. *Phys. Rev. E*, 69(2):021610–, 2004. https://link.aps.org/doi/10.1103/PhysRevE.69.021610.

[106] T. Halpin-Healy. Extremal paths, the stochastic heat equation, and the three-dimensional Kardar-Parisi-Zhang universality class. *Phys. Rev. E*, 88(4): 042118–, 2013. https://link.aps.org/doi/10.1103/PhysRevE.88.042118.

[107] Y. Shim and D. P. Landau. Dynamic finite-size scaling of the normalized height distribution in kinetic surface roughening. *Phys. Rev. E*, 64(3):036110–, 2001. https://link.aps.org/doi/10.1103/PhysRevE.64.036110.

[108] T. Paiva and F. D. A. Aarão Reis. Height and roughness distributions in thin films with Kardar–Parisi–Zhang scaling. *Surface Science*, 601(2):419–424, 2007. https://www.sciencedirect.com/science/article/pii/S0039602806010661.

[109] T. Halpin-Healy. $(2+1)$-dimensional directed polymer in a random medium: Scaling phenomena and universal distributions. *Phys. Rev. Lett.*, 109:170602, 2012. https://doi.org/10.1103/PhysRevLett.109.170602.

[110] T. Halpin-Healy and G. Palasantzas. Universal correlators and distributions as experimental signatures of $(2+1)$-dimensional Kardar-Parisi-Zhang growth. *Europhys. Lett.)*, 105(5):50001, 2014. http://dx.doi.org/10.1209/0295-5075/105/50001.

[111] M. Lässig. Quantized scaling of growing surfaces. *Phys. Rev. Lett.*, 80(11): 2366–2369, 1998. https://link.aps.org/doi/10.1103/PhysRevLett.80.2366.

[112] F. Colaiori and M. A. Moore. Upper critical dimension, dynamic exponent, and scaling functions in the mode-coupling theory for the Kardar-Parisi-Zhang equation. *Phys. Rev. Lett.*, 86(18):3946–3949, 2001. https://link.aps.org/doi/10.1103/PhysRevLett.86.3946.

[113] K. J. Wiese. On the perturbation expansion of the KPZ equation. *Journal of Statistical Physics*, 93(1):143–154, 1998. https://doi.org/10.1023/B:JOSS.0000026730.76868.c4.

[114] L. Canet, H. Chaté, B. Delamotte, and N. Wschebor. Nonperturbative renormalization group for the Kardar-Parisi-Zhang equation. *Phys. Rev. Lett.*, 104:150601, 2010. https://link.aps.org/doi/10.1103/PhysRevLett.104.150601.

[115] L. Canet, H. Chaté, B. Delamotte, and N. Wschebor. Nonperturbative Renormalization Group for the Kardar-Parisi-Zhang equation: General framework and first applications. *Phys. Rev. E*, 84:061128, 2011. http://link.aps.org/doi/10.1103/PhysRevE.84.061128.

[116] T. Kloss, L. Canet, and N. Wschebor. Nonperturbative renormalization group for the stationary Kardar-Parisi-Zhang equation: Scaling functions and amplitude ratios in $1+1$, $2+1$, and $3+1$ dimensions. *Phys. Rev. E*, 86(5): 051124, 2012. https://link.aps.org/doi/10.1103/PhysRevE.86.051124.

[117] V. Savona, C. Piermarocchi, A. Quattropani, P. Schwendimann, and F. Tassone. Optical properties of microcavity polaritons. *Phase Transitions*, 68(1):169–279, 1999. https://doi.org/10.1080/01411599908224518.

[118] G. D. Mahan. *Many-Particle Physics*. Springer, 3rd edition edition, 2008.

[119] D. Squizzato. *Exploring Kardar-Parisi-Zhang universality class: From the dynamics of exciton-polariton condensates to stochastic interface growth with temporally correlated noise*. Thesis, Université Grenoble Alpes, 2019. https://tel.archives-ouvertes.fr/tel-02494207.

[120] H. Deng, H. Haug, and Y. Yamamoto. Exciton-polariton Bose-Einstein condensation. *Rev. Mod. Phys.*, 82:1489–1537, 2010. https://link.aps.org/doi/10.1103/RevModPhys.82.1489.

[121] H. Deng, G. Weihs, C. Santori, J. Bloch, and Y. Yamamoto. Condensation of semiconductor microcavity exciton polaritons. *Science*, 298(5591):199–202, 2002. https://www.science.org/doi/abs/10.1126/science.1074464.

[122] J. Kasprzak, M. Richard, S. Kundermann, A. Baas, P. Jeambrun, J. M. J. Keeling, F. M. Marchetti, M. H. Szymańska, R. André, J. L. Staehli, V. Savona, P. B. Littlewood, B. Deveaud, and L. S. Dang. Bose–Einstein condensation of exciton polaritons. *Nature*, 443(7110):409–414, 2006. https://doi.org/10.1038/nature05131.

[123] A. Amo, J. Lefrère, S. Pigeon, C. Adrados, C. Ciuti, I. Carusotto, R. Houdré, E. Giacobino, and A. Bramati. Superfluidity of polaritons in semiconductor microcavities. *Nature Physics*, 5(11):805–810, 2009. https://doi.org/10.1038/nphys1364.

[124] J. J. Hopfield. Theory of the contribution of excitons to the complex dielectric constant of crystals. *Phys. Rev.*, 112:1555–1567, 1958. https://link.aps.org/doi/10.1103/PhysRev.112.1555.

[125] D. S. Dovzhenko, S. V. Ryabchuk, Y. P. Rakovich, and I. R. Nabiev. Light–matter interaction in the strong coupling regime: Configurations, conditions, and applications. *Nanoscale*, 10(8):3589–3605, 2018. http://dx.doi.org/10.1039/C7NR06917K.

[126] P. Comaron. *Phase transitions and quench dynamics in driven-dissipative condensates*. Thesis, Newcastle University, 2018. http://theses.ncl.ac.uk/jspui/handle/10443/4255.

[127] A. Chiocchetta, A. Gambassi, and I. Carusotto. Laser operation and Bose-Einstein condensation: Analogies and differences, 2015. https://arxiv.org/abs/1503.02816.

[128] V. DeGiorgio and Marlan O. Scully. Analogy between the laser threshold region and a second-order phase transition. *Phys. Rev. A*, 2:1170–1177, 1970. https://link.aps.org/doi/10.1103/PhysRevA.2.1170.

[129] R. Graham and H. Haken. Laserlight — first example of a second-order phase transition far away from thermal equilibrium. *Zeitschrift für Physik*, 237(1): 31–46, 1970. https://doi.org/10.1007/BF01400474.

[130] T. Byrnes, N-Y. Kim, and Y. Yamamoto. Exciton–polariton condensates. *Nature Physics*, 10(11):803–813, 2014. https://doi.org/10.1038/nphys3143.

[131] R. M. Stevenson, V. N. Astratov, M. S. Skolnick, D. M. Whittaker, M. Emam-Ismail, A. I. Tartakovskii, P. G. Savvidis, J. J. Baumberg, and J. S. Roberts. Continuous wave observation of massive polariton redistribution by stimulated scattering in semiconductor microcavities. *Phys. Rev. Lett.*, 85: 3680–3683, 2000. https://link.aps.org/doi/10.1103/PhysRevLett.85.3680.

[132] J. J. Baumberg, P. G. Savvidis, R. M. Stevenson, A. I. Tartakovskii, M. S. Skolnick, D. M. Whittaker, and J. S. Roberts. Parametric oscillation in a vertical microcavity: A polariton condensate or micro-optical parametric oscillation. *Phys. Rev. B*, 62:R16247–R16250, 2000. https://link.aps.org/doi/10.1103/PhysRevB.62.R16247.

[133] A. Baas, J.-Ph. Karr, M. Romanelli, A. Bramati, and E. Giacobino. Quantum degeneracy of microcavity polaritons. *Phys. Rev. Lett.*, 96:176401, 2006. https://link.aps.org/doi/10.1103/PhysRevLett.96.176401.

[134] I. Carusotto and C. Ciuti. Spontaneous microcavity-polariton coherence across the parametric threshold: Quantum Monte Carlo studies. *Phys. Rev. B*, 72: 125335, 2005. https://link.aps.org/doi/10.1103/PhysRevB.72.125335.

[135] L. S. Dang, D. Heger, R. André, F. Bœuf, and R. Romestain. Stimulation of polariton photoluminescence in semiconductor microcavity. *Phys. Rev. Lett.*, 81: 3920–3923, 1998. https://link.aps.org/doi/10.1103/PhysRevLett.81.3920.

[136] M. Richard, J. Kasprzak, R. André, R. Romestain, L. S. Dang, G. Malpuech, and A. Kavokin. Experimental evidence for nonequilibrium Bose condensation of exciton polaritons. *Phys. Rev. B*, 72:201301, 2005. https://link.aps.org/doi/10.1103/PhysRevB.72.201301.

[137] M. Richard, J. Kasprzak, R. Romestain, R. André, and L. S. Dang. Spontaneous coherent phase transition of polaritons in CdTe microcavities. *Phys. Rev. Lett.*, 94:187401, 2005. https://link.aps.org/doi/10.1103/PhysRevLett.94.187401.

[138] A. Ferrier, A. Zamora, G. Dagvadorj, and M. H. Szymańska. Searching for the kardar-parisi-zhang phase in microcavity polaritons. *Phys. Rev. B*, 105:205301, May 2022. https://link.aps.org/doi/10.1103/PhysRevB.105.205301.

[139] A. Zamora, L. M. Sieberer, K. Dunnett, S. Diehl, and M. H. Szymańska. Tuning across universalities with a driven open condensate. *Phys. Rev. X*, 7:041006, 2017. https://doi.org/10.1103/PhysRevX.7.041006.

[140] M. Wouters and I. Carusotto. Excitations in nonequilibrium Bose-Einstein condensates. *Phys. Rev. Lett*, 99:140402, 2007. https://doi.org/10.1103/PhysRevLett.99.140402.

[141] M. Wouters and V. Savona. Stochastic classical field model for polariton condensates. *Phys. Rev. B*, 79:165302, 2009. https://doi.org/10.1103/PhysRevB.79.165302.

[142] L.P. Pitaevskii and S. Stringari. *Bose-Einstein condensation*. International Series of Monographs on Physics. Clarendon Press, 2003.

[143] D. Porras, C. Ciuti, J. J. Baumberg, and C. Tejedor. Polariton dynamics and Bose-Einstein condensation in semiconductor microcavities. *Phys. Rev. B*, 66: 085304, 2002. https://link.aps.org/doi/10.1103/PhysRevB.66.085304.

[144] A. Chiocchetta and I. Carusotto. Non-equilibrium quasi-condensates in reduced dimensions. *Europhys. Lett.*, 102(6):67007, 2013. https://doi.org/10.1209/0295-5075/102/67007.

[145] M. Wouters and I. Carusotto. Superfluidity and critical velocities in nonequilibrium Bose-Einstein condensates. *Phys. Rev. Lett.*, 105:020602, 2010. https://link.aps.org/doi/10.1103/PhysRevLett.105.020602.

[146] F. Baboux, D. De Bernardis, V. Goblot, V. N. Gladilin, C. Gomez, E. Galopin, L. Le Gratiet, A. Lemaître, I. Sagnes, I. Carusotto, and et al. Unstable and stable regimes of polariton condensation. *Optica*, 5(10):1163, 2018. https://doi.org/10.1364/OPTICA.5.001163.

[147] M. Richard. Private communication, 2019.

[148] Q. Fontaine, D. Squizzato, F. Baboux, I. Amelio, A. Lemître, Morassi M., I. Sagnes, L. Le Gratiet, A. Harouri, M. Wouters, I. Carusotto, A. Amo, M. Richard, A. Minguzzi, L. Canet, S. Ravets, and J. Bloch. Observation of KPZ universal scaling in a one-dimensional polariton condensate, 2021. https://arxiv.org/abs/2112.09550.

[149] M. H. Szymańska, J. Keeling, and P. B. Littlewood. Nonequilibrium quantum condensation in an incoherently pumped dissipative system. *Phys. Rev. Lett.*, 96: 230602, 2006. https://link.aps.org/doi/10.1103/PhysRevLett.96.230602.

[150] C. W. Gardiner and M. J. Davis. The stochastic Gross–Pitaevskii equation: II. *Journal of Physics B: Atomic, Molecular and Optical Physics*, 36(23):4731–4753, 2003. https://doi.org/10.1088/0953-4075/36/23/010.

[151] D. Manzano. A short introduction to the Lindblad master equation. *AIP Advances*, 10(2):025106, 2020. https://doi.org/10.1063/1.5115323.

[152] C. W. Gardiner and P. Zoller. *Quantum noise*. Springer - Verlag, 2000.

[153] R. J. Glauber. Coherent and incoherent states of the radiation field. *Phys. Rev.*, 131:2766–2788, 1963. https://link.aps.org/doi/10.1103/PhysRev.131.2766.

[154] E. C. G. Sudarshan. Equivalence of semiclassical and quantum mechanical descriptions of statistical light beams. *Phys. Rev. Lett.*, 10:277–279, 1963. https://link.aps.org/doi/10.1103/PhysRevLett.10.277.

[155] K. Husimi. Some formal properties of the density matrix. *Proceedings of the Physico-Mathematical Society of Japan. 3rd Series*, 22(4):264–314, 1940. 10.11429/ppmsj1919.22.4_264.

[156] V. N. Gladilin, K. Ji, and M. Wouters. Spatial coherence of weakly interacting one-dimensional nonequilibrium bosonic quantum fluids. *Phys. Rev. A*, 90: 023615, 2014. https://doi.org/10.1103/PhysRevA.90.023615.

[157] K. Ji, V. N. Gladilin, and M. Wouters. Temporal coherence of one-dimensional nonequilibrium quantum fluids. *Phys. Rev. B*, 91:045301, 2015. https://doi.org/10.1103/PhysRevB.91.045301.

[158] L. He, L. M. Sieberer, E. Altman, and S. Diehl. Scaling properties of one-dimensional driven-dissipative condensates. *Phys. Rev. B*, 92:155307, 2015. https://doi.org/10.1103/PhysRevB.92.155307.

[159] D. Squizzato, L. Canet, and A. Minguzzi. Kardar-Parisi-Zhang universality in the phase distributions of one-dimensional exciton polaritons. *Phys. Rev. B*, 97: 195453, 2018. https://doi.org/10.1103/PhysRevB.97.195453.

[160] K. Rojan, Y. Léger, G. Morigi, M. Richard, and A. Minguzzi. Enhanced second-order nonlinearity for THz generation by resonant interaction of exciton-polariton Rabi oscillations with optical phonons. *Phys. Rev. Lett*, 119: 127401, 2017. https://doi.org/10.1103/PhysRevLett.119.127401.

[161] D. Squizzato, K. Deligiannis, A. Minguzzi, and L. Canet. in preparation, 2023.

[162] Y. T. Fukai and K. A. Takeuchi. Kardar-Parisi-Zhang interfaces with curved initial shapes and variational formula. *Phys. Rev. Lett*, 124:060601, 2020. https://doi.org/10.1103/PhysRevLett.124.060601.

[163] F. Bornemann. On the numerical evaluation of Fredholm determinants. *Mathematics of Computation*, 79(270):871–915, 2009. https://doi.org/10.1090/S0025-5718-09-02280-7.

[164] F. Bornemann. On the numerical evaluation of distributions in random matrix theory: A review, 2010. https://arxiv.org/abs/0904.1581v5.

[165] G. Tosi, G. Christmann, N. G. Berloff, P. Tsotsis, T. Gao, Z. Hatzopoulos, P. G. Savvidis, and J. J. Baumberg. Sculpting oscillators with light within a nonlinear quantum fluid. *Nature Physics*, 8(3):190–194, 2012. https://doi.org/10.1038/nphys2182.

[166] T. Langen, S. Erne, R. Geiger, B. Rauer, T. Schweigler, M. Kuhnert, W. Rohringer, Igor E. Mazets, T. Gasenzer, and J. Schmiedmayer. Experimental observation of a generalized Gibbs ensemble. *Science*, 348(6231):207, 2015. http://dx.doi.org/10.1126/science.1257026.

[167] T. Schweigler, V. Kasper, S. Erne, I. Mazets, B. Rauer, F. Cataldini, T. Langen, T. Gasenzer, J. Berges, and J. Schmiedmayer. Experimental characterization of a quantum many-body system via higher-order correlations. *Nature*, 545(7654): 323–326, 2017. https://doi.org/10.1038/nature22310.

[168] G. Dagvadorj, J. M. Fellows, S. Matyjaśkiewicz, F. M. Marchetti, I. Carusotto, and M. H. Szymańska. Nonequilibrium phase transition in a two-dimensional driven open quantum system. *Phys. Rev. X*, 5:041028, 2015. https://doi.org/10.1103/PhysRevX.5.041028.

[169] K. Dunnett, A. Ferrier, A. Zamora, G. Dagvadorj, and M. H. Szymańska. Properties of the signal mode in the polariton optical parametric oscillator regime. *Phys. Rev. B*, 98:165307, 2018. https://doi.org/10.1103/PhysRevB.98.165307.

[170] O. K. Diessel, S. Diehl, and A. Chiocchetta. Emergent Kardar-Parisi-Zhang phase in quadratically driven condensates. *Phys. Rev. Lett.*, 128(7):070401–, 2022. https://link.aps.org/doi/10.1103/PhysRevLett.128.070401.

[171] V. N. Gladilin and M. Wouters. Interaction and motion of vortices in nonequilibrium quantum fluids. *New Journal of Physics*, 19(10):105005, 2017. http://dx.doi.org/10.1088/1367-2630/aa83a1.

[172] V. N. Gladilin and M. Wouters. Multivortex states and dynamics in nonequilibrium polariton condensates. *Journal of Physics A: Mathematical and Theoretical*, 52(39):395303, 2019. http://dx.doi.org/10.1088/1751-8121/ab3abc.

[173] E. Altman, L. M. Sieberer, L. Chen, S. Diehl, and J. Toner. Two-dimensional superfluidity of exciton polaritons requires strong anisotropy. *Phys. Rev. X*, 5: 011017, 2015. https://doi.org/10.1103/PhysRevX.5.011017.

[174] L. M. Sieberer, G. Wachtel, E. Altman, and S. Diehl. Lattice duality for the compact Kardar-Parisi-Zhang equation. *Phys. Rev. B*, 94(10):104521–, 2016. https://link.aps.org/doi/10.1103/PhysRevB.94.104521.

[175] G. Wachtel, L. M. Sieberer, S. Diehl, and E. Altman. Electrodynamic duality and vortex unbinding in driven-dissipative condensates. *Phys. Rev. B*, 94:104520, 2016. https://doi.org/10.1103/PhysRevB.94.104520.

[176] P. Comaron, I. Carusotto, M. H. Szymańska, and N. P. Proukakis. Non-equilibrium Berezinskii-Kosterlitz-Thouless transition in driven-dissipative condensates (a). *Europhys. Lett.*, 133(1):17002, 2021. http://dx.doi.org/10.1209/0295-5075/133/17002.

[177] G. Roumpos, M. Lohse, W. H. Nitsche, J. Keeling, M. H. Szymańska, P. B. Littlewood, A. Löffler, S. Höfling, L. Worschech, A. Forchel, and Y. Yamamoto. Power-law decay of the spatial correlation function in exciton-polariton condensates. *Proc. Natl. Acad. Sci. USA*, 109(17):6467, 2012. http://www.pnas.org/content/109/17/6467.abstract.

[178] D. Caputo, D. Ballarini, G. Dagvadorj, C. Sánchez Muñoz, M. De Giorgi, L. Dominici, K. West, L. N. Pfeiffer, G. Gigli, F. P. Laussy, M. H. Szymańska, and D. Sanvitto. Topological order and thermal equilibrium in polariton condensates. *Nature Materials*, 17(2):145–151, 2018. https://doi.org/10.1038/nmat5039.

[179] D. E. Wolf. Kinetic roughening of vicinal surfaces. *Phys. Rev. Lett.*, 67(13): 1783–1786, 1991. https://link.aps.org/doi/10.1103/PhysRevLett.67.1783.

[180] U. C. Täuber and E. Frey. Universality classes in the anisotropic Kardar-Parisi-Zhang model. *Europhys. Lett.*, 59(5):655, 2002. http://stacks.iop.org/0295-5075/59/i=5/a=655.

[181] L. Chen and J. Toner. Universality for moving stripes: A hydrodynamic theory of polar active smectics. *Phys. Rev. Lett.*, 111(8):088701–, 2013. https://link.aps.org/doi/10.1103/PhysRevLett.111.088701.

[182] Q. Mei, K. Ji, and M. Wouters. Spatiotemporal scaling of two-dimensional nonequilibrium exciton-polariton systems with weak interactions. *Phys. Rev. B*, 103(4):045302–, 2021. https://link.aps.org/doi/10.1103/PhysRevB.103.045302.

[183] T. Kloss, L. Canet, and N. Wschebor. Strong-coupling phases of the anisotropic Kardar-Parisi-Zhang equation. *Phys. Rev. E*, 90:062133, 2014. http://link.aps.org/doi/10.1103/PhysRevE.90.062133.

[184] I. S. Aranson, S. Scheidl, and V. M. Vinokur. Nonequilibrium dislocation dynamics and instability of driven vortex lattices in two dimensions. *Phys. Rev. B*, 58(21):14541–14547, 1998. https://link.aps.org/doi/10.1103/PhysRevB.58.14541.

[185] K. Deligiannis, D. Squizzato, A. Minguzzi, and L. Canet. Accessing Kardar-Parisi-Zhang universality sub-classes with exciton polaritons. *EPL (Europhysics Letters)*, 132(6):67004, 2020. http://dx.doi.org/10.1209/0295-5075/132/67004.

[186] S. T. Bramwell, J-Y. Fortin, P. C. W. Holdsworth, S. Peysson, J-F. Pinton, B. Portelli, and M. Sellitto. Magnetic fluctuations in the classical XY model: The origin of an exponential tail in a complex system. *Phys. Rev. E*, 63:041106, 2001. https://link.aps.org/doi/10.1103/PhysRevE.63.041106.

[187] N. Takemura, S. Trebaol, M. Wouters, M. T. Portella-Oberli, and B. Deveaud. Polaritonic Feshbach resonance. *Nature Physics*, 10(7):500–504, 2014. https://doi.org/10.1038/nphys2999.

[188] R. Larson and B. H. Edwards. *Multivariate calculus*. Cengage Learning, 2013. ISBN 9781285060293.

[189] J.R. Johansson, P. D. Nation, and F. Nori. QuTiP 2: A Python framework for the dynamics of open quantum systems. *Computer Physics Communications*, 184 (4):1234–1240, 2013. ISSN 0010-4655. https://doi.org/10.1016/j.cpc.2012.11.019.

[190] J.R. Johansson, P. D. Nation, and F. Nori. QuTiP: An open-source python framework for the dynamics of open quantum systems. *Computer Physics Communications*, 183(8):1760–1772, 2012. ISSN 0010-4655. https://doi.org/10.1016/j.cpc.2012.02.021.

[191] T. Sauer. A look back at the Ehrenfest classification. *The European Physical Journal Special Topics*, 226(4):539–549, 2017. https://doi.org/10.1140/epjst/e2016-60344-y.

[192] S. T. Bramwell, J.-Y. Fortin, P. C. W. Holdsworth, S. Peysson, J.-F. Pinton, B. Portelli, and M. Sellitto. Magnetic fluctuations in the classical XY model: The origin of an exponential tail in a complex system. *Phys. Rev. E*, 63:041106, 2001. https://link.aps.org/doi/10.1103/PhysRevE.63.041106.

[193] L. De Broglie. *Recherches sur la théorie des Quanta*. Theses, Migration - université en cours d'affectation, 1924. https://tel.archives-ouvertes.fr/tel-00006807.

[194] E. Wertz, L. Ferrier, D. D. Solnyshkov, R. Johne, D. Sanvitto, A. Lemaître, I. Sagnes, R. Grousson, A. V. Kavokin, P. Senellart, G. Malpuech, and J. Bloch. Spontaneous formation and optical manipulation of extended polariton condensates. *Nature Physics*, 6(11):860–864, 2010. https://doi.org/10.1038/nphys1750.

[195] D. Caputo, D. Ballarini, G. Dagvadorj, C. Sánchez Muñoz, M. De Giorgi, L. Dominici, K. West, Loren N. Pfeiffer, G. Gigli, Fabrice P. Laussy, M. H. Szymańska, and D. Sanvitto. Topological order and thermal equilibrium in polariton condensates. *Nature Materials*, 17(2):145–151, 2018. https://doi.org/10.1038/nmat5039.

[196] V. N. Gladilin and M. Wouters. Noise-induced transition from superfluid to vortex state in two-dimensional nonequilibrium polariton condensates. *Phys. Rev. B*, 100:214506, 2019. https://doi.org/10.1103/PhysRevB.100.214506.